21GRD08 SoMMet

D2: Report on the traceability scheme and uncertainty model for validation of neutron response functions of CRNS neutron-measuring devices under laboratory conditions

Prepared by: CMI, SMU, UHEI, PTB, CIEMAT and ASNR

Organisation name of the lead participant for the deliverable: CMI

Due date of the deliverable: February 2024

Actual submission date of the deliverable: 30 November 2025

Confidentiality Status: PU - Public, fully open (remember to deposit public deliverables in a trusted repository)

Deliverable Cover Sheet

Funded by the European Union. Views and opinions expressed are however those of the author(s) only and do not necessarily reflect those of the European Union or EURAMET. Neither the European Union nor the granting authority can be held responsible for them.

The project has received funding from the European Partnership on Metrology, co-financed from the European Union's Horizon Europe Research and Innovation Programme and by the Participating States.

Deliverable **D2** of project 21GRD08 SoMMet

Report on the traceability scheme and uncertainty model for validation of neutron response functions of CRNS neutron-measuring devices under laboratory conditions

Authors:
Zdenek Vykydal (CMI), Jaroslav Šolc (CMI), Jan Rusňák (CMI), Pavol Blahušiak (SMU), Markus Köhli (UHEI), Jannis Weimar (UHEI), María de los Ángeles Millán-Callado (PTB), Miroslav Zboril (PTB), Roberto Méndez (CIEMAT) and Nelson Magalotti (ASNR)

Institutions:
CMI – Czech Metrology Institute, Czech Republic
SMU – Slovenský metrologický ústav, Slovak Institute of Metrology, Slovakia
UHEI – University of Heidelberg, Germany
PTB – Physikalisch-Technische Bundesanstalt, the National Metrology Institute of Germany
CIEMAT – Centro de Investigaciones Energéticas, Medioambientales y Tecnológicas, Energy, Environment and Technology Research Centre, Spain
ASNR – L'Autorité de sûreté nucléaire et de radioprotection, Nuclear Safety and Radiation Protection Authority in France, formerly IRSN

Glossary

API: Application Programming Interface

BSS: Bonner Sphere Spectrometer

CRNS: Cosmic-Ray Neutron Sensing

ECV: Essential Climate Variable

ENDF/B: Evaluated Nuclear Data File/B

EPS: Expanded Polystyrene

GM counter: Geiger-Müller counter

GPS: Global Positioning System

GSM: Global System for Mobile Communications

HDPE: High-Density Polyethylene

IEC: International Electrotechnical Commission

IP67: Ingress Protection rating indicating dust and water resistance.

IR: Infrared

ISO: International Organization for Standardization

MC: Monte Carlo (referring to the simulation method)

MCA: Multichannel Analyzer

MCNP: Monte Carlo N-Particle (A specific particle transport code)

MWPC: Multiwire Proportional Counter

NMI: National Metrology Institute

NPM: Neutron Pulse Monitor

PET: Polyethylene Terephthalate

PMT: Photomultiplier Tube

PP: Polypropylene

PSD: Pulse-Shape Discrimination

SDI-12: Serial Data Interface at 1200 baud (A common communication protocol for environmental sensors) sf: Spontaneous Fission (as in ^{252}Cf(sf))

SI: International System of Units (Système International)

SWC: Soil Water Content

UV: Ultraviolet

WLS: Wavelength Shifter

Institutions & Facilities

ASNR: L'Autorité de sûreté nucléaire et de radioprotection, Nuclear Safety and Radiation Protection Authority in France, formerly IRSN (Institut de radioprotection et de sûreté nucléaire)

CEM: Spanish Metrology Centre

CIEMAT: Centro de Investigaciones Energéticas, Medioambientales y Tecnológicas, Energy, Environment and Technology Research Centre (Spain)

CMI: Český metrologický institut, Czech Metrology Institute

LMRI: Ionizing Radiation Metrology Laboratory (Spain)

LPN: Neutron Standards Laboratory (Spain)

NPL: National Physical Laboratory (UK)

PIAF: PTB Ion Accelerator Facility

PTB: Physikalisch-Technische Bundesanstalt (National Metrology Institute of Germany)

SMU: Slovenský metrologický ústav, Slovak Institute of Metrology

TABLE OF CONTENTS

Summary

This document, deliverable D2, is the second of eight technical deliverables of the project 21GRD08 SoMMet (hereafter: SoMMet). The project has received funding from the European Partnership on Metrology, co-financed by the European Union's Horizon Europe Research and Innovation Programme and by the Participating States (Funder name: European Partnership on Metrology; Funder ID: 10.13039/100019599; Grant number: 21GRD08 SoMMet).

Soil moisture measurements at point scales, conducted in agriculture and hydrology by practitioners (e.g., farmers, agronomists) or by scientists treating soil moisture as an Essential Climate Variable (ECV), are not immediately representative of moisture levels at larger scales relevant for practical applications. Point-scale measurements typically employ invasive, physical tactile sensors that are subject to local heterogeneities. While complex sampling designs and interpolation methods can be implemented to overcome this limitation, their uncertainties must be reduced, and practical calibration guidelines need to be developed. Earth observation via remote sensing enables real-time, continuous assessment of soil moisture at the kilometre scale; however, intermediate-scale methods like cosmic-ray neutron sensing (CRNS) are required to bridge the gap between point measurements and remote sensing. This necessitates the establishment of appropriate validation practices for the deep-sensing CRNS method. These practices should integrate supporting data on soil properties, moisture profiles, and vegetation, harmonizing different methods across scales through a holistic yet metrologically traceable approach.

As a first step, the CRNS probes currently deployed at various outdoor sites must be characterized in the well-described neutron reference fields of neutron metrology laboratories. This characterization is essential to understand their response, to model the response using particle transport codes, and to use such a validated model to calculate the influence of various external conditions (e.g., altitude, water content, snow cover, proximity to buildings) on probe behaviour.

This report provides the traceability scheme and uncertainty model for validating the neutron response functions of CRNS devices under laboratory conditions.

1 Introduction

Correct soil moisture estimation is a fundamental prerequisite for many applications, including agriculture, meteorological forecasting, flood and drought prediction, and general water accounting and management. Traditional methods typically provide point-scale measurements but are affected by soil heterogeneity, which can lead to a significant misinterpretation of hydrological conditions.

A completely different alternative is provided by satellite remote sensing approaches, which are typically based on microwave radiation (1 mm – 1 m). Compared to point-scale methods, satellite observations cover large areas, making them more suitable for hydrological applications. However, the signal is sensitive only to the uppermost centimetres of the soil layer and suffers from several limitations. These include a limited capability to penetrate vegetation, an inability to measure soil ice, sensitivity to surface roughness, and a low temporal resolution (on the order of weeks).

Over the last decade, a proximal geophysical method has been developed to overcome the operational challenges and bridge the gap between point-scale and remote sensing approaches: Cosmic-Ray Neutron Sensing (CRNS).

However, this novel approach suffers from a lack of metrologically traceable measurement methods and harmonization in the interpretation of results provided by different probe types. This report aims to provide the traceability scheme and uncertainty model for validating the calculated neutron response functions of CRNS neutron-measuring devices under laboratory conditions.

1.1 Review of the metrological facilities capable of traceable CRNS response validation

A primary step in the work conducted for activity A1.3.1 was to review existing metrology facilities within the consortium that can be used for the SI-traceable validation and characterization of neutron-measuring devices employed in the CRNS method. Input from activity A1.1.4 and the project's Stakeholder Committee (A5.1.1) were utilized for this task. The number of reviewed facilities was expanded to four institutes, including the Slovak Institute of Metrology (SMU).

1.1.1 Czech Metrology Institute (CMI)

The Czech Metrology Institute (CMI), the National Metrology Institute (NMI) of the Czech Republic, is responsible for maintaining and developing national standards, ensuring their international traceability, and implementing SI units into practice.

The Laboratory of Neutron Metrology focuses on the development of neutron metrology and maintains and develops the following primary national standards:

- The National Standard for the Emission of Radionuclide Neutron Sources (Manganese Bath)
- The National Standard for Neutron Fluence Rate and Spectral Fluence Rate
- The National Standard for Thermal Neutron Fluence Rate

These standards are used for the routine calibration of instruments in neutron reference fields and can also be used for validating the Monte Carlo (MC) models (from activity A1.3.3) of selected CRNS probes (from activity A1.3.2).

CMI can provide the following neutron reference fields:

- ^{252}Cf radionuclide source, characterized to include room-scattered contributions.
- ^{241}Am-Be radionuclide source, characterized to include room-scattered contributions.
- ^{239}Pu-Be radionuclide source.
- 3”, 4” and 6” polyethylene-moderated ^{252}Cf radionuclide source.
- 14 MeV neutron generator.
- Graphite pile – thermal neutron field.

The calibration method is based on a comparison between the conventionally true fluence rates at specified locations and the values indicated by the instrument. Radionuclide neutron sources are characterized by their emission rate (measured in a manganese bath), their anisotropy factor, and their energy spectrum. The contribution of room-scattered neutrons and linear air attenuation to the instrument reading is either determined and corrected for using the generalized distance variation method or the shadow cone method (as per ISO 8529), or it is spectrally characterized using a calibrated extended-range Bonner sphere spectrometer and accounted for (for ^{252}Cf and ^{241}Am-Be fields).

The 14 MeV neutron generator is characterized using a calibrated extended-range Bonner sphere spectrometer in terms of neutron spectral fluence rate per monitor unit.

In both cases, the instrument being calibrated is placed on the calibration bench at a specific distance from the source (see Figure 1). The maximum load capacity of the calibration bench is 50 kg. The maximum dimensions of the instrument being calibrated depend on its shape and its distance from the source and are approximately 40 cm.

The graphite pile (see Figure 1d) is characterized by a validated MC model. The instrument is placed in front of the graphite opening, and its size is limited by the dimensions of the opening to approximately 30 cm. The maximum load capacity of the pile bench is 30 kg.

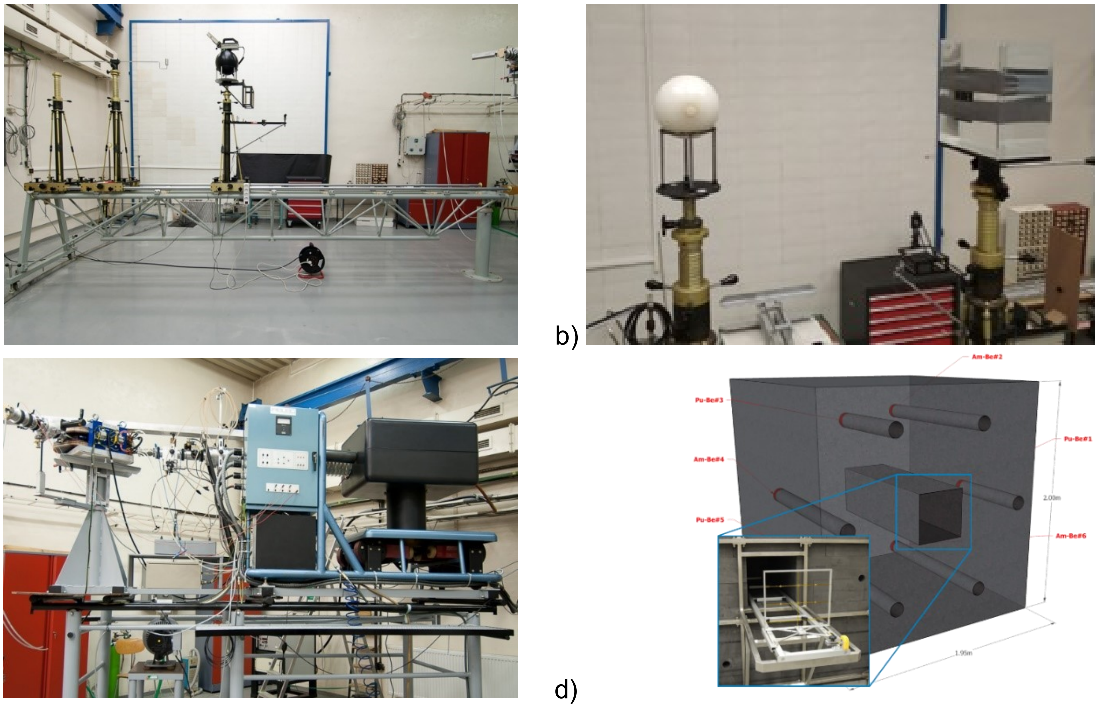

a) b) c) d)

Figure 1. Laboratory of Neutron Metrology at CMI. a) Calibration bench with a ^{241}Am-Be source irradiating a neutron ambient dose equivalent rate meter. b) A polyethylene-moderated ^{252}Cf source irradiating a neutron personal dosimeter on an ISO water slab phantom. c) The 14 MeV neutron generator. The irradiated instrument is placed on the same calibration bench used for radionuclide neutron source irradiations. d) The graphite pile as a source of thermal neutrons, with a detail from the field characterization using gold foils.

1.1.2 Physikalisch-Technische Bundesanstalt (PTB)

The Physikalisch-Technische Bundesanstalt (PTB) is Germany's national metrology institute (NMI), operating under the Federal Ministry for Economic Affairs and Climate Action. It functions as a high-level scientific and technical authority, meeting the calibration and testing standards of DIN EN ISO/IEC 17025. The "Department 6.4 – Neutron Radiation" at PTB specializes in neutron metrology, spectrometry, and dosimetry. It operates the PTB Ion Accelerator Facility (PIAF) and other irradiation facilities equipped with neutron sources, including thermal neutron fields.

1.1.2.1 Neutron reference fields from radionuclide sources

PTB provides neutron reference fields for calibrating measuring instruments in accordance with ISO 8529 (Parts 1-3) and IEC 61005. Calibrations and irradiations for neutron measuring devices, area dosimeters, and personal dosimeters are overseen by the "6.42 – Neutron Dosimetry" team. Dose equivalent quantities are determined using recommended fluence-to-dose conversion coefficients.

Various neutron reference fields are offered, with the relative standard uncertainty in neutron fluence ranging from 1 % to 3 %, depending on the source:

- ^{252}Cf(sf)
- ^{252}Cf(sf) (15 cm D_2O moderated).
- ^{252}Cf(sf) (15 cm D_2O moderated, 1 mm Cd)
- ^{241}Am-Be (α,n)

The neutron source strength was determined using the primary manganese bath method at the UK's National Physical Laboratory (NPL). Neutron fluence spectra are assessed via spectrometry and neutron transport calculations, with room scatter corrections applied using methods such as shadow objects or distance variations, as specified in ISO 8529-3. Irradiations are conducted in a 7 m × 7 m × 6.5 m room, where sources are positioned remotely and detector distances are controlled automatically (Figure 2).

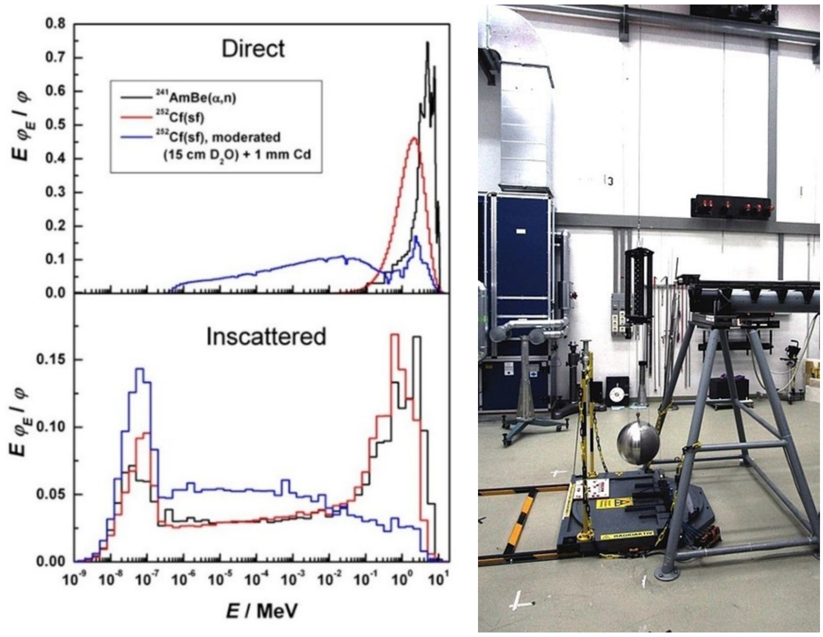

Figure 2. Left, neutron fluence rate as a function of neutron energy for the direct and scattered neutrons at the PTB neutron source irradiation facility. Right, the irradiation facility showing the water tank for source storage and the D_2O moderator sphere.

1.1.2.2 Thermal neutron reference field

PTB maintains a homogeneous 20 cm × 20 cm thermal neutron field, where thermal neutrons constitute 98.4 % of the total neutron fluence and 83 % of the neutron dose equivalent. At the reference position (30 cm from the moderator and 75 cm above the floor), the thermal neutron fluence rate is 68 cm^{-2} s^{-1}, with ambient dose equivalent and personal dose equivalent rates of 2.8 μSv h^{-1} and 2.15 μSv h^{-1}, respectively. This neutron field was characterized by using gold foil activation, Bonner spheres, and MC calculations.

The moderator consists of a 1.5 m × 1.5 m × 1.8 m graphite block containing sixteen embedded ^{241}Am-Be(α,n) sources at distances of 1.25 m and 1.35 m from the front face and heights of 65 cm and 85 cm above the floor (Figure 3). Borated plastic and lead shields are used to minimize neutron and gamma background radiation. A cadmium plate can be employed to subtract thermal neutrons, enabling the measurement of a near-pure thermal neutron field using the difference method.

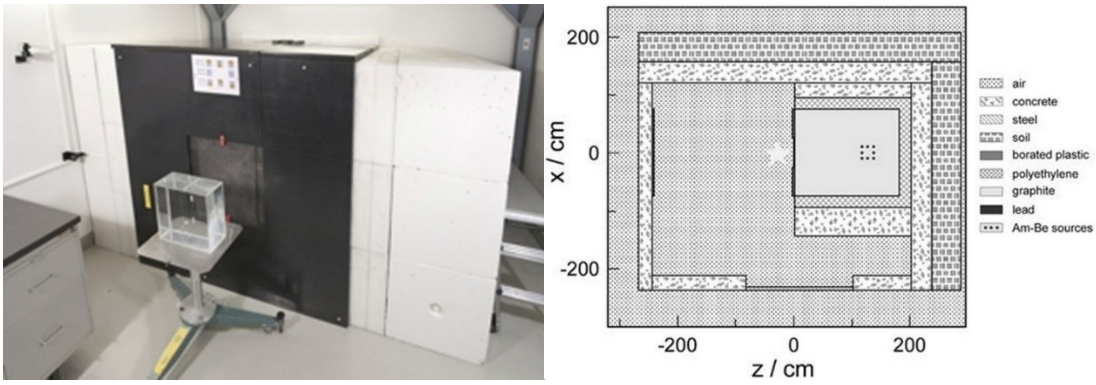

Figure 3. Left, the PTB thermal neutron irradiation facility. Right, a schematic diagram (horizontal cross-section) of the PTB thermal neutron facility.

1.1.2.3 Monoenergetic neutron reference fields

In accordance with ISO 8529, PTB generates monoenergetic neutron reference fields with peak energies from 24 keV to 19 MeV at the PIAF facility (see

Table 1). These fields are produced using nuclear reactions such as ^{7}Li(p,n), D(d,n), T(p,n), and T(d,n). PIAF comprises a 2 MV Tandetron accelerator and an energy-variable isochronous cyclotron, which provide ion beams in continuous or pulsed mode. Other (p,n), (d,n), and (α,n) reactions can also be used to generate neutrons with both monoenergetic and broad energy distributions.

Neutron fluence is measured using a stable ^{3}He counter, which is traceable to primary standards. The neutron energy distribution is determined via time-of-flight techniques with liquid scintillators, while a calibrated GM (Geiger-Müller) counter monitors the photon dose fraction.

Table 1. Fluxes and ambient dose equivalent rates for the monoenergetic neutron fields at PTB. The parameters $<E_n>$ and ΔE_n represent the average energy and energy spread of the neutron distribution, respectively. The maximum fluence rates and ambient dose equivalent rates, measured at 1 meter from the production target, are denoted by (dΦ/dt) and (dH^*(10)/dt). Additionally, ($\Phi_s c/\Phi$) indicates the proportion of the total neutron fluence attributable to neutrons scattered within the target.

Reaction	$<E_n>$ MeV	ΔE_n MeV	Target	($d\Phi/dt$) $cm^{-2}.s^{-1}$	Φ_{sc}/Φ %	($dH^*(10)/dt$) $mSv.h^{-1}$
^{7}Li(p,n)^{7}Be	0.024	0.010	Li	2.5×10^{2}	6.4	0.02
^{7}Li(p,n)^{7}Be	0.144	0.015	Li	7.1×10^{2}	2.8	0.34
^{7}Li(p,n)^{7}Be	0.250	0.012	Li	3.5×10^{2}	5.4	0.26
^{7}Li(p,n)^{7}Be	0.565	0.009	Li	1.6×10^{3}	1.6	2.0
^{3}H(p,n)^{3}He	1.2	0.108	Ti(T)	2.0×10^{3}	3.1	3.1
^{3}H(p,n)^{3}He	2.5	0.127	Ti(T)	4.9×10^{3}	1.4	7.3
^{2}H(p,n)^{3}He	5.0	0.200	D_2-Gas	5.2×10^{3}	<1.0	7.5
^{2}H(p,n)^{3}He	8.0	0.200	D_2-Gas	1.9×10^{4}	<1.0	27.5
^{3}H(d,n)^{4}He	14.8	0.431	Ti(T)	1.3×10^{4}	3.0	24.3
^{3}H(d,n)^{4}He	19.0	0.300	Ti(T)	8.5×10^{2}	1.2	1.8

The neutron production target is located in a large experimental hall with a low-mass gridded floor and an open space below the target to minimize background from back-scattered low-energy neutrons (Figure 4). The facility is designed to reduce contributions from backscattered neutron radiation to less than 5 %.

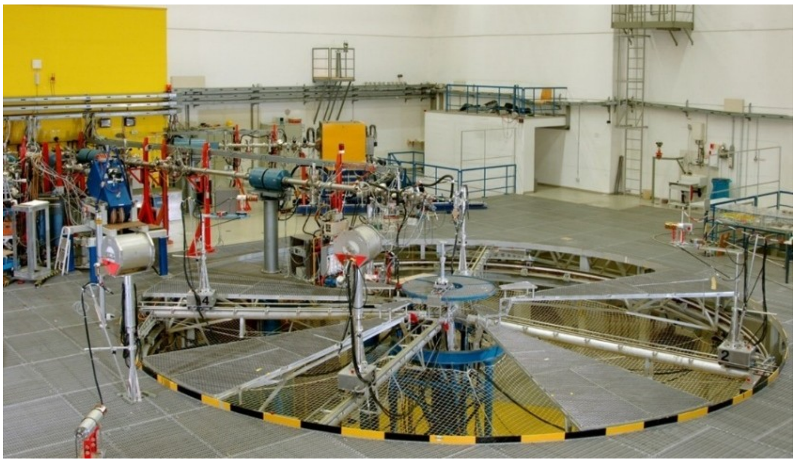

Figure 4. The low-scattering experimental hall at PIAF. The neutron-production target is mounted at the end of the beamline above the opening in the grid floor.

1.1.3 Centro de Investigaciones Energéticas, Medioambientales y Tecnológicas (CIEMAT)

The Centro de Investigaciones Energéticas, Medioambientales y Tecnológicas (CIEMAT) is a public research organization under the Ministry of Science and Innovation, focusing on energy, environment, and related technologies.

The CIEMAT-LMRI (Laboratorio de Metrología de Radiaciones Ionizantes, Ionizing Radiation Metrology Laboratory) is the laboratory associated with the Spanish Metrology Centre (CEM) in the field of ionizing radiation, as designated by Royal Decree 533/1996. It is responsible, on behalf of the state, for preserving, maintaining, and disseminating the national standards for ionizing radiation units.

Specifically, CIEMAT-LMRI is dedicated to preserving, maintaining, and disseminating the National Standards for the quantities of Activity (of a radionuclide), Kerma (for X- and gamma-rays), and Absorbed Dose, as defined in Act ITC/2581/2006. A neutron fluence standard is scheduled to be incorporated in the coming months.

CIEMAT-LMRI maintains primary standards for activity and secondary standards for photon air kerma and neutron emission. Relevant to this project, the LPN (Laboratorio de Patrones Neutrónicos, Neutron Standards Laboratory), as part of CIEMAT-LMRI, has developed the National Standard of Neutron Fluence Rate based on ^{252}Cf, ^{241}Am-Be, and D_2O-moderated ^{252}Cf neutron sources.

As part of the LPN's expansion, the installation of a manganese bath (as a primary standard) and a thermal neutron pile are planned for the following year.

The irradiation room is an 8 m × 8 m × 8 m bunker featuring a 3-meter-long bench where equipment to be calibrated is positioned (Figure 5). Neutron sources are stored underwater, and an automated system allows for their remote manipulation from the control room. The bench is robust, enabling the placement of heavy instruments (up to 200 kg), such as some CRNS models (from activity A1.3.2), to validate MC simulations (from activity A1.3.3) using the following neutron fields:

- ^{252}Cf
- ^{241}Am-Be
- D_2O-moderated ^{252}Cf
- H_2O-moderated ^{252}Cf

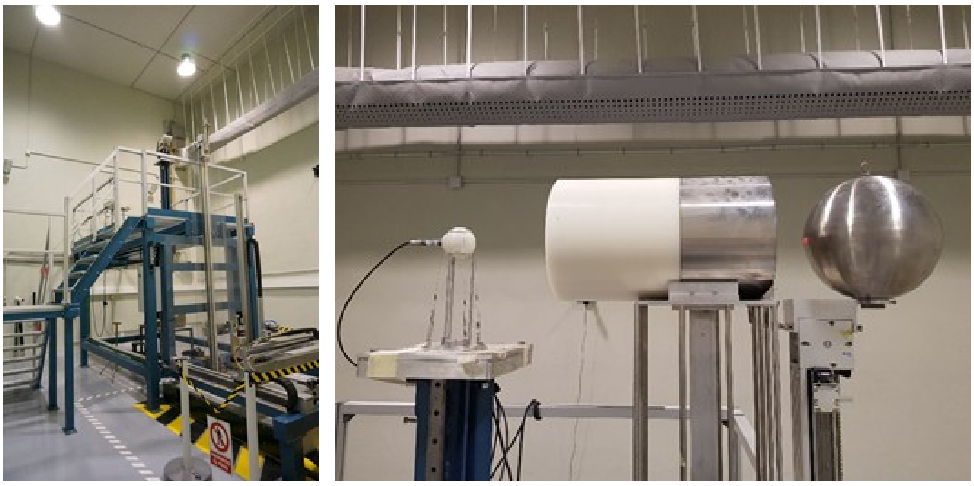

Figure 5. Positioning bench at LPN (left). D_2O-moderated ^{252}Cf source and shadow cylinder (right).

Shadow cones are available for the three primary neutron sources (Figure 5), and there is extensive experience in calibrating large detectors with custom-made shadow cones.

An extended-range Bonner sphere spectrometer (BSS) capable of measuring with eight spheres simultaneously has also been developed (Figure 6) and can be applied to characterize environmental neutron fields.

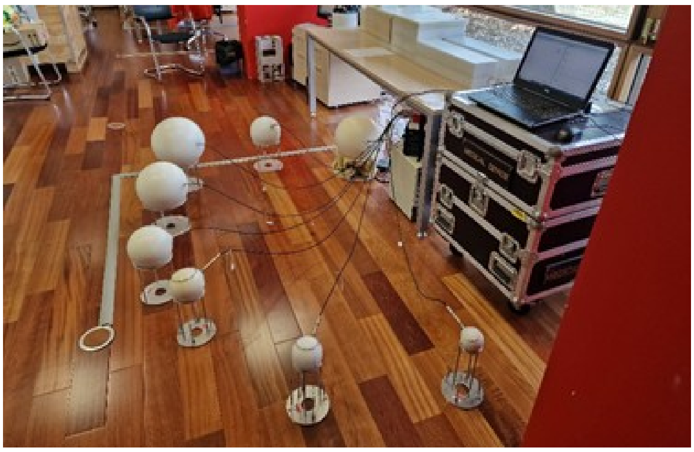

Figure 6. The extended-range Bonner Sphere Spectrometer (BSS) of CIEMAT.

1.1.4 Slovak Institute of Metrology (SMU)

The Slovak Institute of Metrology (SMU) is the Slovak national metrology institute (NMI). SMU maintains national standards for ionizing radiation and provides metrological services, verification, calibration, and testing for national stakeholders at the highest metrological level in the Slovak Republic. One of the maintained standards is the National Neutron Standard No. NE 016/98, which is a secondary standard. This standard is used to ensure the traceability of neutron quantities for strategic entities in the Slovak Republic, such as nuclear power plants, the Ministry of the Interior, the Ministry of Defence, Civil Defence, and public health authorities.

This standard is based on two separate systems: a Bonner sphere spectrometer and a system for neutron field measurement using radionuclide sources (^{241}Am-Be, ^{239}Pu-Be, and ^{252}Cf). The first device is used to determine neutron qualities and the neutron spectrum in known or unknown fields, while the second device generates the neutron fields necessary for transferring the unit to lower-order standards and measuring devices.

The irradiation room for national standard NE 016/98 is a neutron laboratory measuring 10 m × 10 m × 8 m, featuring an approximately 3-meter-long measuring bench where equipment to be calibrated is positioned (Figure 7). Neutron sources are stored in a polyethylene-shielded carousel below floor level, and an automated system allows for their remote manipulation from the control room.

Recently, the standard polyethylene Bonner sphere spectrometer was extended with specific metallic spheres, designated 4Pb5_7″, 4W5_7″, and 5Pb7_9″ (Figure 8). To determine the emission rate of neutron sources used at SMU at a primary level, an in-house manganese bath is currently under development.

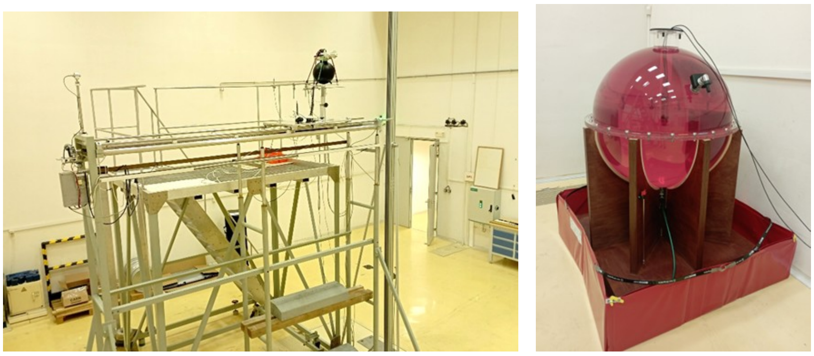

Figure 7. Measuring bench at SMU (left). Manganese bath under development at SMU (right).

Figure 8. The extended-range Bonner sphere spectrometer at SMU.

The calibration method follows the same principles as previously described in 1.1.1, being based on a comparison between conventionally true fluence rates at specified locations and the values indicated by the instrument. Radionuclide neutron sources are characterized by their emission rate, anisotropy factor, and energy spectrum. The contribution of room-scattered neutrons and linear air attenuation to the instrument reading is determined using the generalized distance variation method (ISO 8529).

1.1.5 L'Autorité de sûreté nucléaire et de radioprotection (ASNR)

ASNR, the French Nuclear Safety and Radiation Protection Authority (formerly IRSN – Institut de radioprotection et de sûreté nucléaire), operates and is developing a large technical platform at the Cadarache centre (Bouches du Rhône) for neutron metrology and calibration of neutron measuring instruments, particularly for radiation protection. Having been designated the national holder of neutron dosimetry reference standards by France's national testing laboratory (LNE), ASNR must be able to produce perfectly controlled neutron fields and take measurements that are as accurate as possible. The platform is composed of CEZANE and AMANDE facilities which produce all the neutron reference field types recommended by international standards (ISO 8529 and ISO 12789) for calibrating neutron measuring instruments.

The AMANDE and CEZANE facilities are at the centre of a 300-meter radius exclusion zone. This is unique worldwide for this type of facility and means that neutrons can be generated in structurally light experiment halls (with metallic walls) limiting the proportion of scattered neutrons at the calibration point.

1.1.5.1 CEZANE - Van Gogh irradiator

The VAN GOGH irradiator consists of the two main radioactive sources recommended by standard ISO 8529-1: ^{241}AmBe and ^{252}Cf.

When they are not in use, these sources are stored in a polyethylene container. Using compressed air in a guide tube, the sources are taken to their irradiation position 3.2 m above the ground, which limits the background noise due to neutrons scattered by the ground. A motorized calibration bench is used to position the instruments at the source or at any distance between 0 and 2 m.

To produce an energy distribution that is closer to those encountered in the workplace, the ^{252}Cf source can be placed in the centre of a moderating heavy water sphere of radius 15 cm, with a 1.2 mm thick aluminium shell to which an 0.8 mm thick cadmium shell can be added. The contribution of the scattered neutrons can be evaluated both with shadow cone and semi-empirical methods.

Neutron flux values for both sources were determined directly from measurements of the neutron emission rate (number of neutrons emitted per second), performed in a manganese bath at the Laboratoire National Henri Becquerel (LNHB at CEA Saclay).

The fluxes and dose equivalent rates (individual and ambient, on 17th May 2024) at 75 cm from the source are presented in Table 2.

Calibration activities in this irradiator are accredited by the French accreditation committee (COFRAC), under the designation LA2.55 (scope available on www.cofrac.fr).

Table 2. Neutron fluxes and dose equivalent rates (ambient and personal) for the Van Gogh sources.

Quantity	^{241}**Am-Be**	^{252}**Cf**	**(^{252}Cf+D_2O)$_{/Cd}$**
Flux (cm^{-2}.s^{-1})	501	1722	1469
H*(10) (µSv.h^{-1})	698	2386	603
H_p(10) (µSv.h^{-1})	732	2480	629

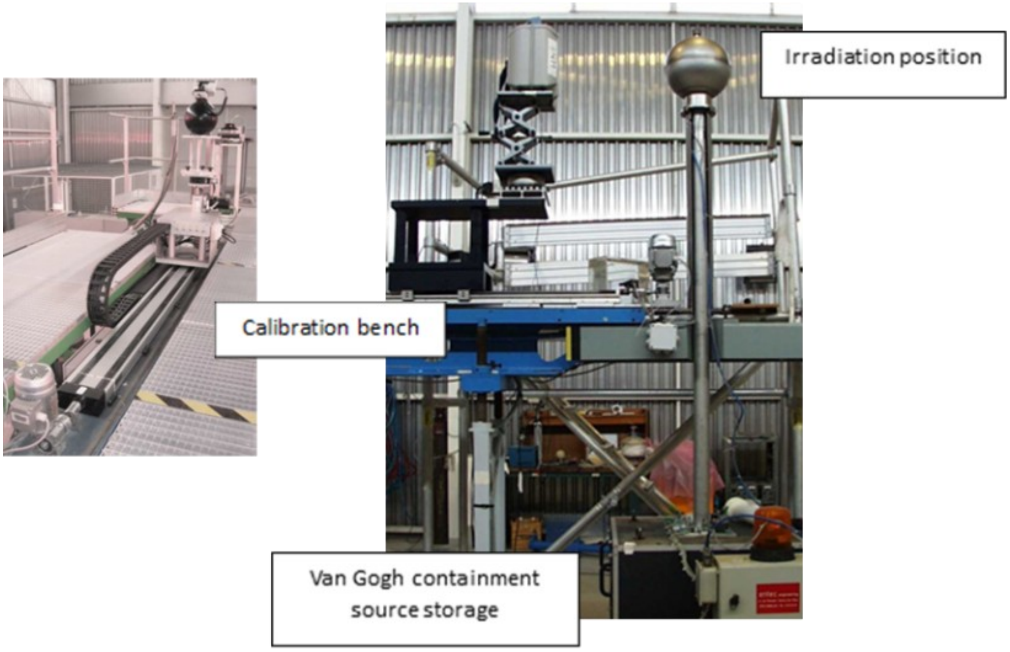

Figure 9. Van Gogh neutron irradiator of ASNR.

1.1.5.2 CEZANE - SAMES T400 neutron generator

The T400 neutron generator is a 400 kV electrostatic accelerator bringing deuterons (deuterium nucleus) up to an energy of between 150 and 400 keV. These accelerated deuterons are sent to a deuterated titanium (TiD) target where their interactions with the deuterium atoms generate quasi-monoenergetic neutrons of around 3 MeV.

T400 nominally operates at an energy of 350 keV with a beam intensity of 2 mA and it is used for high flux irradiation, 10^9 n·s^{-1}, with a flux of around 10^4 cm^{-2} s^{-1} at 1 m.

The neutron fluence is determined and monitored using the associated particle method: 3 silicon diodes are placed at the back of the target (175° angle) and detect the protons emitted simultaneously with the neutrons.

The devices being tested can be placed at between 0 and 2 m from the target along the axis of the deuteron beam.

The accelerator can be coupled with two different devices, CANEL and BLOG, which allow to produce respectively a realistic field, i.e. one with similar characteristics to the neutron fields encountered in the workplace, and a thermal one (to be characterized).

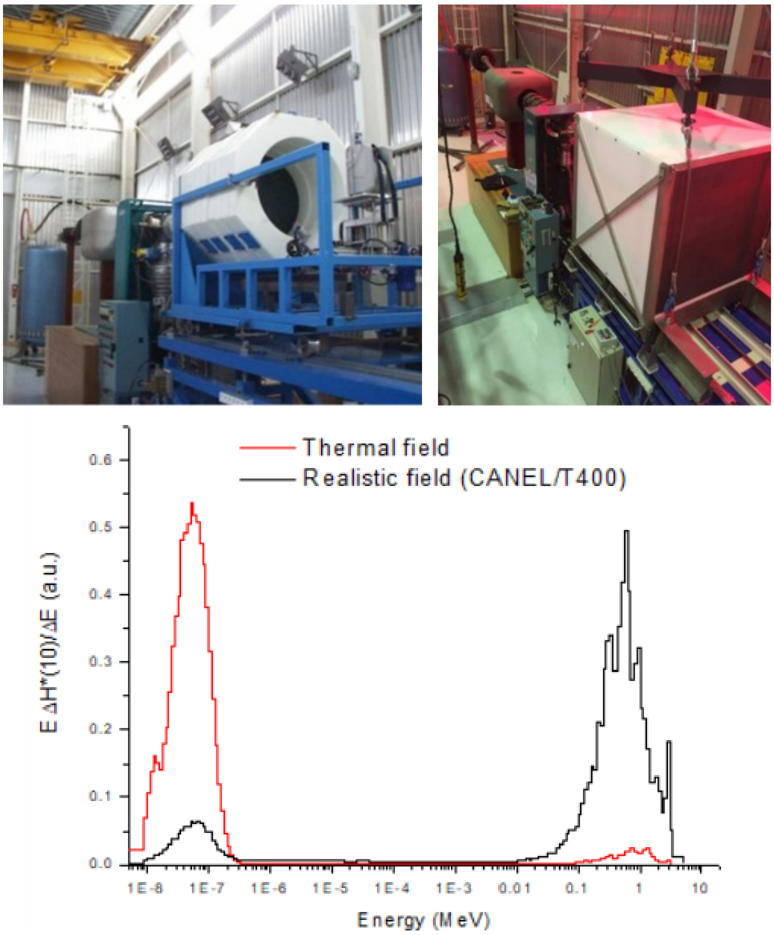

Figure 10. The CANEL (top left) and BLOG (top right) devices and the associated neutron fields (bottom).

1.1.5.3 AMANDE

The AMANDE facility (Accelerator for metrology and neutron applications in external dosimetry), produces reference monoenergetic neutron fields for two purposes: neutron metrology related to fluence and dose equivalent, and testing and calibration of neutron detectors and dosimeters for several specific energies in a large range (between 2 keV and 20 MeV).

Because of its characteristics, and particularly its capacity to deliver monoenergetic neutron fields, the AMANDE facility can be used to study the variation in response of a measuring device (such as a dosimeter, flowmeter, spectrometer, etc.) to different neutron energy levels.

The ion accelerator used at the AMANDE facility is a 2 MV Tandetron^{TM}. It has been specially designed for very low energy dispersion from the ion beam (approximately 500 eV) and very high energy stability (approximately 100 eV). It can be used in continuous or pulsed mode and can produce proton or deuteron beams with energies ranging from 100 keV to 4 MeV (i.e. twice the maximum high voltage). In pulsed mode, neutron time-of-flight measurements can be made.

The neutron flux at 1 m and at 0° is $7 \cdot 10^3$ $cm^{-2} \cdot s^{-1}$, with limitations due to target heating and radiological zoning.

Care has been taken with AMANDE's 400 m² experiment hall. To reduce the amount of neutron scattering polluting the monoenergetic neutron fields, a minimum amount of material has been placed in the experiment hall, and the hall walls have been optimized. The target is 7.2 meters above ground, and the hall has thin metallic walls with which there is little neutron interaction.

An automated system is used for precise, reproducible positioning of the detectors at between 0.5 m and 6 m from the target, within an angular range of –150° to +150° with respect to the ion beam axis.

Finally, the experiment hall is equipped with a temperature and humidity control system, which uses an air curtain around the calibration zone to keep the ambient conditions within the specifications laid down by international standards for radiation protection instrument calibration.

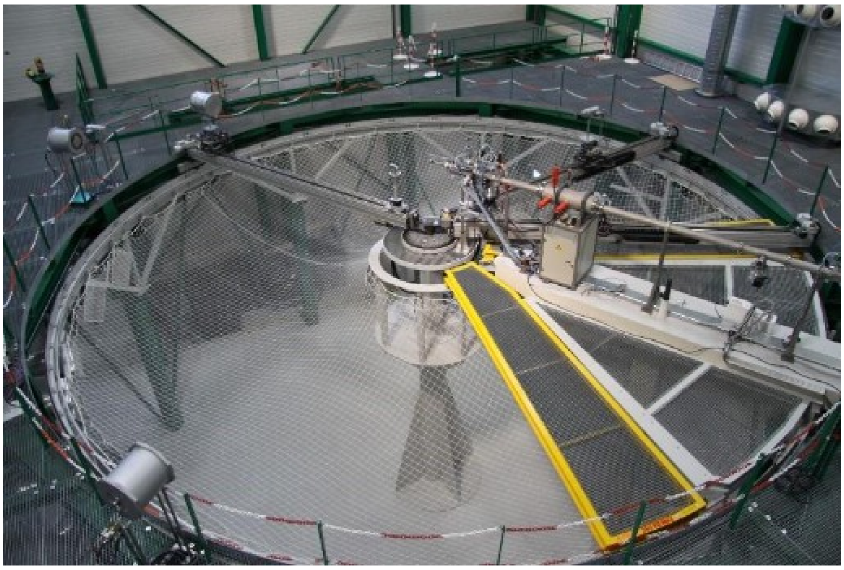

Figure 11. The AMANDE irradiation hall at ASNR.

A 'long counter' detector is used to determine the reference neutron fluence on AMANDE with a relative uncertainty of around 3 %. This detector consists of a cylindrical tube filled with ^{3}He gas placed in a moderator. The detector geometry is optimized to give a constant response throughout the energy range in question (between a few eV and several MeV). So that it is linked to the national reference standards for neutron fluence, the long counter is periodically calibrated to the sources of Van Gogh irradiator.

The fluence where the instrument to be calibrated is situated is always determined using the long counter before calibration takes place. The reference fluence is monitored during instrument calibration by neutron detectors (known as 'monitors') permanently installed in the experiment hall. The dose equivalents are obtained by applying a conversion factor to fluence, given in international standards (ISO, ICRU, ICRP).

1.2 Review and selection of CRNS probes for laboratory characterization

The goal of activity A1.3.2 is to review state-of-the-art CRNS devices currently available on the market and used in existing and emerging CRNS networks, utilizing input from activity A1.1.4 and the project's Stakeholder Committee (A5.1.1). Based on this review, three different types of CRNS devices were selected for detailed modelling and characterization in neutron metrology laboratories.

1.2.1 Detection principle

Several neutron detection technologies are appropriate for soil moisture measurements using cosmic neutrons, each with specific advantages and disadvantages:

1.2.1.1 ^3He and BF_3 proportional counters

Most CRNS probes used for research are based on ^3He or BF_3 proportional counters. These are tubes filled with ^3He or BF_3 gas, with an axial electrode forming an isotropic electric field inside the tube. Incoming neutrons undergo nuclear reactions with the gas nuclei, producing electrically charged particles. These particles ionize the surrounding gas, and the resulting charge—proportional to the deposited energy—is collected by the applied electric field and counted by the read-out electronics. These proportional counters are typically shielded by a layer of high-density polyethylene (HDPE) to suppress incoming thermal neutrons and to moderate epithermal neutrons, thereby enhancing the detection of neutrons in the epithermal to fast energy range relevant for CRNS.

The rapidly decreasing global supply of ^3He has resulted in a tenfold price increase over the last 20 years, prompting the search for alternatives. The BF_3 proportional counter is a common alternative to helium-based neutron detectors for soil moisture monitoring in agricultural and hydrological applications. However, the high toxicity of BF_3 and its relatively high cost (though lower than ^3He) limit its widespread use.

1.2.1.2 Boron-lined proportional counter

This detector, specially designed for CRNS, consists of an aluminium tube filled with a gas mixture of 90 % argon and 10 % CO_2, and a central electrode made of gold-plated tungsten wire. The inner wall of the cylinder is covered with a copper foil coated with a 1.5 µm thin layer of B_4C as a neutron converter. The detector tubes are surrounded by a modular moderator of 25–35 mm thickness and a removable thermal neutron shield made of Gd_2O_3. Additional moderator sheets placed between the base units allow for modular shielding and adjustment of the specific energy response function. When the system is configured such that moderator sheet inlays are placed between rows of counter tubes, information about the neutron spectrum can be retrieved by comparing the count rates of the differently moderated rows, similar to the principle of Bonner sphere spectrometers.

1.2.1.3 Scintillation detectors

In scintillation materials, high-energy charged particles or photons can excite valence electrons to the conduction band. A released electron subsequently recombines with a hole in the valence band, emitting a photon in the UV, visible, or near-IR range. The number of photons produced is proportional to the energy deposited by the primary particle. The emitted light pulses are collected by a photocathode. Electrons emitted from the photocathode are accelerated by an applied high voltage and amplified at the dynodes of an attached photomultiplier tube (PMT), producing an electric pulse proportional to the absorbed energy. By incorporating a neutron converter, scintillation detectors can also be used for neutron detection.

Inorganic scintillators loaded with ^{6}Li are sensitive to thermal neutrons. Using pulse-height discrimination and pulse-shape analysis, neutrons can be distinguished from gamma photons in mixed radiation fields.

Organic liquid scintillators and, more recently, some plastic scintillators can be utilized for fast neutron detection. Neutrons are distinguished from gamma radiation using pulse-shape analysis. Although liquid scintillators have higher scintillation efficiency, their toxicity and chemical and fire hazards limit their use in commercial applications.

1.2.2 Access to technical documentation

Current MC codes allow for the precise and detailed calculation of a neutron instrument's response function. However, their application requires access to detailed technical drawings and the material composition of the CRNS probe. Since the availability of an MC model validated by calibration measurements is highly beneficial for understanding and harmonizing data from different probe types, this criterion must be given special attention.

1.2.3 Size and weight

The relatively low flux of cosmic neutrons requires detectors with high efficiency and/or large volumes. Some systems are designed to be modular, allowing their size to be increased when necessary (e.g., for mobile measurements). However, a review of available neutron calibration facilities shows that most are equipped to calibrate instrumentation that is considerably more compact than the average CRNS probe. Therefore, the experimental validation of neutron response functions for CRNS devices may require the development of new calibration procedures.

1.2.4 Mobile measurements

Most CRNS systems are designed as stationary detectors. However, some can be installed in a vehicle to perform mobile measurements and cover larger areas.

1.2.5 Availability within consortium

The CRNS device types selected for this activity were intended to be provided by the project participants operating them at their test-field sites for laboratory characterization. However, this was not feasible. Consequently, device manufacturers were approached, and the devices characterized in this activity were either purchased or borrowed specifically for the project. This situation significantly impacted the laboratory measurement campaigns: the devices arrived later than planned, and subsequent measurements had to be postponed due to scheduling conflicts with other activities in the neutron metrology laboratories. These two factors are the primary reasons for the delay in this deliverable.

1.3 Examples of commercial CRNS systems

CRS-1000

Producer	Hydroinnova LLC
Country	USA
Detector	- Bare ^{3}He proportional counter - Polyethylene-moderated ^{3}He proportional counter
Count rate	~1000 counts per hour (cph)
Size	80 cm height
Weight	15 kg
Installation	Static / Mobile
Other sensors	GPS, time, temperature, humidity, air pressure
Data transmission	GSM, Iridium satellite

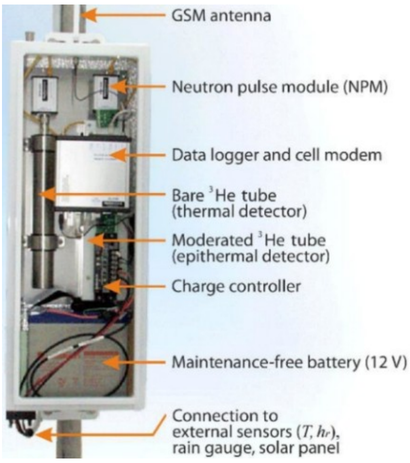

The CRS-1000 system consists of a bare and a moderated ^{3}He neutron detector, two advanced neutron pulse detecting modules (NPMs), and a data logger with integrated telemetry, including barometric pressure, humidity, and temperature sensors. Its data logger also supports common external sensors, such as capacitance probes, water content reflectometers, tipping bucket rain gauges, and additional sensors commonly used in environmental measurements. Data received via a remote data link can be displayed and plotted in near real-time on a password-protected web page and can also be accessed directly from a MySQL database.

Website: https://hydroinnova.com/ps_soil.html

Finapp 3

Producer	Finapp S.r.l.
Country	Italy
Detectors	- Inorganic scintillator EJ-420/426 (^{6}Li dispersed in ZnS(Ag)) - Plastic scintillator (EJ-299-33A) with Pulse-Shape Discrimination (PSD)
Count rate	~1000 cph
Size	40 x 30 x 20 cm
Weight	5 kg
Installation	Static / Mobile (Finapp 5 model)
Other sensors	GPS, time, temperature, humidity, air pressure
Data transmission	GSM

The Finapp 3 is a lightweight, compact detector constructed from plastic and metallic materials. Its two different scintillator types allow for the differentiation of thermal, epithermal, and fast neutron spectrum components, which is critical for soil moisture measurements. The system features a modular design for customization and enables real-time measurements. Its compact size makes it suitable for mobile applications, such as detecting water leaks along aqueducts pipes.

Website: https://www.finapptech.com/en/why-finapp

System S1

Producer	StyX Neutronica GmbH
Country	Germany
Detector	^{10}B-lined proportional counter with gadolinium thermal neutron shielding
Count rate	~1000 cph
Size	Ø20 x 150 cm height
Weight	15-60 kg
Installation	Static / Mobile (upon request)
Other sensors	GPS, time, temperature, humidity, air pressure
Data transmission	Wifi, GSM

The System S1 consists of a solid ^{10}B-lined proportional counter filled with an $Ar:CO_2$ gas mixture and a gadolinium coating to improve the signal-to-noise ratio for soil moisture measurements. It includes proprietary detector electronics and a data logger with integrated telemetry (barometric pressure, humidity, temperature). An SDI-12 interface supports a variety of user-specific environmental sensors. Data from large networks can be collected, visualized, and accessed via a web interface in real-time.

Website: https://www.styx-neutronica.de

Radetech RDT

Producer	Radiation Detection Technologies, Inc.
Country	United States
Detector	Lithium Foil Multiwire Proportional Counter (MWPC)
Count rate	~1500 cph
Size	60 x 25 x 15 cm
Weight	5 kg
Installation	Static / Mobile (upon request)
Other sensors	GPS, time, temperature, humidity, air pressure
Data transmission	GSM

This system utilizes a new and affordable technology for soil moisture monitoring, employing a cosmic-ray neutron sensor with high neutron sensitivity and a large sensing area.

Website: https://radectech.com/

1.4 Distribution of the instruments for calibration and modelling

Following the review of commercially available CRNS devices, three primary probes and one backup device were selected:

- Hydroinnova CRS-1000
- StyX Neutronica System S1
- Finapp 3
- Hydroinnova CRS-2000/B

The selection was based on the following criteria:

- Detection principle and construction
- Availability within the SoMMet consortium
- Access to technical documentation
- Field usage and availability of historical data

The information on probe construction and material composition was used to prepare MC models and to distribute the different CRNS probes to various project partners for measurement. A summary of the capabilities of the available neutron calibration facilities, in relation to the requirements of the CRNS probes, led to the following conclusions:

- Most facilities are equipped to calibrate relatively compact instrumentation (size < 50 cm, weight < 50 kg), and some CRNS probes exceed these limits.
- CRNS probes are designed to operate at very low neutron fluence rates—approximately three orders of magnitude lower than the neutron fields typically used for standard neutron instrumentation. Calibration facilities must therefore be capable of providing reference fields with correspondingly low emission rates.

The specific construction of the CRNS probes (e.g., long, heavy cylinders) may require adaptations to standard calibration techniques, such as the use of custom shadow cones. Considering these limitations and the availability of the different laboratories, the selected probes were distributed for characterization as follows:

- Finapp 3 (Finapp)
  - **CMI:** MC (Monte Carlo) modelling; measurement in broad-range neutron fields.
  - **SMU:** MC modelling; measurement in broad-range neutron fields.
  - **PTB:** Measurement in broad-range and monoenergetic neutron fields.
- CRS-1000 (Hydroinnova)
  - **PTB:** MC modelling.
  - **PTB:** Measurement in broad-range and monoenergetic neutron fields.
- System S1 (StyX Neutronica)
  - **PTB:** MC modelling.
  - **PTB:** Measurement in broad-range and monoenergetic neutron fields.
- CRS-2000/B (Hydroinnova)
  - **CIEMAT:** MC modelling.
  - **CIEMAT:** Measurement in broad-range neutron fields.
  - **PTB:** Measurement in monoenergetic neutron fields.

2 Traceability scheme

2.1 Traceability of soil water content

Although this report deals specifically with the traceability of the neutron signal from CRNS probes under laboratory conditions, it is necessary to address the overarching goal: obtaining traceable information on volumetric water content at the field scale. CRNS devices are designed to measure the total neutron flux in the epithermal energy range as a proxy quantity. The primary measurement is not an absolute neutron flux value, but rather the relative change in neutron flux induced by a change in volumetric water content. Influences on the signal from factors such as biomass, lattice water, temperature, air pressure variation, solar activity, air humidity, and the incoming neutron flux and spectrum must be considered within the traceability chain.

To amend these influences on the soil moisture signal, adjustments for the aforesaid factors must be implemented. It is therefore crucial to differentiate between the direct measurement –a relative neutron signal within a specific part of the epithermal neutron energy spectrum– and the derived information, which is the field-scale soil water content. A suggested traceability scheme that combines the traceability of the neutron signal with that of the soil water content is shown in Figure 12.

The primary standard for traceability would be the volumetric water content in the desired support volume (specifically, the amount of unbound water). This support volume could be defined, for example, within a radius of 178.4 m and a depth of 0.20 m.

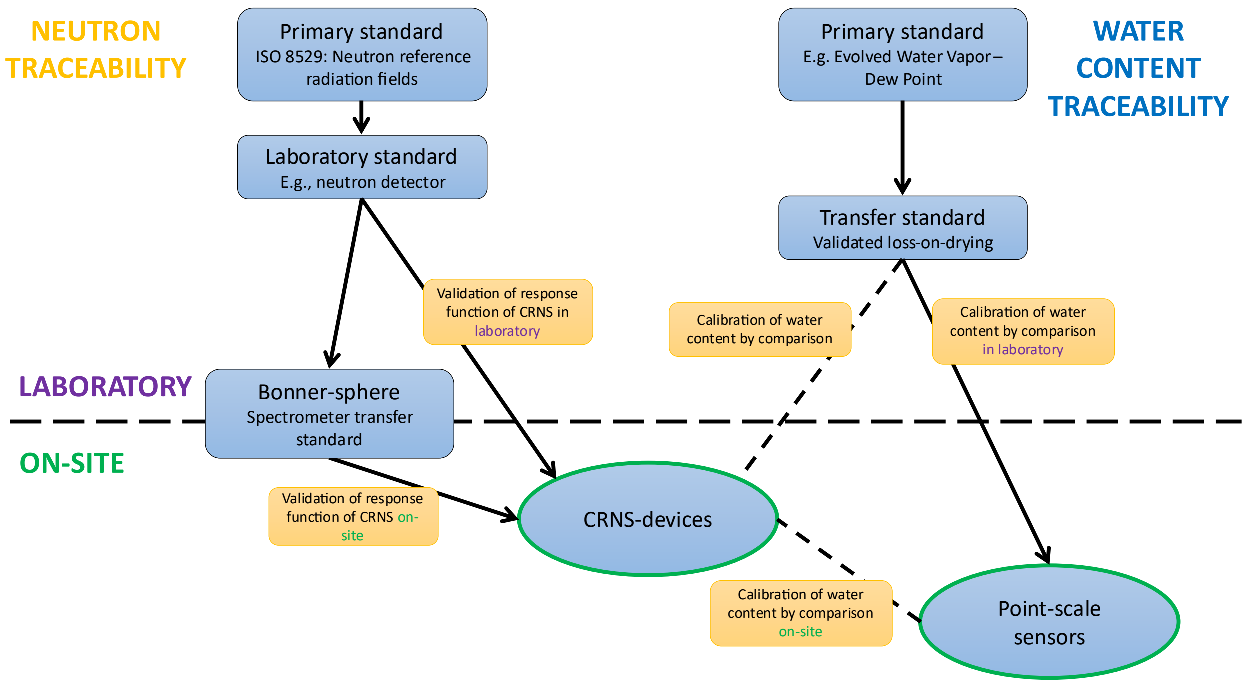

Figure 12. Traceability scheme for CRNS devices developed within the SoMMet project, showing how metrological traceability is achieved for both neutron counts and soil water content.

This report focuses on the neutron traceability branch under laboratory conditions, specifically on the validation of CRNS MC models and their corresponding response functions (e.g., energy, directional).

2.2 Traceability of the relative epithermal neutron flux as the underlying measurand

CRNS measures an underlying physical quantity —often termed the "signal"— to infer volumetric water content. This measurement integrates over a specific support volume with a characteristic shape and an inherent, spatially inhomogeneous sensitivity. For CRNS, this volume is approximately a circular area with a radius of several hundred meters and a depth of several decimetres in the soil, with its precise shape modulated by factors such as biomass, terrain, and air humidity.

CRNS devices are designed to measure the total neutron flux in the epithermal energy range. The primary measurand is not the absolute neutron flux, but the relative change in this flux induced by a change in volumetric water content. The neutron count rate used to calculate volumetric water content is not the raw, natural neutron flux. It is a corrected value, normalized for variations in air pressure, air humidity, and the incoming neutron flux—a theoretical quantity derived from these corrections. A non-uniform sensitivity across different energies within the epithermal range is not necessarily a disadvantage and can be incorporated into an individual CRNS probe's specific calibration. However, this energy-dependent weighting must remain stable over time and be independent of changes in volumetric water content. Conversely, any significant contribution to the signal from outside the target epithermal range (e.g., from thermal neutrons) constitutes a source of inaccuracy.

Therefore, a thorough investigation using neutron reference fields is required to characterize a CRNS probe's response to a given neutron energy spectrum. This investigation was conducted within Task 1.3 as a laboratory-based calibration of the most common CRNS probe types. In parallel, MC models of the selected probes were developed and validated using these calibration data (see Section 3 of this report).

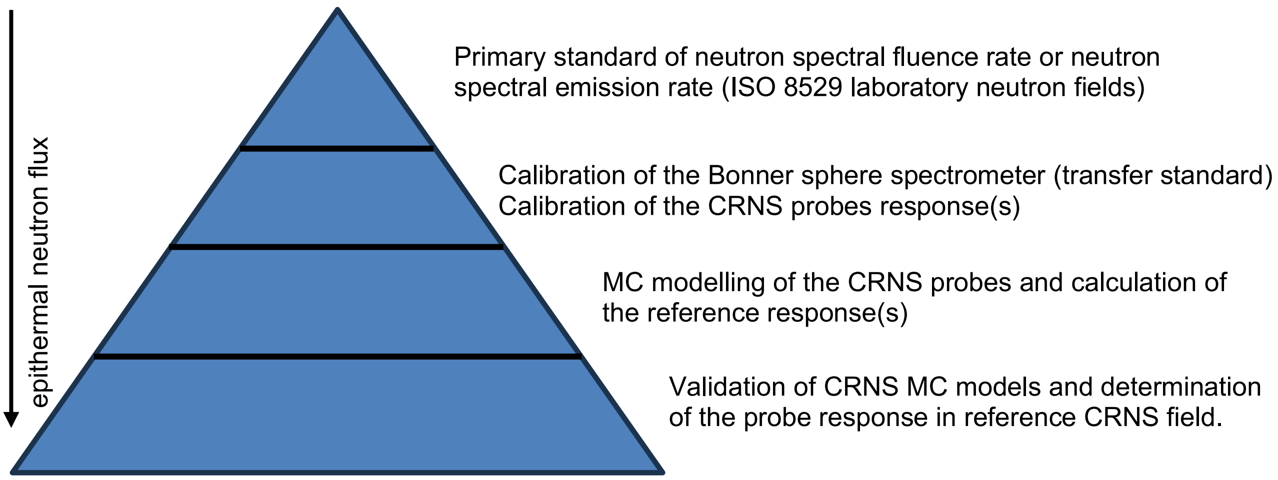

Figure 13. Traceability pyramid of the neutron signal, showing the dissemination from standard neutron fields in the laboratory to CRNS devices installed in the field.

The aim is for the individual signal changes from each CRNS probe in the field to be traceable to a change in a specific part of the epithermal neutron energy spectrum.

Several open questions remain regarding the traceability chain for changes in the weighted epithermal neutron flux.

The first question is how to address the difference between the natural neutron flux and a technical neutron flux. The natural neutron flux requires corrections for air pressure, incoming neutron flux, and absolute air humidity to isolate changes due to soil moisture. This is not an issue for a purely technical neutron flux generated in a laboratory.

A second question concerns the fact that CRNS devices do not need to determine the absolute value of the neutron flux they receive, but only a consistent fraction of it. Furthermore, these devices do not need to measure the full epithermal neutron spectrum and can have an implicit, non-uniform sensitivity to different energies within the epithermal range.

Finally, it is an open question whether the intrinsic background signal of the CRNS probes and Bonner spheres needs to be determined. Such a determination could be critical because the relevant changes in the CRNS signal are partially concealed by the probe's own background.

These questions will be addressed in the next phase of the SoMMet project. The validated MC models of the selected CRNS probes summarized in this report will be instrumental in answering them.

3 Validation of MC models and assessment of uncertainties

This work was planned in several sequential steps, contingent upon the availability of instrumentation, information, and calibration facilities:

- Preparation of the MC model using the available information on material composition, technical specifications, and detection principle.
- Measurement in reference fields, including broad range, monoenergetic, open, and shielded configurations.
- Adaptation of the MC model to the measurement geometry. The large size and unique energy response of CRNS devices, which differ significantly from standard neutron radiation instrumentation, required the adaptation of standard neutron calibration techniques.
- Validation of the MC model, including an estimation of the model uncertainty.

The procedure described above was applied to each selected CRNS instrument and is summarized in the following subchapters.

3.1 Finapp - Model 3

The Finapp detector is a compact system designed for thermal neutron detection with low sensitivity to gamma radiation. It consists of a layered structure of sheets sensitive to thermal neutrons and wavelength shifters (WLS) to collect light via a photomultiplier tube (PMT). The thermal neutron-sensitive sheets comprise a homogeneous matrix of fine lithium fluoride and zinc sulphide phosphor (ZnS:Ag) particles compactly dispersed in a colourless silicon binder. The lithium is enriched in ^{6}Li

to >95 %. The detector assembly is wrapped in a 15 mm thick HDPE cover to enhance the sensitivity to epithermal neutrons.

The neutron detection mechanism is based on the nuclear reaction $^{6}Li(n,\alpha)^{3}H$:

$$^{6}Li + {}^{1}n \rightarrow {}^{3}H + {}^{4}He + 4.78\ MeV$$

This reaction has a cross-section of 941 barn for thermal neutrons (0.025 eV). The resulting triton and alpha particles excite the ZnS:Ag phosphor, producing a broad blue-fluorescent spectrum with a prompt scintillation decay time of 200 ns.

The ZnS:Ag scintillator is also sensitive to muons and electrons. Discrimination between neutrons and muons is performed using a Pulse Shape Discrimination (PSD) algorithm covered by a Finapp patent. The detector is read out using a head-on PMT.

The detector is available in four hardware models differing in scintillator dimensions. Model 3 was selected for characterization because it is the smallest and least sensitive model, making it suitable for characterization in neutron metrology laboratories, which utilize relatively intense reference fields.

The neutron detector, data logger unit, and weather sensors are housed in an IP67-rated enclosure for outdoor use. Data telemetry is accomplished via a low-power GSM modem, with local backup storage on an SD card (e.g., during reference irradiations where GSM signal may be unavailable).

Measured data are transmitted via GSM to Finapp servers at preset intervals and processed using the proprietary PSD algorithm. Users can access the data through a web interface or a customizable API service for further processing.

To cross-check the results and enhance the validation's credibility, the Finapp 3 probe was characterized independently by CMI and SMU in broad-spectrum neutron reference fields.

3.1.1 MC model (CMI)

An input file for the MCNP particle transport code was prepared based on information from the manufacturer regarding the detector's dimensions and composition. The model was subsequently cross-checked against physical measurements performed by CMI on the provided detector sample.

The main components of the model are summarized below and depicted in detail in Figure 14:

1. **High-density polyethylene (HDPE):** CH_2; density 0.97 g/cm³.
2. **“Very light plastic polymer”:** Approximated by PVC (C_2H_3Cl); density 0.007 g/cm³.
3. **EJ-426 Thermal neutron detector:** A mixture of LiF and ZnS in a 1:3 ratio; density 1.544 g/cm³. The lithium is enriched in ^{6}Li to >95 %, with a ^{6}Li density of 8.81×10^{21} atoms/cm³. The support layer is polyester (PET, Mylar) with a density of 1.40 g/cm³.
4. **EJ-280 wavelength shifter:** Polyvinyltoluene; density 1.023 g/cm³.
5. **Outer box:** Approximated by PVC (C_2H_3Cl); density 1.406 g/cm³.
6. **Aluminium alloy:** EN-AW-5083, according to the supplier's material data sheet; density 2.66 g/cm³.

7. **Battery lead:** Approximated by a custom material ("literina"); density 3.05 g/cm³, calculated from the battery's total weight (2168 g, including polypropylene casing) and the estimated lead volume (678 cm³).

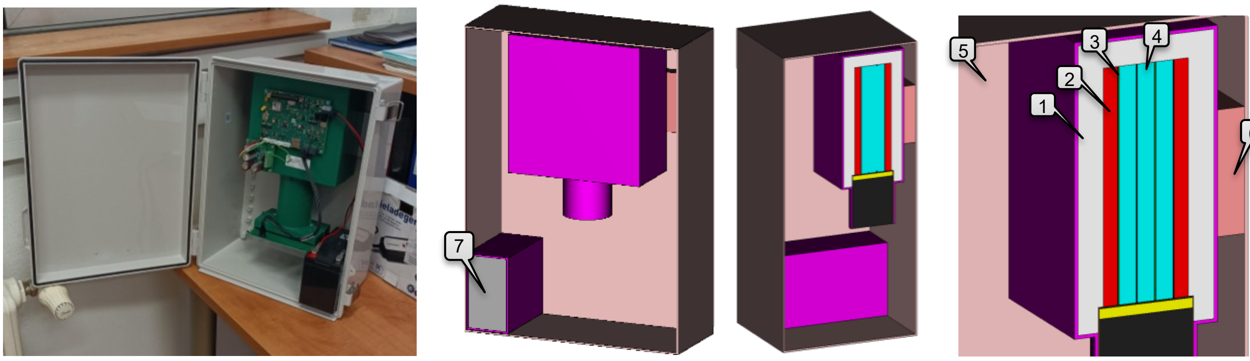

Figure 14. Photograph of the Finapp 3 detector and its corresponding MCNP model prepared by CMI.

The calculations were performed using the MCNP6.3 neutron transport code with the ENDF/B-VIII.0 data library at a temperature of 296 K, which includes the S(α,β) treatment for low-energy neutrons.

3.1.1.1 Simulated quantities in the first MC model

The following quantities were simulated in the initial model:

- Number of ^{6}Li(n,α)T interactions and neutron absorption (per sheet and total).
- Neutron fluence at the detector position in the absence of the detector.

An initial comparison of the calculations with the measured neutron response in ^{252}Cf and ^{241}Am-Be broad-spectrum neutron fields revealed a discrepancy of more than 50 %, varying with the neutron spectrum. Numerous calculations were performed, varying key MC model parameters such as:

- HDPE moderator density (1)
- Light plastic density (2)
- Scintillator density (3)
- Wavelength shifter density (4)

It was found (see Figure 15) that modifying these model parameters, even to unrealistic values, did not significantly influence the relative results, as each model version required its own weighting factor.

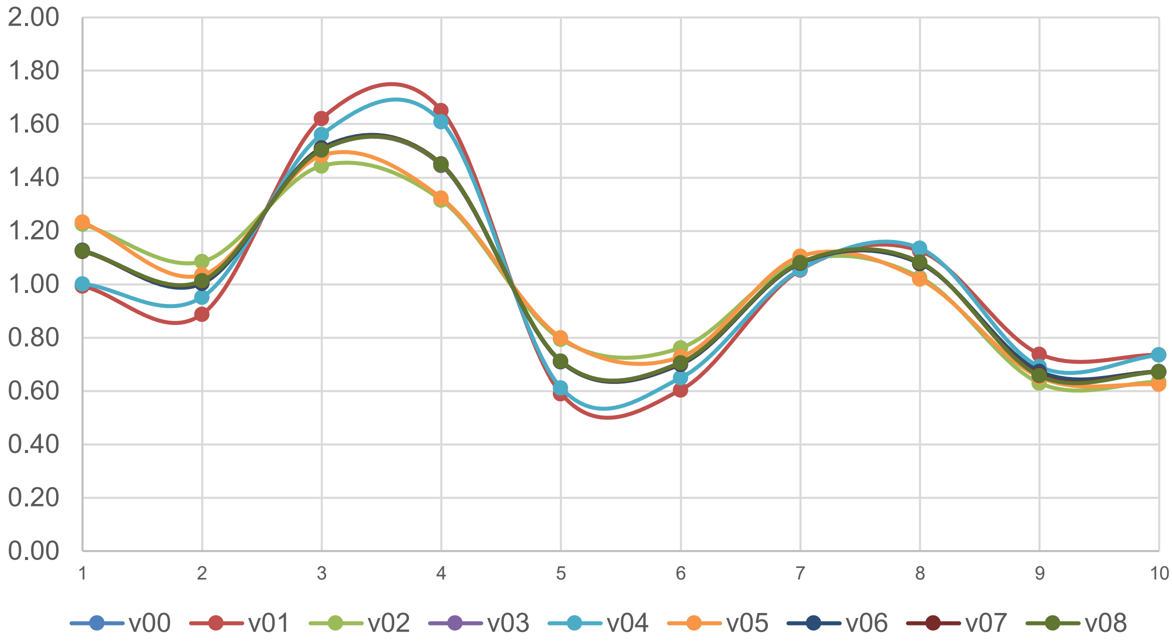

Figure 15. Relative comparison of the MC calculation output and measurements for 10 different irradiation geometries and neutron spectra, across 9 MC models with different parameters.

Several factors could explain this discrepancy, including a non-optimal CMI shadow cone for the instrument's cubic shape, and the unknown energy and angular dependence of the light collection efficiency and the neutron signal PSD selection algorithm. To minimize some sources of discrepancy, the MC model was enhanced to include the full irradiation room (see Figure 16). This model includes the Finapp 3 detector and the neutron source with its measured characteristics (emission rate and angular anisotropy).

3.1.1.2 Simulated quantities for the final model including full irradiation room

The final, enhanced model simulated the following quantities:

- Number of ^{6}Li(n,α)T interactions and neutron absorption (per sheet and total).
- Proton recoil counts in the scintillator; alpha- and triton counts in the scintillator (all sheets).
- Neutron fluence at the detector position for all irradiation geometries in the absence of the detector.
- Neutron spectra at the detector position and the contribution of individual model cells to this spectrum, in the absence of the detector.

A comparison of the calculations from this enhanced model with the measured neutron responses, along with a discussion of the results, is provided in Section 3.1.2.

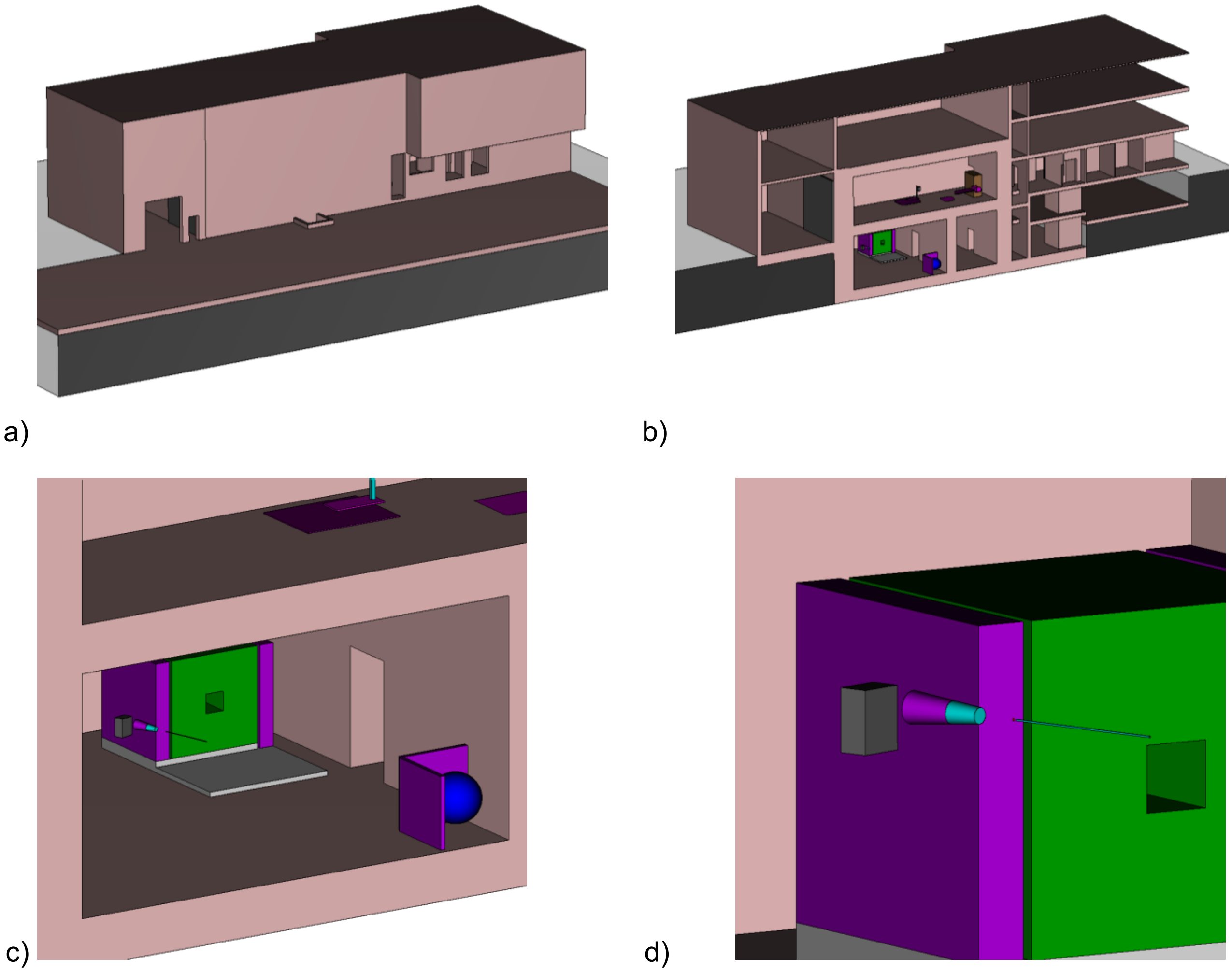

Figure 16. MCNP model of the entire CMI building (a, b) with the underground neutron irradiation room (c, d).

3.1.2 Measurements in the neutron reference fields (CMI)

Under standard field operation, data from the Finapp detector are transmitted via GSM to Finapp servers at one-hour intervals and processed using the proprietary PSD algorithm. The user can then access the data through a web interface or a customizable API service. A sample of the standard data output is shown in Figure 17.

```
#Datetime;neutrons;muons;gamma;integration_time(s);V_in(Volt);temperature_in(°C);temperature_ext(°C);ur(%);pressure(hPa)
2023-09-04 14:00:00;885;3349;0;122;12.1;26.3;0.0;0.0;995.9
2023-09-04 15:00:00;946;3127;0;3581;12.1;27.7;0.0;0.0;995.9
2023-09-04 16:00:00;861;3168;0;3588;12.2;28.2;0.0;0.0;995.4
2023-09-04 17:00:00;900;3312;0;3585;12.1;28.4;0.0;0.0;995.0
2023-09-04 18:00:00;929;3343;0;3587;12.2;28.4;0.0;0.0;994.8
2023-09-04 19:00:00;948;3170;0;3588;12.2;28.4;0.0;0.0;995.0
2023-09-04 20:00:00;964;3227;0;3588;12.2;28.3;0.0;0.0;994.9
2023-09-04 21:00:00;906;3225;0;3588;12.2;28.2;0.0;0.0;995.2
2023-09-04 22:00:00;933;3333;0;3589;12.1;28.0;0.0;0.0;995.4
2023-09-04 23:00:00;935;3418;0;3588;12.1;27.9;0.0;0.0;995.5
2023-09-05 00:00:00;891;3223;0;3590;12.1;27.8;0.0;0.0;995.5
2023-09-05 01:00:00;960;3192;0;3588;12.1;27.7;0.0;0.0;995.4
2023-09-05 02:00:00;941;3181;0;3591;12.1;27.6;0.0;0.0;995.2
2023-09-05 03:00:00;934;3265;0;3589;12.1;27.5;0.0;0.0;995.0
2023-09-05 04:00:00;963;3262;0;3590;12.1;27.4;0.0;0.0;994.6
```

Figure 17. Standard API output (https://www.finapptech.com/finapp/api/getCSV_id.php?ID=120&D=1).

The standard one-hour interval is unsuitable for laboratory testing. Therefore, the API output was customized by Finapp engineers to provide data at five-minute intervals. As the tested instrument was not equipped with a gamma detector or external sensors, these data fields were removed. The number of registered triggers and high-voltage (HV) stability monitoring were added to the modified output (see Figure 18).

```
timestamp[UTC+2];neutrons_count;muons_count;trigger_number;integration_time[s];temperature;HighVoltage[V];Battery[V]
2023-10-03 07:03:27;81;295;546;303;27.17;682.5;12.29
2023-10-03 07:08:28;91;274;588;302;27.17;682.5;12.27
2023-10-03 07:13:31;102;237;571;302;27.17;682.5;12.27
2023-10-03 07:18:33;90;283;604;302;27.15;682.5;12.28
2023-10-03 07:23:36;74;313;582;303;27.13;682.5;12.24
2023-10-03 07:28:39;117;237;603;303;27.14;682.5;12.27
2023-10-03 07:33:41;100;285;616;302;27.13;682.5;12.29
2023-10-03 07:38:43;94;260;597;302;27.12;682.5;12.27
2023-10-03 07:43:54;105;238;584;303;27.12;682.5;12.27
2023-10-03 07:48:56;79;288;600;311;27.1;682.5;12.31
2023-10-03 07:53:59;92;251;580;302;27.1;682.5;12.29
2023-10-03 07:59:01;98;282;609;302;27.09;682.5;12.22
2023-10-03 08:04:04;97;274;569;303;27.09;682.5;12.23
2023-10-03 08:09:06;92;249;600;302;27.08;682.5;12.27
```

Figure 18. Modified API output (https://finapptech.com/finapp/api/detectordata/index.php?id=158).

Since GSM signals are typically unavailable in neutron calibration laboratories due to thick concrete shielding, data were stored asynchronously on the internal SD card during irradiations and uploaded to the Finapp servers afterward. Consequently, the processed data were available for validation with a delay of a few hours.

As identified during the project's background research phase, a major challenge is the disparity in neutron fluence rates: CRNS probes are designed for environmental fluxes on the order of 10^{-2} cm^{-2} s^{-1}, while neutron metrology laboratories typically operate with fluxes between 10^{2} cm^{-2} s^{-1} and 10^{4} cm^{-2} s^{-1}. Therefore, it was not feasible to use the 14 MeV neutron generator or the thermal reference field for these irradiations. Only the two weakest available neutron sources (^{241}Am-Be and ^{252}Cf) could be used. To adjust the MC model output, several different irradiation conditions were required, which were established as detailed in Table 3.

Table 3. Irradiation geometries/setups used for MC model adjustment.

Irradiation number	Source	Neutron spectrum	Irradiation geometry	Distance (cm)
1	^{241}Am-Be	direct + scattered	front	100 cm
2	^{241}Am-Be	direct + scattered	front	150 cm
3	^{241}Am-Be	direct + scattered	front	200 cm
4	^{241}Am-Be	direct + scattered	front	250 cm
5	^{241}Am-Be	direct + scattered	side	100 cm
6	^{241}Am-Be	direct + scattered	side	150 cm
7	^{241}Am-Be	direct + scattered	side	200 cm
8	^{241}Am-Be	direct + scattered	side	250 cm
9	^{241}Am-Be	scattered	front	100 cm
10	^{241}Am-Be	scattered	front	150 cm
11	^{241}Am-Be	scattered	front	200 cm
12	^{241}Am-Be	scattered	front	250 cm
13	^{241}Am-Be	scattered	side	100 cm
14	^{241}Am-Be	scattered	side	150 cm
15	^{241}Am-Be	scattered	side	200 cm
16	^{241}Am-Be	scattered	side	250 cm
17	^{252}Cf	direct + scattered	front	100 cm
18	^{252}Cf	direct + scattered	front	150 cm
19	^{252}Cf	direct + scattered	front	200 cm
20	^{252}Cf	direct + scattered	front	250 cm
21	^{252}Cf	direct + scattered	side	100 cm
22	^{252}Cf	direct + scattered	side	150 cm
23	^{252}Cf	direct + scattered	side	200 cm
24	^{252}Cf	direct + scattered	side	250 cm
25	^{252}Cf	scattered	front	100 cm
26	^{252}Cf	scattered	front	150 cm
27	^{252}Cf	scattered	front	200 cm
28	^{252}Cf	scattered	front	250 cm
29	^{252}Cf	scattered	side	100 cm
30	^{252}Cf	scattered	side	150 cm
31	^{252}Cf	scattered	side	200 cm
32	^{252}Cf	scattered	side	250 cm
33-57	^{241}Am-Be	direct + scattered	rotation 15 deg step	100 cm
58-84	^{252}Cf	direct + scattered	rotation 15 deg step	200 cm

A total of 84 irradiations, combining different neutron sources, irradiation distances, and geometries, were performed to obtain the device's response in spectrally and directionally diverse broad-spectrum neutron reference fields, as detailed below:

^{241}Am-Be source (CMI no. 06)

- Type: AMN.30
- Capsule type: X.21, Ø7.8 mm × 15 mm
- Emission rate: 6.767×10^{4} s^{-1} ± 0.96 % (*k* = 1) to 19.9.2023
- Emission anisotropy @ 90 deg: 1.017 ± 0.67 % (*k* = 1)
- Fluence rate @ 110 cm:
  - Direct neutrons: 0.4479 cm^{-2} s^{-1} ± 1.2 % (*k* = 1)
  - Direct + scattered neutrons: 0.604 cm^{-2} s^{-1} ± 3.2 % (*k* = 1) (BS spectrometer)

^{252}Cf source (CMI no. 02)

- Type: NC252M11
- Capsule type: spherical head, Ø7 mm × 15 mm
- Emission rate: 6.231×10^{4} s^{-1} ± 1.30 % (*k* = 1) to 19.9.2023
- Emission anisotropy @ 90 deg: 1.02 ± 1.00 % (*k* = 1)
- Fluence rate @ 110 cm:
  - Direct neutrons: 0.4170 cm^{-2} s^{-1} ± 1.7 % (*k* = 1)
  - Direct + scattered neutrons: 0.590 cm^{-2} s^{-1} ± 3.3 % (*k* = 1) (BS spectrometer)

CMI shadow cone

- Front diameter: 10 cm
- Length: 50 cm (20 cm Iron, 30 cm HDPE)
- Back diameter: 20 cm

Finapp 3 geometry

- Distance: Measured from the source centre to the detector sensitive volume centre.
- Front geometry: See Figure 19.
- Side geometry: Rotated 90 deg clockwise around vertical axis.

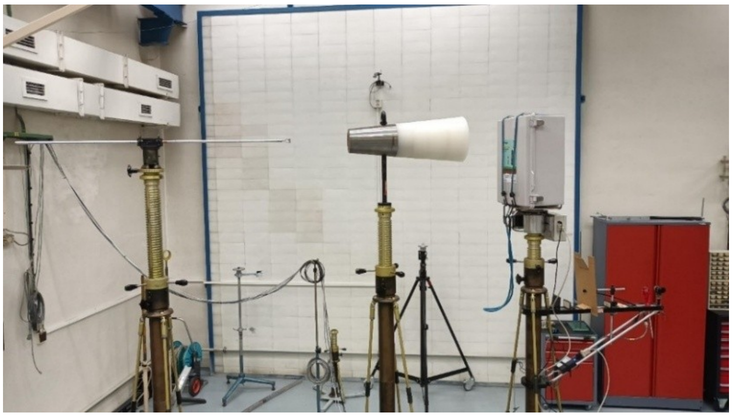
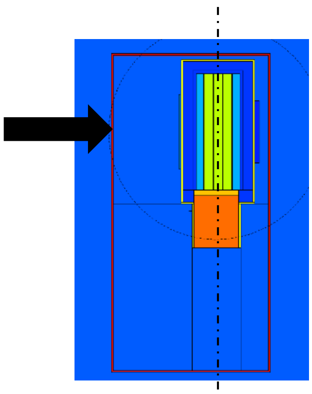

Figure 19. Photograph of irradiation setup no. 25 (^{252}Cf source, shadow cone, front irradiation, distance of 100 cm) (left). Detail of the irradiation geometry with an arrow indicating the direction of irradiation and the vertical rotation axis (right).

The irradiations described above were used for the absolute adjustment of the MC model predictions, as described in more detail in the following section. Additional irradiations were performed to obtain an independent dataset for verifying the adjusted MC model. These included irradiations with the same sources at different distances, a ^{252}Cf source moderated by a 3-inch polyethylene sphere (see Table 4), and measurements in the monoenergetic neutron fields at the PTB PIAF facility (see

Table **5**).

Table 4. Irradiation geometries/setups used for MC model validation at CMI.

Irradiation number	Source	Neutron spectrum	Irradiation geometry	Distance (cm)
85	^{241}Am-Be	direct + scattered	front	110 cm
86	^{241}Am-Be	direct + scattered	side	110 cm
87	^{241}Am-Be	scattered	front	110 cm
88	^{241}Am-Be	scattered	side	110 cm
89	^{252}Cf	direct + scattered	front	110 cm
90	^{252}Cf	direct + scattered	side	110 cm
91	^{252}Cf	scattered	front	110 cm
92	^{252}Cf	scattered	side	110 cm
93	^{252}Cf + 3“PE	direct + scattered	side	95 cm
94	^{252}Cf + 3“PE	scattered	side	95 cm

Table 5. Irradiation geometries/setups used for MC model validation at the PIAF facility of PTB.

Irradiation number	Neutron field	Neutron spectrum	Irradiation geometry	Distance (cm)
95	1.2 MeV	direct + scattered	front	653 cm
96	1.2 MeV	direct + scattered	side	653 cm
97	1.2 MeV	scattered	front	653 cm
98	1.2 MeV	scattered	side	653 cm
99	150 keV	direct + scattered	front	653 cm
100	150 keV	direct + scattered	side	653 cm
101	150 keV	scattered	front	653 cm
102	150 keV	scattered	side	653 cm
103	24 keV	direct + scattered	front	458 cm
104	24 keV	direct + scattered	side	458 cm
105	24 keV	scattered	front	458 cm
106	24 keV	scattered	side	458 cm

3.1.3 Validation of MC model (CMI)

The validation of the two Finapp 3 models, prepared independently by CMI and SMU, was conducted in two steps. First, the MC adjustment coefficient was determined using reference irradiation data. Then, this adjusted model was used to calculate the response under different conditions.

The data from the irradiations summarized in Table 3 were used for the MC model adjustment. As the Finapp 3 data were recorded asynchronously to the irradiation times, only data points where the device was exposed for an entire 5-minute measurement interval were selected. The neutron signal counts from these selected data points were summed, and the statistical uncertainty was determined from the total count. The average neutron count rate during the stable irradiation period was calculated from the recorded measurement time and normalized to the emission rate of the neutron source used.

The same geometry was simulated using the enhanced model described in Figure 16. The simulation output is the number of neutrons absorbed in all four sensitive sheets (layer 3 on Figure 14) per unit volume and per source neutron. This value was multiplied by the total sensitive volume ($4 \times 6.272\ cm^3 = 25.088\ cm^3$) to enable a direct comparison with the emission-rate-normalized detector response.

For each irradiation geometry, the dimensionless Monte Carlo-to-measurement ratio, S_0 was calculated as:

$$S_0 = \frac{M}{R/B}$$

where:

- M is the MC-calculated neutron absorptions in the scintillator sheets (multiplied by the sheet volume) per source neutron,
- R is the detector neutron count rate [cps],
- B is the neutron emission rate [s^{-1}].

The mean value, $\bar{S}$, of the 84 S_0 values from the reference irradiations was calculated, and the standard deviation was used to estimate its uncertainty:

$$\bar{S} = 1.47 \pm 10\ \%$$

This result indicates that the MC model predicts 47 % more events than were measured. This discrepancy is likely because the MCNP calculation does not account for all inefficiencies in the detection chain (e.g., light collection efficiency, neutron selection algorithm), meaning the actual instrument sensitivity is lower than theoretically expected.

The value $\bar{S}$ is used hereafter as the MC model scaling factor. The formula for the Monte Carlo-to-measurement ratio can thus be rewritten as:

$$S = \frac{M/\bar{S}}{R/B}$$

The MC-to-measurement ratios for the adjustment measurements are plotted in Figure 20, Figure 21 and Figure 22. The error bars displayed include the following components:

- Combined uncertainty of the emission rate *B*: ~1 %
- Statistical uncertainty of MC calculation: ~0.5 %
- Estimated systematic uncertainty of the MC model: 5 %
- Uncertainty of the MC-to-measurement scaling factor: 10 %

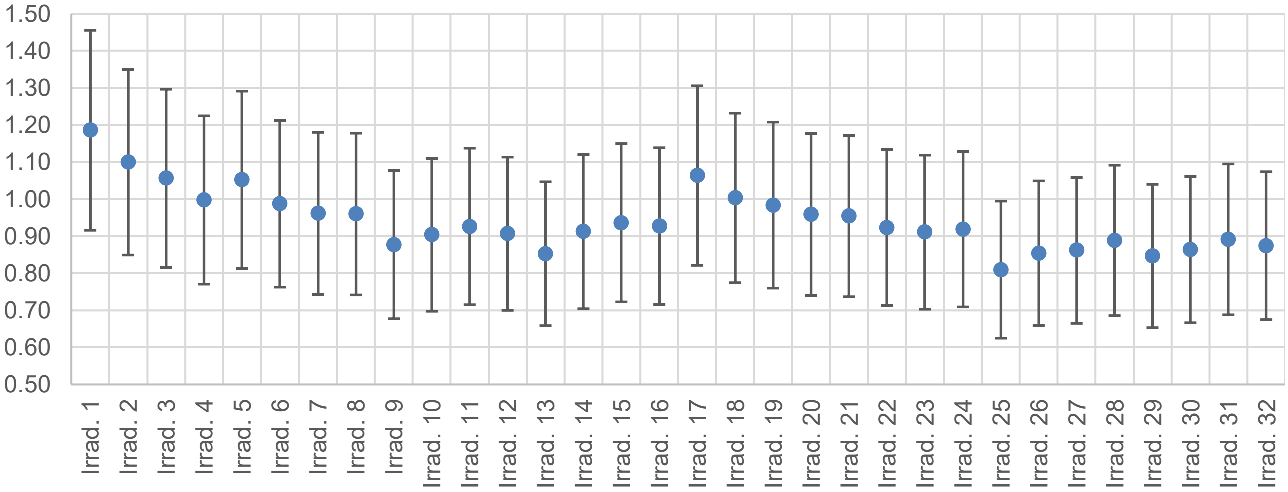

Figure 20. MC-to-measurement ratio for irradiation setups no. 1-32 (various sources, distances, and geometries; see Table 3). Error bars correspond to k = 2 (~95 % coverage for a normal distribution).

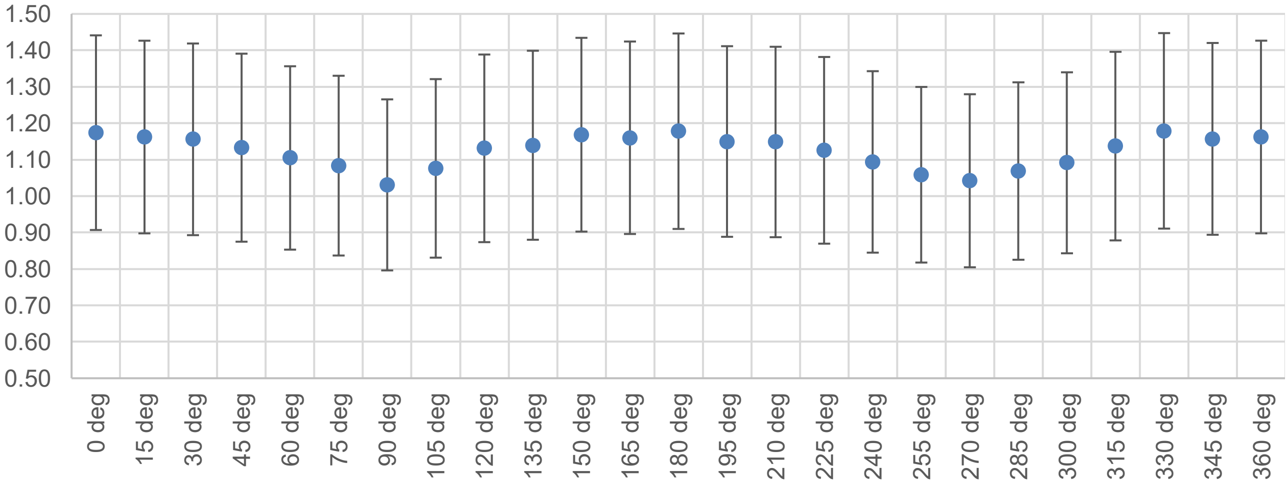

Figure 21. MC-to-measurement ratio for irradiation setups no. 33-57 (^{241}Am-Be source, 15° step rotation, distance 100 cm). Error bars correspond to k = 2.

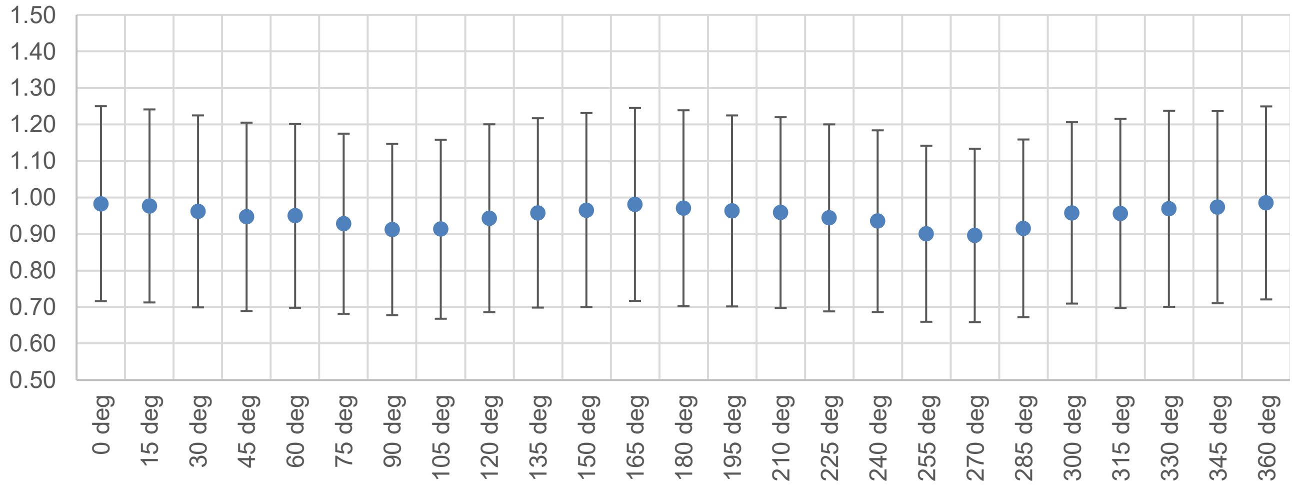

Figure 22. MC-to-measurement ratio for irradiation setups no. 58-84 (^{252}Cf source, 15° step rotation, distance 200 cm). Error bars correspond to k = 2.

The MC scaling factor $\bar{S}$ was subsequently verified using 16 different irradiation setups. In these validations, the reference quantity was the neutron spectral fluence rate, so the MC-to-measurement ratio S was calculated as:

$$S = \frac{\frac{M/\Phi_M}{\bar{S}}}{R/\dot{\Phi}_R}$$

where:

- M is the MC-calculated neutron absorptions in the scintillator sheets (multiplied by the sheet volume) per source neutron,
- Φ_M is the MC-calculated fluence per source neutron at the detector position in the absence of the detector [cm^{-2}],
- R is the detector neutron count rate [cps],
- $\dot{\Phi}_R$ is the reference fluence rate [cm^{-2} s^{-1}].

The MC-to-measurement ratios for these validation measurements are plotted in Figure 23 and Figure 24. The displayed error bars include:

- Combined uncertainty of the neutron fluence: ~1.5 – 3.5 %
- Statistical uncertainty of the MC calculation: ~0.5 %
- Estimated systematic uncertainty of the MC model: 5 %
- Uncertainty of the MC-to-measurement scaling factor: 10 %

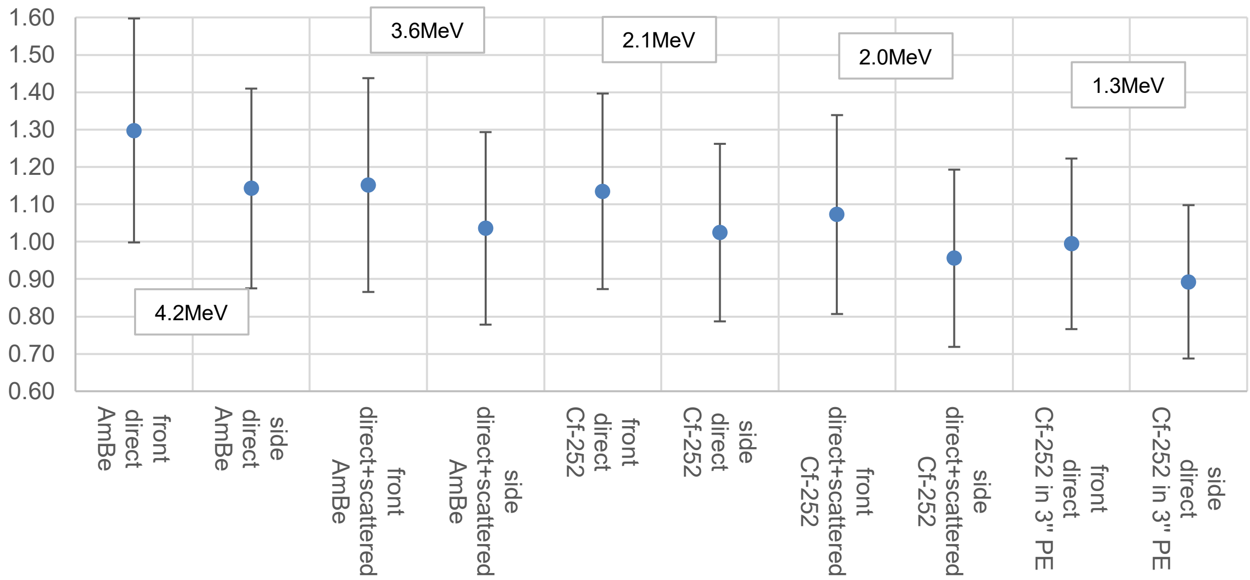

Figure 23. MC-to-measurement ratio for irradiation setups no. 85-94 (various CMI broad-spectrum neutron fields; see the overview of irradiations in Table 3). Error bars correspond to k = 2.

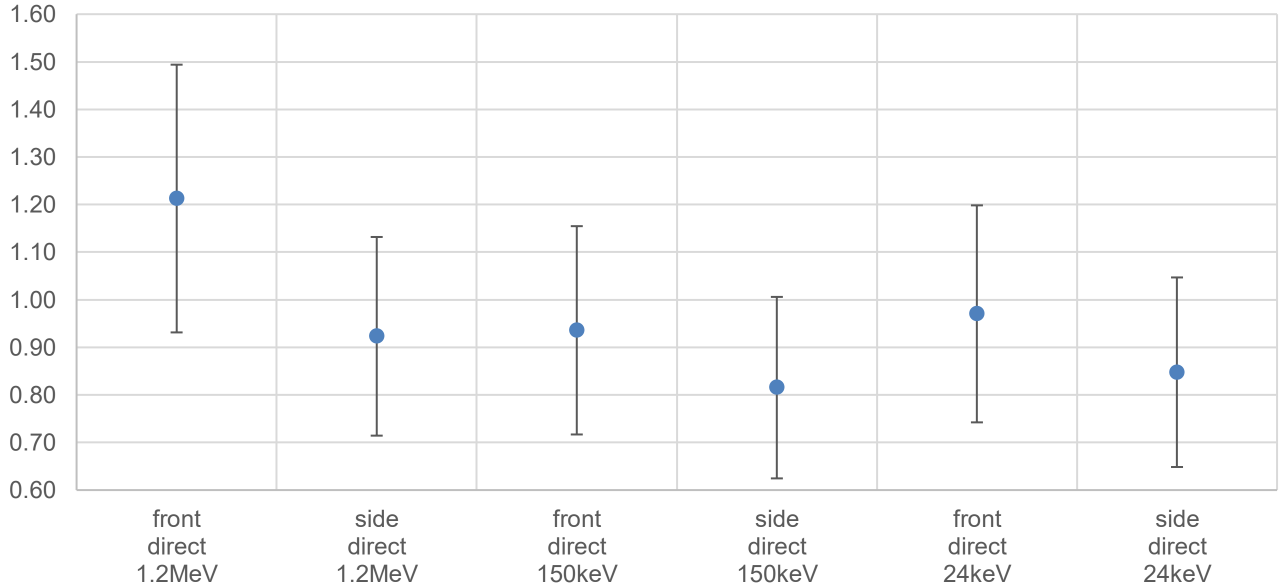

Figure 24. MC-to-measurement ratio for irradiation setups no. 95-106 (PTB monoenergetic neutron fields at PIAF; see Table **5**). Error bars correspond to k = 2.

3.1.4 Temperature stability test (CMI)

CRNS probes are designed for outdoor operation under conditions that can differ significantly from well-controlled laboratory environments. The neutron-sensitive detector and its associated electronics are enclosed in a plastic box, where internal temperatures can become elevated under direct sunlight. This test aimed to assess the potential influence of temperature on the device's response.

Test conditions were as follows:

- The probe was placed in a 1 m³ CMI climate chamber (see Figure 25).
- The neutron source was located outside the chamber.
- The probe was shielded by polyethylene (PE) bricks to reduce the Finapp 3 count rate to <50 cps.
- The tested temperature range was -20°C to +60°C, in 10°C steps.
- The temperature program consisted of a 1-hour transition phase followed by a 3-hour stabilization phase at each target temperature.
- The Finapp 3's internal temperature sensor was used to monitor the temperature inside the plastic enclosure.

A promoted feature of the Finapp 3 probe is its detection of muons and high-energy neutrons via its proprietary Pulse Shape Discrimination (PSD) algorithm. Both the neutron and muon channels were evaluated during this test. The measured count rates, averaged over the corresponding time periods, are summarized in

Table **6**. The uncertainties stated in

Table **6** and the text below consider statistical uncertainties only.

Table 6. Neutron and muon count rates averaged over consecutive time intervals during the temperature stability test.

Start date and time	End date and time	Preset temperature	n = Neutron rate	u(n) [%]	m = Muon rate	u(m) [%]
27.02.2024 16:15	27.02.2024 17:15	20 to -20	41.53	0.27	0.68	2.10
27.02.2024 17:15	27.02.2024 20:15	-20	41.37	0.15	0.62	1.24
27.02.2024 20:15	27.02.2024 21:15	-20 to -10	41.46	0.27	0.62	2.17
27.02.2024 21:15	28.02.2024 00:15	-10	41.54	0.15	0.63	1.24
28.02.2024 00:15	28.02.2024 01:15	-10 to 0	41.43	0.27	0.60	2.22
28.02.2024 01:15	28.02.2024 04:15	0	41.59	0.15	0.59	1.27
28.02.2024 04:15	28.02.2024 05:15	0 to 10	41.62	0.27	0.61	2.20
28.02.2024 05:15	28.02.2024 08:15	10	41.56	0.15	0.60	1.27
28.02.2024 08:15	28.02.2024 09:15	10 to 20	41.72	0.27	0.59	2.24
28.02.2024 09:15	28.02.2024 12:15	20	41.69	0.15	0.62	1.23
28.02.2024 12:15	28.02.2024 13:15	20 to 30	41.68	0.28	0.70	2.17
28.02.2024 13:15	28.02.2024 16:15	30	41.66	0.15	0.68	1.18
28.02.2024 16:15	28.02.2024 17:15	30 to 40	41.48	0.27	0.68	2.11
28.02.2024 17:15	28.02.2024 20:15	40	41.61	0.15	0.69	1.17
28.02.2024 20:15	28.02.2024 21:15	40 to 50	41.39	0.27	0.72	2.05
28.02.2024 21:15	29.02.2024 00:15	50	41.46	0.15	0.66	1.20
29.02.2024 00:15	29.02.2024 01:15	50 to 60	41.45	0.27	0.62	2.21
29.02.2024 01:15	29.02.2024 04:15	60	41.18	0.15	0.60	1.26
29.02.2024 04:15	29.02.2024 05:15	60 to 20	41.06	0.27	0.59	2.27
29.02.2024 05:15	29.02.2024 06:15	20	40.94	0.27	0.56	2.33

Figure 25. CMI climate chamber with an internal volume of 1 m³ (left). Detail of the Finapp 3 device during the test inside the climate chamber (right).

3.1.4.1 Evaluation of the neutron count rates

The neutron counts statistics correspond to approximately 12,000 counts per 5-minute measurement period. Figure 26 does not show any significant influence of temperature changes on the neutron count rate. The relative standard deviation calculated from the data in Figure 27 is about 0.5 %. Considering other sources of uncertainty in CRNS measurements, it can be concluded that the neutron signal is not temperature-dependent within the tested range.

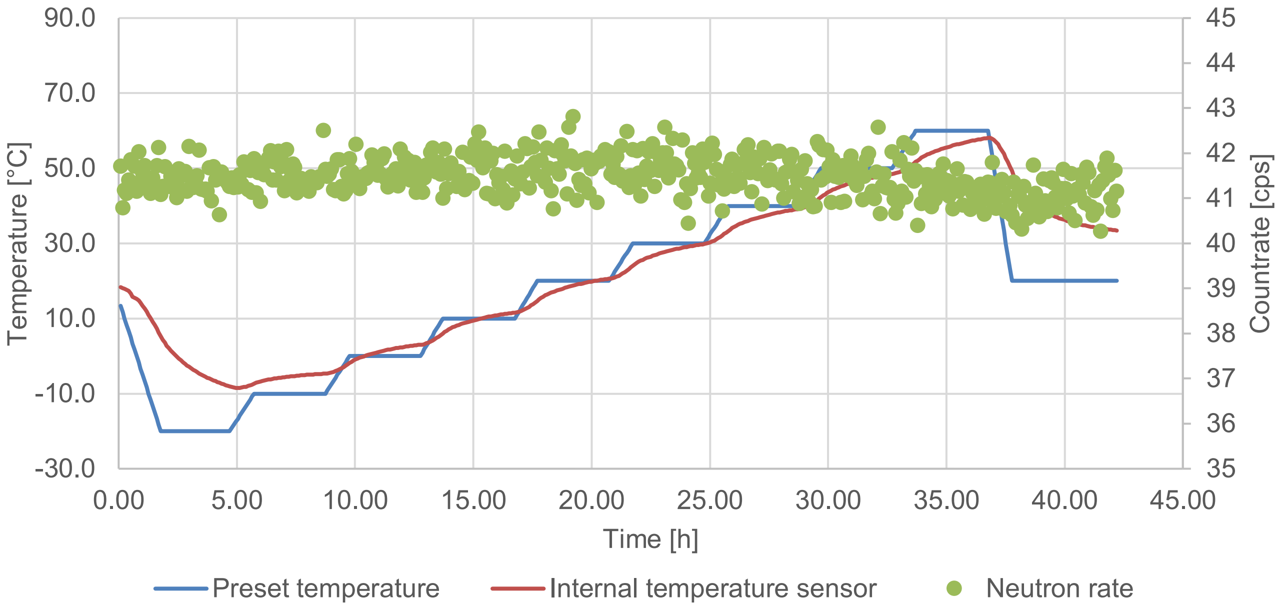

Figure 26. Neutron count rate (5-minute measurement steps) during the consecutive steps of the temperature test. Preset and internally measured temperatures are indicated.

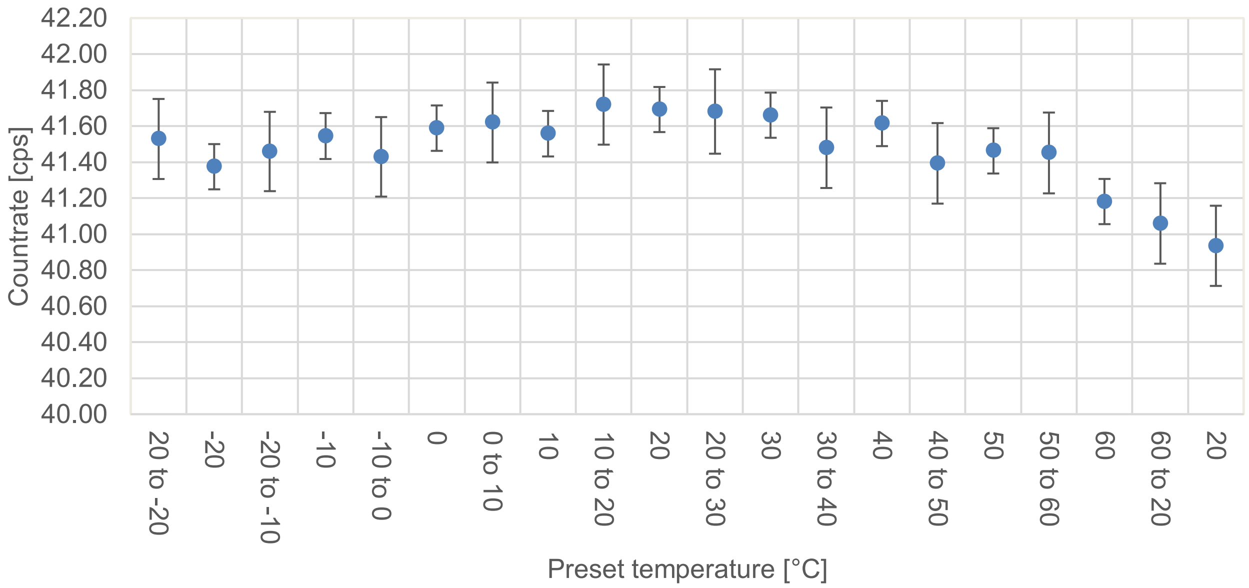

Figure 27. Average neutron count rate during the consecutive steps of the temperature test. Error bars correspond to k = 2.

3.1.4.2 Evaluation of the muon count rates

The muon count statistics correspond to approximately 200 counts per 5-minute measurement period, resulting in a more scattered plot than for neutrons, as shown in Figure 28. No clear trend can be identified. The data presented in Figure 29 show significant deviations, which might be related to the natural diurnal variation of the muon flux. However, more data would be required to support this hypothesis. The relative standard deviation calculated from the data in Figure 29 is approximately 7 %.

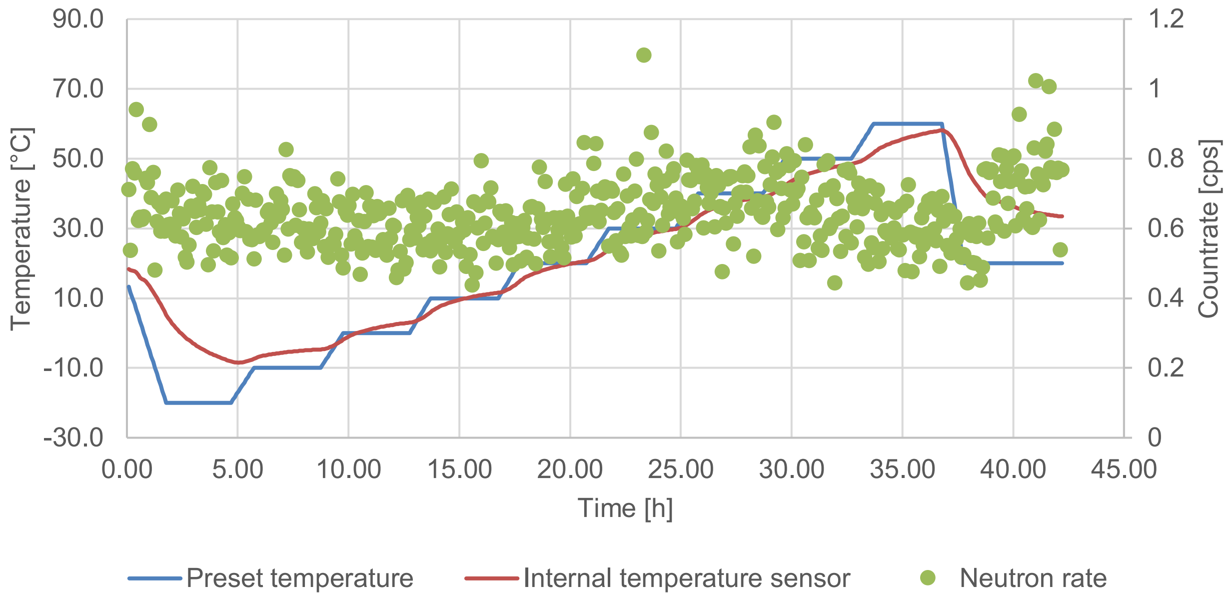

Figure 28. Muon count rate (5-minute measurement steps) during the consecutive steps of the temperature test. Preset and internally measured temperatures are indicated.

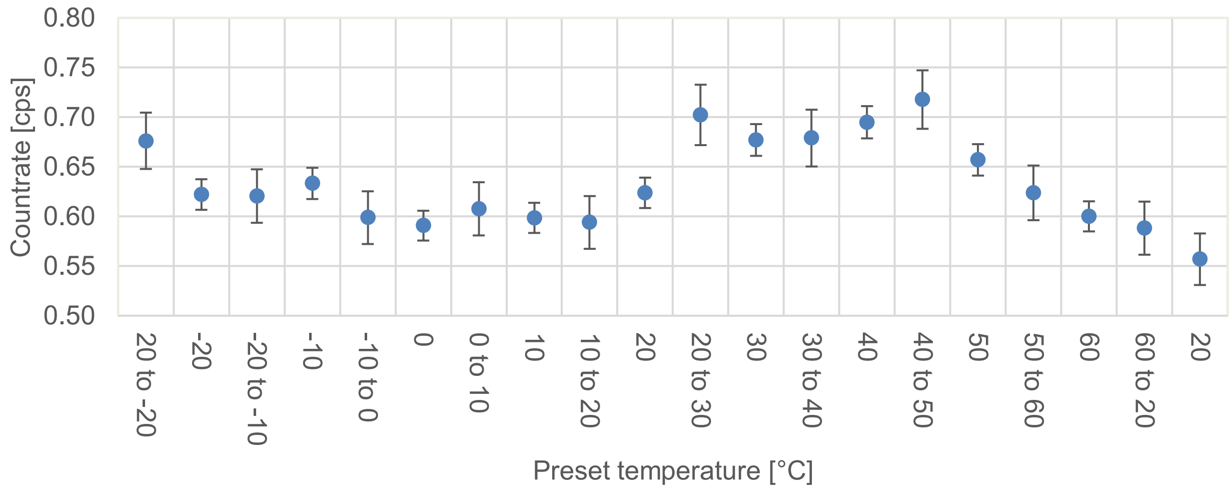

Figure 29. Average muon count rate during the consecutive steps of the temperature test. Error bars correspond to k = 2.

3.1.5 MC model (SMU)

An input file for the MCNP particle transport code was prepared based on information from the manufacturer regarding the detector's dimensions and composition. This model was cross-checked by SMU through physical measurements of the provided detector sample after the CMI measurements were completed (Figure 30). Due to insufficiently detailed information on material composition, some materials were defined according to the “Compendium of Material Composition Data for Radiation Transport Modeling”:

https://mcnp.lanl.gov/pdf_files/TechReport_2021_PNNL_PNNL-15870Rev.2_DetwilerMcConnEtAl.pdf

The main components of the model, also depicted in Figure 31, are summarized below:

1. **High-density polyethylene: CH_2:** density 0.965 g/cm³ (from Compendium).
2. **Expanded polystyrene (EPS):** Approximated as C_8H_8; density 0.007 g/cm³ (SMU approximation).
3. **EJ-426 thermal neutron detector:** A mixture of LiF and ZnS in a 1:3 ratio; density 1.544 g/cm³. Enriched in ^{6}Li to >95 %, with a ^{6}Li density of 8.81×10^{21} atoms/cm³ (same as CMI model). The simulated volume of each EJ-426 sheet is 6.183 cm³.
4. **Support layer: Polyester (PET, Mylar):** density 1.40 g/cm³ (same as CMI). The simulated volume of each PET layer is 4.830 cm³.
5. **EJ-280 wavelength shifter:** Polyvinyltoluene; density 1.023 g/cm³ (same as CMI).
6. **Outer box:** Approximated by Polypropylene (PP), C_3H_6; density 0.9 g/cm³ (from Compendium).
7. **Aluminium alloy:** 2024-O; density 2.78 g/cm³ (from Compendium).
8. **Battery lead:** Approximated by “clear lead” from the Compendium; density 11.35 g/cm³. The simulated battery weight does not correspond to the physical battery weight (7691 g total, including PP casing, for a lead volume of 678 cm³).

The calculations were performed using the MCNP6.2 neutron transport code with the ENDF/B-VII.0 data library at a temperature of 296 K, which includes the S(α,β) treatment for low-energy neutrons.

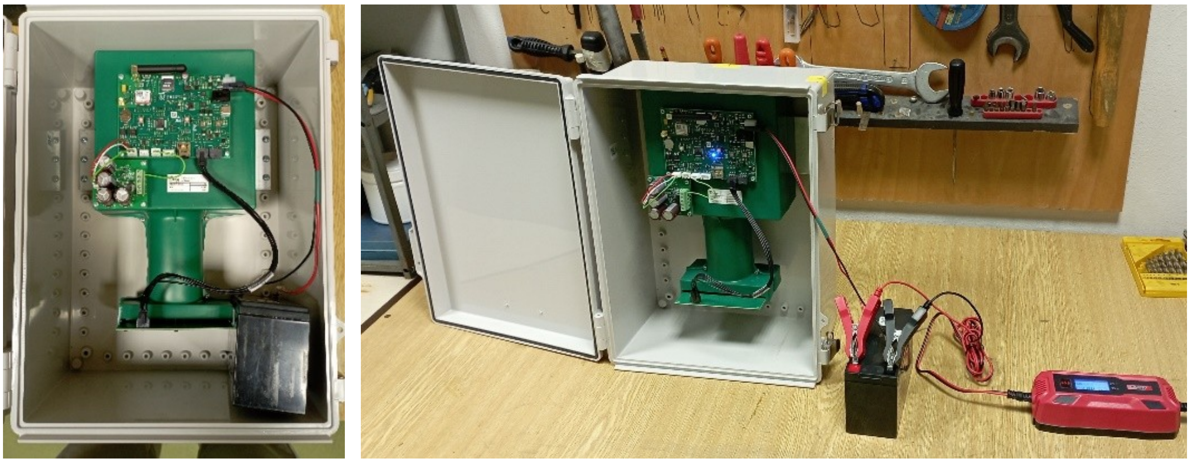

Figure 30. Interior photo of the Finapp 3 case (left). Photo of the detector during charging (right).

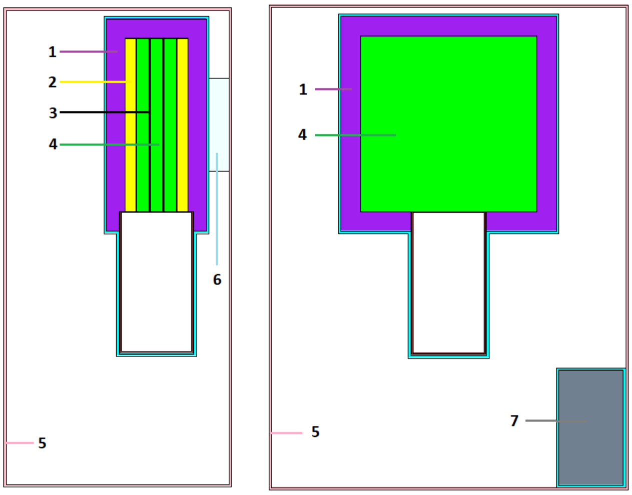

Figure 31. MCNP model of Finapp 3 prepared by SMU.

After finalizing the model, the response function of the Finapp 3 device was determined as a function of neutron energy. The fluence response functions, R, were computed for different faces of the device (Figure 32), as:

$$R[\mathrm{cm}^2] = R_x V S$$

where:

- Rx is the reaction rate [cm^{-3} s^{-1}],
- V is the volume of active part of detector (EJ-426 scintillator) [cm^3],
- S is the frontal surface of detector with moderator [cm^2].

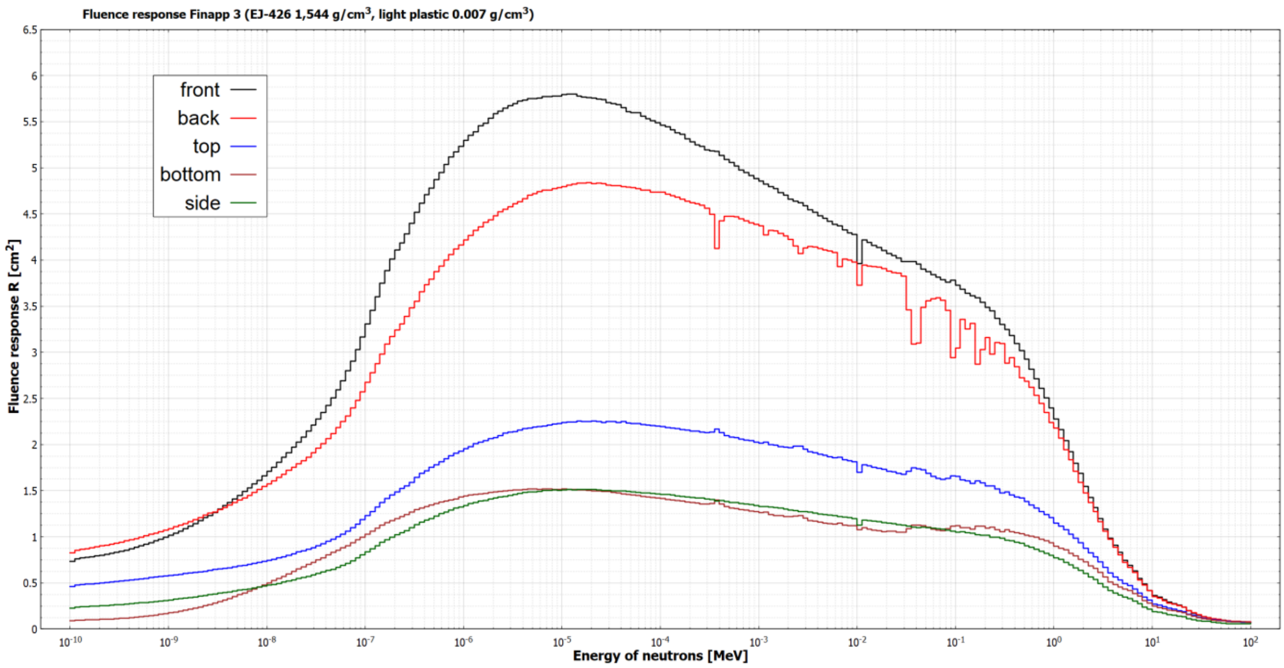

Figure 32. Response functions calculated with MCNP for the Finapp 3 device for all irradiation faces.

3.1.5.1 Simulated quantities in the initial MC model

The initial MCNP models focused on neutron reactions producing tritons, alpha particles, or the total neutron absorption cross-section. However, the ENDF/B-VII.0 library lacks specific data for the ^{6}Li(n,α) reaction. Therefore, it was decided to use the ^{6}Li(n,t) reaction rate, which corresponds to the total neutron absorption, as the simulation output.

The desired result of the Finapp 3 simulations is the fluence response function. However, validating the MC geometric model against real conditions was a necessary first step. Colleagues from CMI performed preliminary experimental measurements in different neutron fields. Preliminary MCNP calculations for Am-Be and Cf point sources were then compared with this CMI data (see Figure 33). The best agreement achieved with the CMI measurements was approximately 6.7 %.

The material composition of certain components in the Finapp 3 MC model (specifically, component 2 – the light plastic material, and component 3 – the EJ-426 scintillator) was varied to test the influence of these parameters on the results.

Following these preliminary MC calculations and subsequent measurements at PTB, a final set of measurements was conducted in the SMU neutron reference fields. Based on all acquired data, an updated and refined MC model was created.

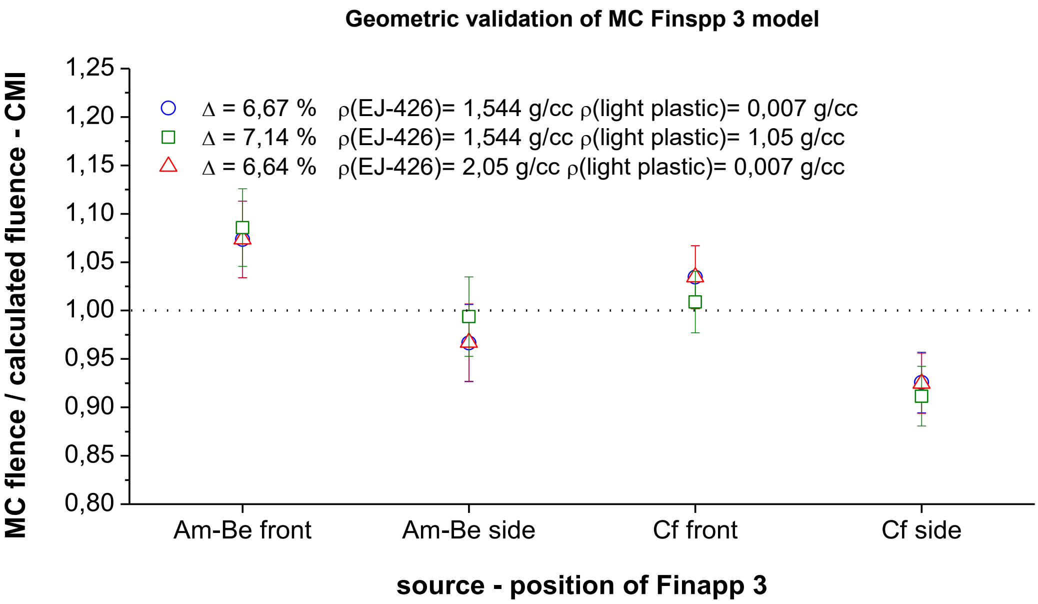

Figure 33. Preliminary relative comparison of the MCNP calculation (SMU) with experimental measurements of the Finapp 3 probe from CMI.

3.1.5.2 Simulated quantities in the updated MC model with the SMU irradiation room

The final enhanced model (Figure 34) simulated the following quantities:

- Number of $^{6}Li(n,\alpha)T$ interactions and total neutron absorption (all sheets).
- Proton recoil counts in the scintillator; alpha- and triton counts in the scintillator (all sheets).
- Neutron spectra at the detector position.
- Preliminary fluence response for various detector orientations.

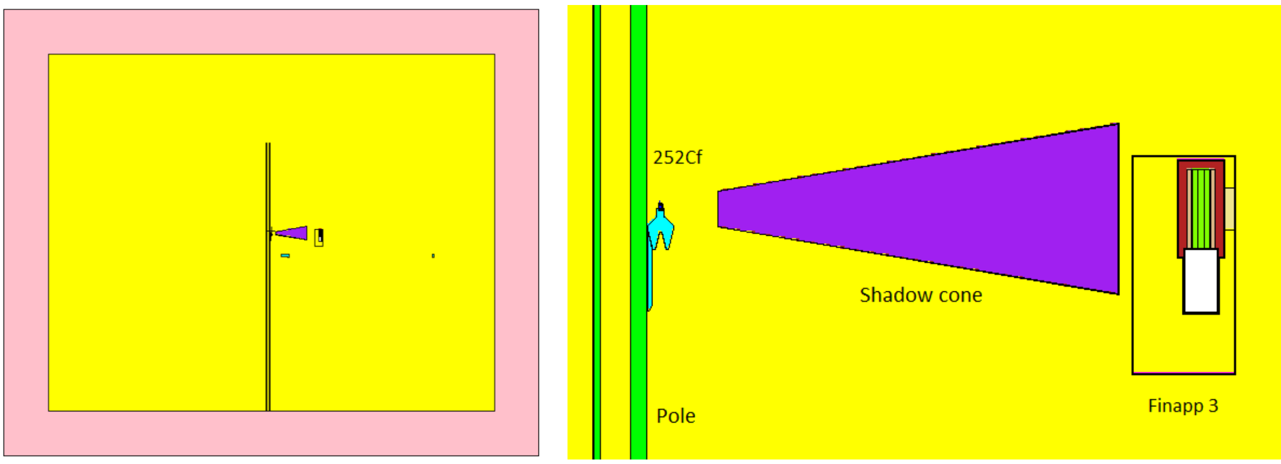

Figure 34. MCNP model of the SMU neutron irradiator room, showing a detailed modelled setup.

A comparison of the calculations from this enhanced model with the measured neutron responses, along with a discussion of the results, is provided in Section 3.1.7.

3.1.6 Measurements in the neutron reference fields (SMU)

Similar to the CMI setup, only the weakest ^{241}Am-Be and ^{252}Cf neutron sources could be used at SMU. Various irradiation conditions were established to adjust the MC model output, as detailed in

Table **7** and Table 8. A total of 44 irradiations, combining different neutron sources, distances, and geometries, were performed to characterize the device's response in diverse broad-spectrum neutron reference fields.

Source specifications:

^{241}Am-Be source (SMU no. 9003)

- Type: AMN.01
- Capsule type: EN 11, Ø13.4 mm × 17.1 mm
- Emission rate: 6.521×10^{4} s^{-1} ± 7.25 % (k = 1) to 14.5.2023
- Emission anisotropy @ 90 deg: 1.03 ± 1.00 % (k = 1)
- Fluence rate @ 110 cm:
  - Direct neutrons: 0.4601 cm^{-2} s^{-1} ± 8.29 % (k = 1)

^{252}Cf source (SMU no. 9-9/01)

- Type: NC252M11
- Capsule type: spherical head, Ø7 mm × 15 mm
- Emission rate: 2.014×10^{4} s^{-1} ± 5.96 % (k = 1) to 14.5.2024
- Emission anisotropy @ 90 deg: 1.018 ± 1.00 % (k = 1)
- Fluence rate @ 110 cm:
  - Direct neutrons: 0.1342 cm^{-2} s^{-1} ± 6.1 % (k = 1)

Table 7. Irradiation geometries used for MC model adjustment (Setups 1-13).

Irradiation number	Source	Neutron spectrum	Irradiation geometry	Distance (cm)
1	^{241}Am-Be	direct + scattered	front	75 cm
2	^{241}Am-Be	direct + scattered	front	95 cm
3	^{241}Am-Be	direct + scattered	front	110 cm
4	^{241}Am-Be	direct + scattered	side	75 cm
5	^{241}Am-Be	direct + scattered	side	95 cm
6	^{241}Am-Be	direct + scattered	side	110 cm
7	^{241}Am-Be	direct + scattered	back	95 cm
8	^{241}Am-Be	direct + scattered	back	110 cm
9	^{241}Am-Be	direct + scattered	top	75 cm
10	^{241}Am-Be	direct + scattered	top	95 cm
11	^{241}Am-Be	direct + scattered	top	110 cm
12	^{241}Am-Be	direct + scattered	bottom	75 cm
13	^{241}Am-Be	direct + scattered	bottom	110 cm

Table 8. Irradiation geometries/setups used for MC model adjustment.

Irradiation number	Source	Neutron spectrum	Irradiation geometry	Distance (cm)
14	^{241}Am-Be	scattered	front	95 cm
15	^{241}Am-Be	scattered	front	110 cm
16	^{241}Am-Be	scattered	side	95 cm
17	^{241}Am-Be	scattered	side	110 cm
18	^{241}Am-Be	scattered	back	95 cm
19	^{241}Am-Be	scattered	top	95 cm
20	^{241}Am-Be	scattered	top	110 cm
21	^{241}Am-Be	scattered	bottom	110 cm
22	^{252}Cf	direct + scattered	front	75 cm
23	^{252}Cf	direct + scattered	front	95 cm
24	^{252}Cf	direct + scattered	front	110 cm
25	^{252}Cf	direct + scattered	side	75 cm
26	^{252}Cf	direct + scattered	side	95 cm
27	^{252}Cf	direct + scattered	side	110 cm
28	^{252}Cf	direct + scattered	back	75 cm
29	^{252}Cf	direct + scattered	back	95 cm
30	^{252}Cf	direct + scattered	back	110 cm
31	^{252}Cf	direct + scattered	top	75 cm
32	^{252}Cf	direct + scattered	top	95 cm
33	^{252}Cf	direct + scattered	top	110 cm
34	^{252}Cf	direct + scattered	bottom	75 cm
35	^{252}Cf	direct + scattered	bottom	110 cm
36	^{252}Cf	scattered	front	95 cm
37	^{252}Cf	scattered	front	110 cm
38	^{252}Cf	scattered	side	95 cm
39	^{252}Cf	scattered	side	110 cm
40	^{252}Cf	scattered	back	95 cm
41	^{252}Cf	scattered	back	110 cm
42	^{252}Cf	scattered	top	95 cm
43	^{252}Cf	scattered	top	110 cm
44	^{252}Cf	scattered	bottom	110 cm

SMU shadow cone – A non-ISO cone, atypical design covered with a 1 mm thick cadmium plate.

- Front diameter: 6 cm
- Length: 70.5 cm (only HDPE inside)
- Back diameter: 30 cm

Finapp 3 geometry

- Distance: Measured from source centre to the centre of the detector's sensitive volume.
- Orientations: Front, Side (90° vertical), Back (180° vertical), Top (90° horizontal), Bottom (270° horizontal).

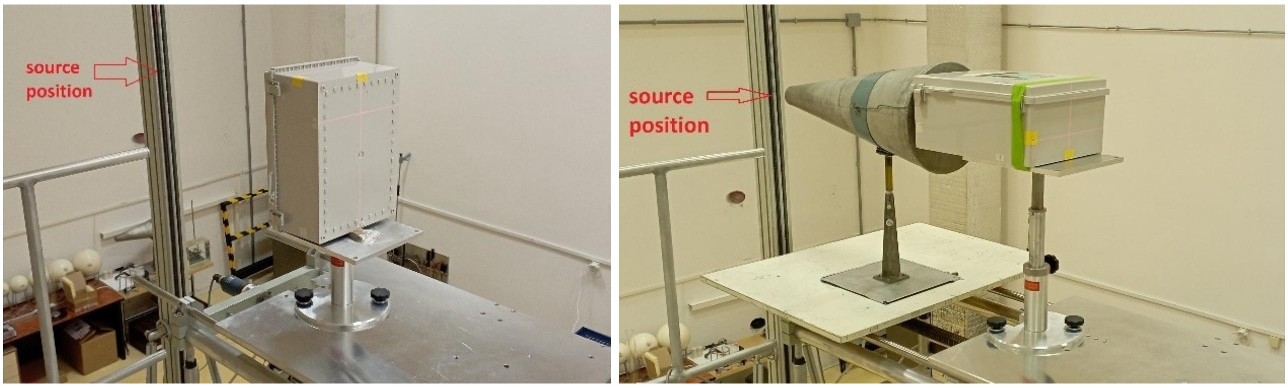

Figure 35. Photograph of irradiation setup no. 1 (^{241}Am-Be source, front irradiation, 75 cm distance) (left) and setup no. 44 (^{252}Cf source, bottom irradiation with shadow cone, 110 cm distance) (right).

3.1.7 Validation of MC model (SMU)

The data from the 44 irradiations (

Table **7** and Table 8) were used for the MC model adjustment. The corresponding geometries were simulated using the enhanced model of the SMU irradiation room (Figure 34). The simulation output was analysed using the triton (F6:T) and alpha (F16:A) deposition tallies in the four sensitive sheets, combined into a pulse-height tally (F8) using the FT8 PHL option. The total active volume of the four sheets is 24.732 cm³. The contribution from proton recoils (F6:H) was found to be insignificant. Finapp 3 data were processed identically to the CMI validation methodology.

The mean scaling factor $\bar{S}$ from the 44 S_0 reference irradiations was calculated, with the standard deviation used as its uncertainty:

$$\bar{S} = 1.29 \pm 12\ \%$$

When the data were categorized by neutron field type, the following values were obtained:

$$\bar{S}_{primary+scattered} = 1.41 \pm 11\ \%$$

$$\bar{S}_{scattered} = 1.10 \pm 11\ \%$$

The MC-to-measurement ratios for the adjustment measurements are plotted in Figure 36 - Figure 39. The error bars include:

- Combined uncertainty of the emission rate *B*: ~7 % (^{241}Am-Be), ~6 % (^{252}Cf)
- Statistical uncertainty of MC calculation: ~1 %
- Estimated systematic uncertainty of the MC model: 5 %
- Uncertainty of the MC to measurement scaling factor: from 11 % to 12 %

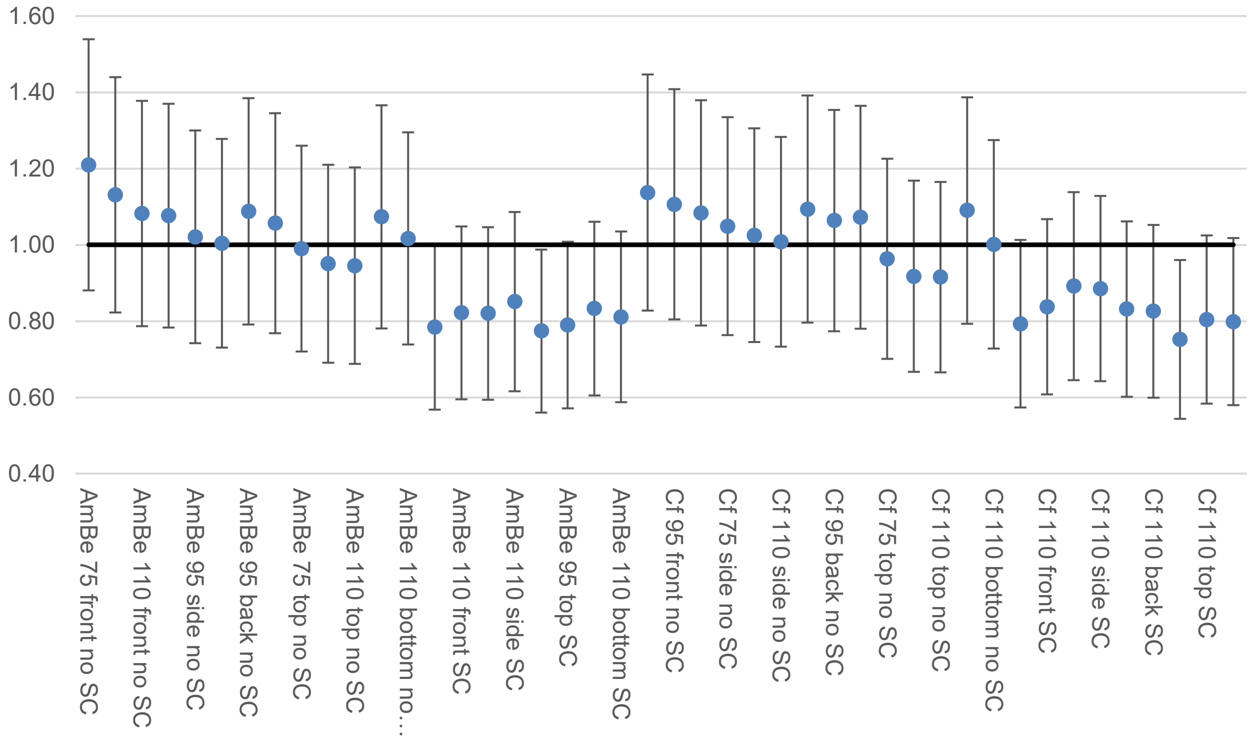

Figure 36. MC-to-measurement ratio for all irradiation setups (see Table **7** and Table 8). Error bars correspond to k = 2.

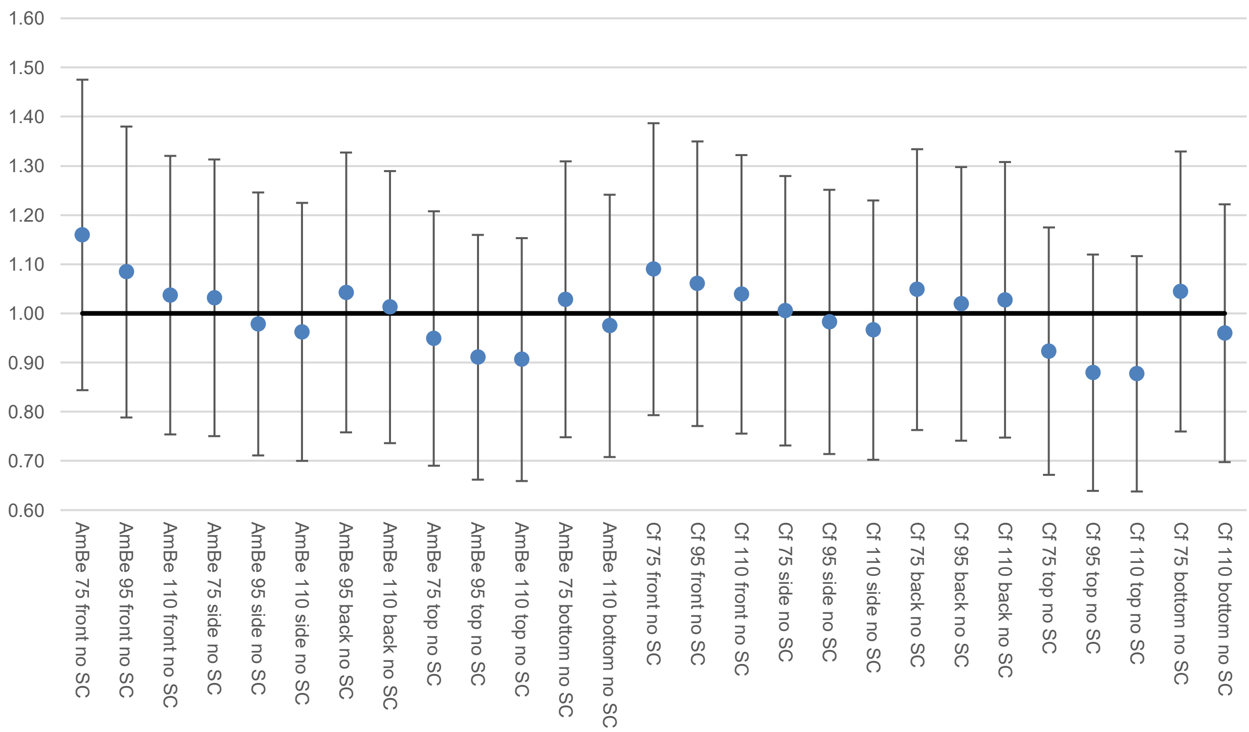

Figure 37. MC-to-measurement ratio for primary + scattered setups (no. 1-12, 22-35). Error bars correspond to k = 2.

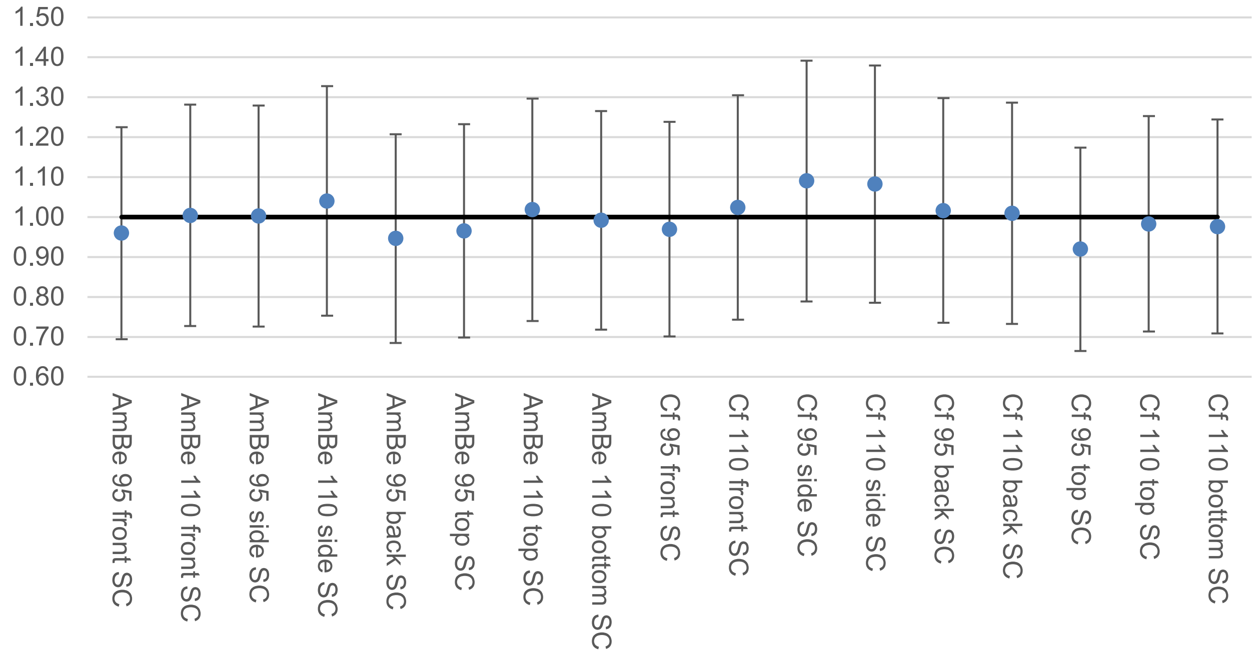

Figure 38. MC-to-measurement ratio for scattered-only setups (13-21, 36-44). Error bars correspond to k = 2.

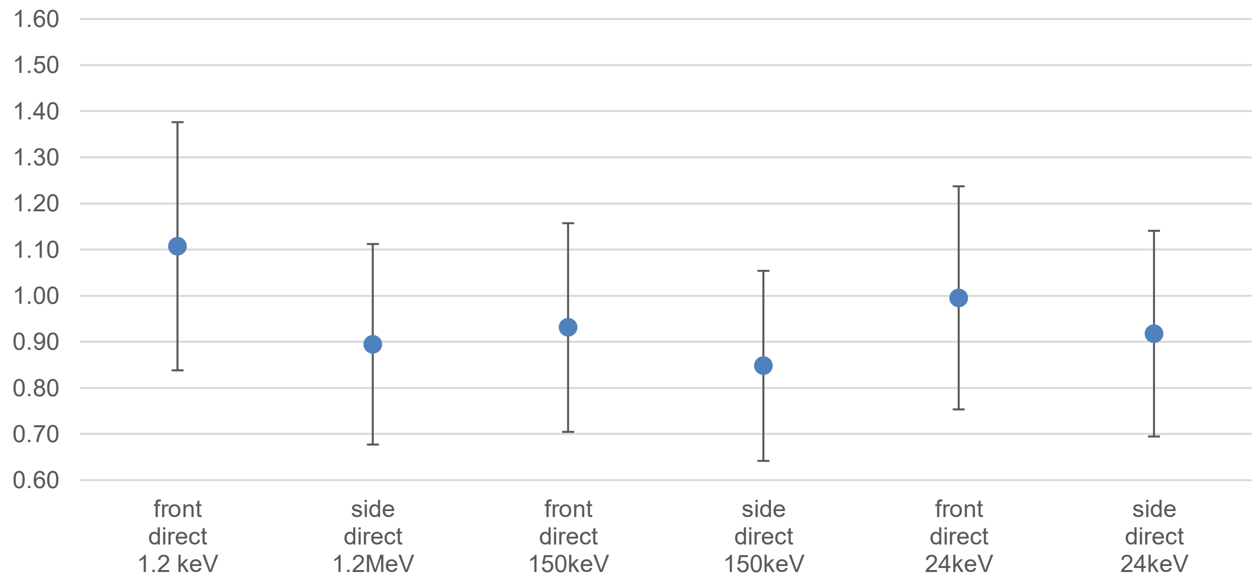

Figure 39. MC-to-measurement ratio for PTB monoenergetic neutron fields (setups 95-106, see

Table **5**), calculated with the SMU Finapp 3 model. Error bars correspond to k = 2.

As previously noted, the shadow cone used at SMU is non-standard. Its dimensions may have caused slight overshielding of the detector.

3.2 Hydroinnova - ^{3}He-based CRS-1000

The CRS-1000 device, developed by Hydroinnova LLC and Quaesta Instruments LLC (USA), is based on gas neutron counters, that are highly sensitive to thermal neutrons while exhibiting low sensitivity to gamma radiation. The system consists of two ^{3}He proportional counters. The neutron detection is based on the nuclear reaction:

$$^3He + ^1n \rightarrow ^1H + ^3H + 764\ keV$$

The products of the reaction deposit energy in the gas volume, ionizing the medium, generating an output pulse proportional to the reaction energy. The cross section of ^{3}He follows an inverse relationship with neutron velocity (1/v) at low energies. To enhance sensitivity to fast neutrons, one of the detectors is enclosed in a high-density polyethylene (HDPE) moderator.

A Neutron Pulse Monitor (NPM), type QI NPM-3100 from Quaesta Instruments LLC, processes and records the detector output. This unit features an integrated high-voltage supply and a multichannel analyzer (MCA), which generates a histogram of pulse-height distributions (Figure 40). The main peak in this distribution corresponds to the full energy deposition of the reaction, while “wall effects” occur when reaction products escape without depositing the whole energy, causing variations in pulse height. This characteristic spectrum allows for monitoring detector stability, optimizing performance, and distinguishing neutron signals from gamma-ray background noise through appropriate threshold settings.

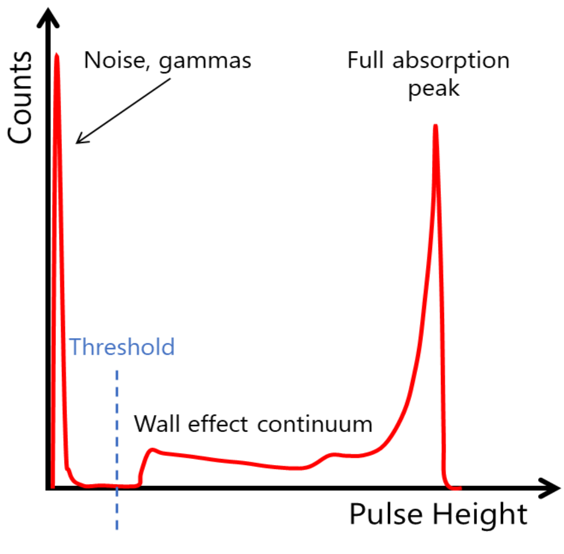

Figure 40. Typical pulse-height spectrum in a ^{3}He detector.

The detectors are housed in a weatherproof metallic enclosure along with meteorological sensors for temperature, pressure, and humidity measurements, and their necessary electronics. These components are managed by an NPM Q-DL-2100 Data Logger/Control Unit, which collects and provides all essential data to the user.

3.2.1 MC model (PTB)

The CRS-1000 device consists of ^{3}He proportional counters: one within a polyethylene moderator and one bare. Instead of analysing the response of each detector separately, the simulation treats the system as a single unit with two outputs. The neutron fluence is simulated on each external face of the outer box (see Figure 41), and the total counts in each detector are then evaluated without disentangling contributions such as internal neutron scattering.

The MCNP model was developed based on information provided by the manufacturer.

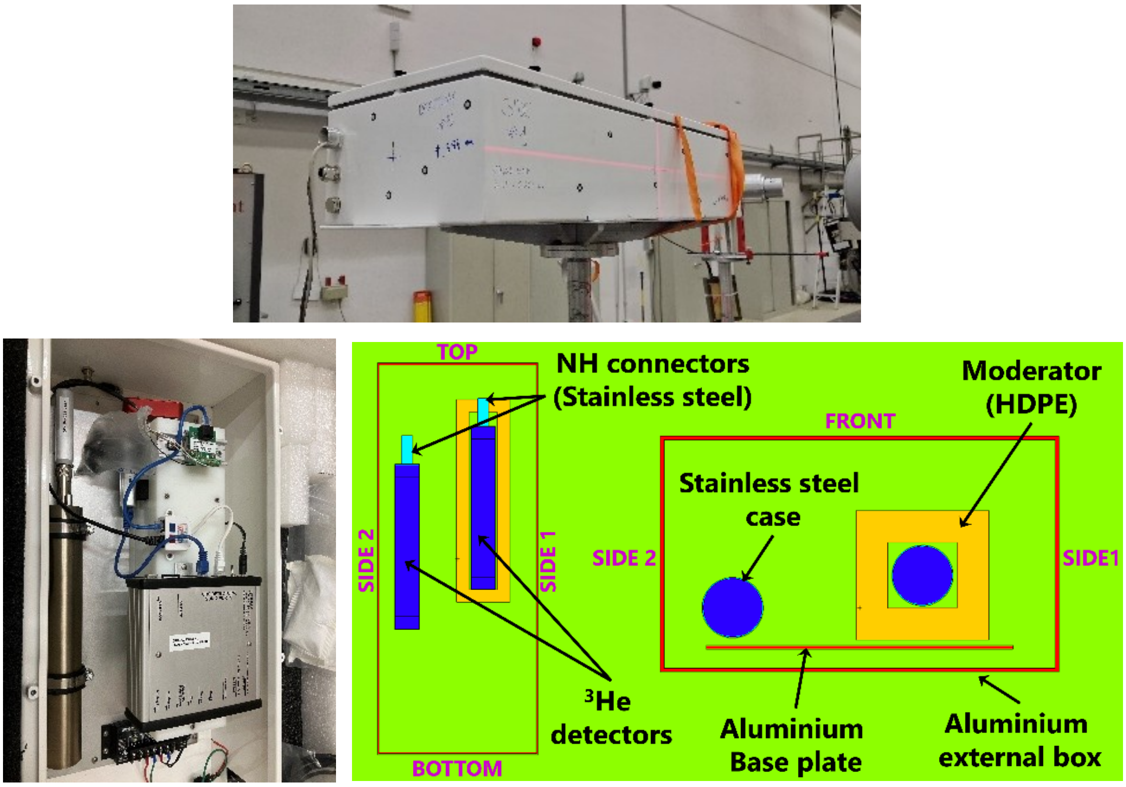

Figure 41. CRS-1000 device: external box (top) and internal arrangement (bottom left). Bottom right: MCNP model of the CRS-1000.

Once the model was finalized, the response function of the device was determined as a function of the neutron energy. Due to the device's geometry, its response is non-symmetrical, varying with the direction of neutron irradiation. Thus, distinct response functions (R) were computed for different faces of the device (Figure 42) as:

$$R[\mathrm{cm}^2] = \frac{M}{\Phi_{\mathrm{MC}}}$$

where:

- M = Number of neutron reactions in the gas volume (calculated by the MCNP model).
- Φ_{MC} = Neutron fluence over the detector's face of interest [cm-2].

The MCNP neutron transport code (v6.1.0) was used for calculations with the ENDF/B-VIII.0 data library at 293.6 K, including S(α,β) treatment for low-energy neutrons. A total of 82 neutron energies from 10^{-9} MeV to 100 MeV were simulated using a plane-parallel monoenergetic neutron source. For each detector, the output was defined as the number of reactions occurring within the active volume of ^{3}He.

According to the MCNP calculations, the response function for the moderated tube has an almost flat response over the energy range of interest (from 1 eV up to 1 MeV) while the bare tube is mostly efficient for thermal neutron energies.

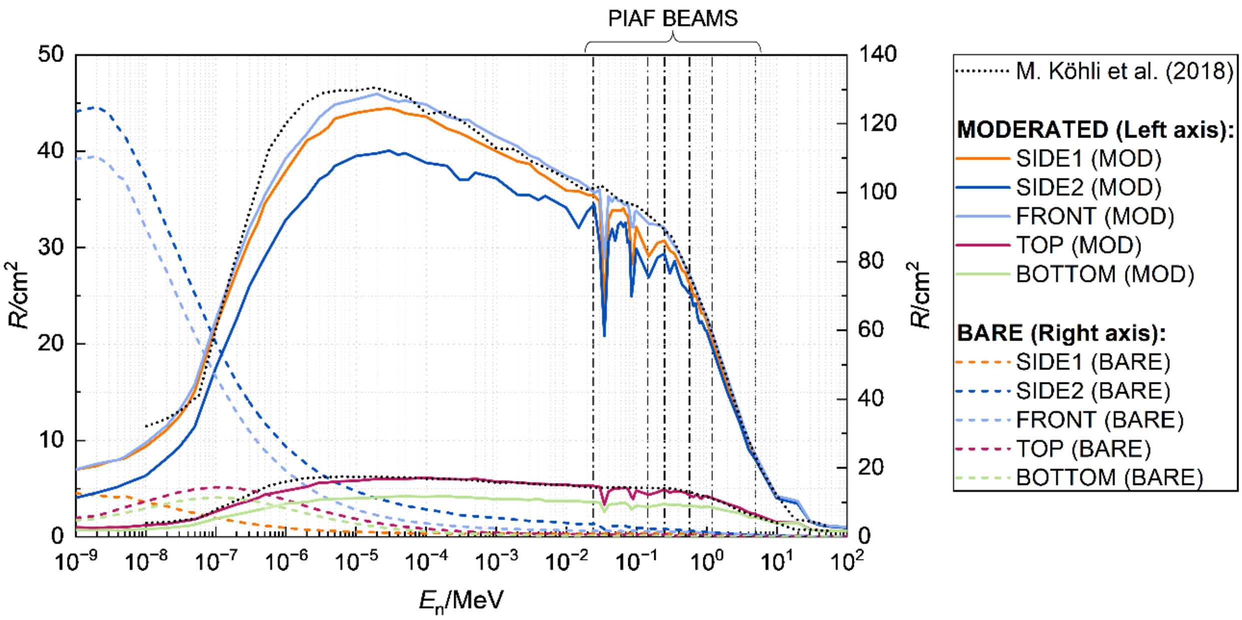

Figure 42. Response functions calculated with MCNP for the CRS-1000 device for both internal detectors (moderated tube in solid lines and bare tube in dashed lines) and all the irradiation faces.

3.2.2 Validation of MC model in the monoenergetic neutron fields (PTB)

To validate the MCNP model, the CRS-1000 has been characterized in monoenergetic neutron reference fields at PTB (PIAF) using six neutron energies (from 24 keV to 5 MeV, see Table 9). The neutron fluence over the detectors was known with a total uncertainty of 3 %, except for the 5 MeV field, which had 7 % uncertainty.

Table 9. Summary of the monoenergetic neutron fields used during the CRS-1000 probe characterization.

E_{ion}/MeV	Reaction	Angle [◦]	E_n/ MeV
1.941	$^{7}Li(p,n)^{7}Be$	80	0.024
1.941	$^{7}Li(p,n)^{7}Be$	0	0.144
2.021	$^{7}Li(p,n)^{7}Be$	0	0.250
2.297	$^{7}Li(p,n)^{7}Be$	0	0.565
2.049	$^{3}H(p,n)^{3}He$	0	1.2
2.360	$^{2}H(d,n)^{3}He$	0	5.0

The detector was placed at 6 meters from the neutron production target at a neutron emission angle of 0° (Figure 43), except for the 24 keV energy, where the detector was placed at 4 meters and 80°. Measurements were taken in five different orientations.

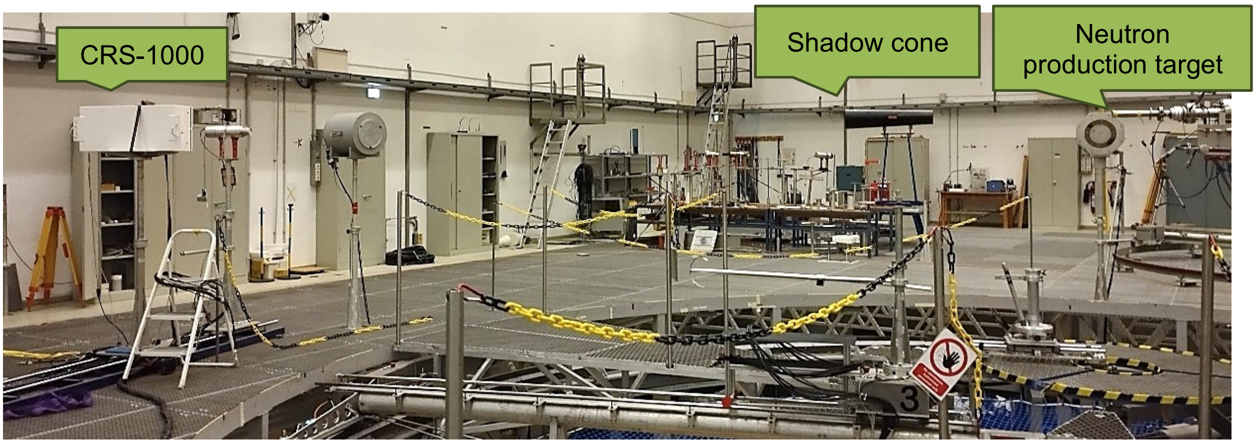

Figure 43. Photograph of the CRS-1000 device placed 6 m from the neutron production target, and the shadow cone in a typical experimental configuration at PIAF.

The high sensitivity of the device (designed for outdoor low-flux conditions) limited the maximum counting rate to 150 counts per second to avoid saturation, pile-up effects, and loss of linearity; increasing the irradiation time and limiting the statistics that could be accumulated.

According to the response functions in Figure 42, the bare detector exhibited higher sensitivity to the low-energy background from scattered neutrons than to neutrons emitted directly from the target. The shadow cone method (illustrated in Figure 43) was used to determine the neutron scattering background. The results indicated that, for the front and side orientations, only 10 % of the signal in the bare detector corresponded to neutrons emitted directly from the target, and less than 5 % for the top and bottom orientations. As in the case of the Finapp probe, the standard shadow cones slightly over-shadow the detector.

Due to low statistics and high background, meaningful data could not be obtained from the bare tube. All reported experimental data corresponds to the moderated tube only.

In addition to the experimental response, the device response to the monoenergetic neutron fields at PIAF was simulated for all irradiation configurations. To simulate the experimental conditions accurately, the neutron source was modelled with a Gaussian energy distribution with a variable full width at half maximum (FWHM) as follows:

- 24 keV → 10 keV FWHM
- 1.2 MeV → 100 keV FWHM
- 5 MeV → 200 keV FWHM
- Other energies → 15 keV FWHM

As in previous sections, to assess the agreement between experiment and simulation, a dimensionless ratio (S_0) was defined:

$$S_o = \frac{R_{\mathrm{MC}}}{R_{exp}}$$

where:
- R_{MC}= Simulated response.
- R_{exp} = Experimental response.

In an ideal case, S_0 = 1 indicates perfect agreement. Table 10 summarizes the experimental R_{exp} and simulated R_{MC}, responses and calculated S_0 values, along with uncertainties for each configuration.

Following the same procedure that has been indicated with the Finapp probe, the mean $\bar{S}$ of the 30 S_0 values was calculated, and the standard deviation was used as estimation of $\bar{S}$ uncertainty:

$$\bar{S} = 0.80 \pm 11\ \%$$

This suggests that the MCNP model underestimates detected events. The discrepancies arise due to incomplete model geometry, cross-section data limitations, and how interactions are modeled within the MCNP code. To correct for this, $\bar{S}$ is introduced as a scaling factor, modifying the Monte Carlo to experimental measurement ratio:

$$S = \frac{R_{\mathrm{MC}}/\bar{S}}{R_{exp}}$$

The MC to measurement ratio for different irradiation setups is plotted in Figure 44, where the error bars include:

- Experimental uncertainties $\boldsymbol{u_{R_{\mathrm{exp}}}}$ (accounts for statistical, fluence, and current uncertainties).
- MC calculation uncertainty $\boldsymbol{u_{R_{\mathrm{MC}}}}$.
- Systematic uncertainty in MC model for different irradiation faces:
  - 2 % (Front, Side 1)
  - 1 % (Side 2)
  - 4 % (Top)
  - 9 % (Bottom)
- Scaling factor uncertainty (11 %).

Table 10. Summary of the experimental response (R_{exp}), the simulated response (R_{MC}) and the MC to measurement ratio before (S_o) and after (S) the adjustment by the scaling factor $\bar{S}$, for each irradiation configuration. All the quantities are written with the corresponding uncertainties.

	E_n / MeV	R_{MC} / cm²	$u_{R_{MC}}$	R_{exp} / cm²	$u_{R_{exp}}$	S_o	u_{S_o}	S	u_S
FRONT	0.024	44.64	0.004	44.80	0.06	0.80	0.05	1.00	0.13
	0.144	40.43	0.004	37.15	0.04	0.87	0.04	1.09	0.13
	0.250	39.52	0.004	37.33	0.07	0.85	0.06	1.06	0.14
	0.565	34.24	0.005	30.45	0.05	0.90	0.04	1.12	0.14
	1.2	26.56	0.005	24.33	0.08	0.87	0.07	1.09	0.15
	5.0	10.60	0.008	9.30	0.15	0.91	0.14	1.14	0.22
SIDE1	0.024	43.06	0.004	41.28	0.04	0.83	0.03	1.04	0.13
	0.144	36.92	0.005	36.88	0.04	0.80	0.03	1.00	0.12
	0.250	37.96	0.004	38.51	0.07	0.79	0.05	0.99	0.13
	0.565	32.53	0.005	35.30	0.04	0.74	0.03	0.92	0.11
	1.2	25.69	0.005	25.25	0.07	0.81	0.06	1.02	0.14
	5.0	10.25	0.009	9.72	0.14	0.84	0.12	1.05	0.19
SIDE2	0.024	39.84	0.004	38.12	0.07	0.84	0.06	1.04	0.14
	0.144	33.70	0.005	31.25	0.05	0.86	0.04	1.08	0.13
	0.250	36.11	0.005	33.69	0.08	0.86	0.07	1.07	0.15
	0.565	30.80	0.005	27.32	0.04	0.90	0.04	1.13	0.14
	1.2	24.47	0.006	22.87	0.08	0.86	0.07	1.07	0.15
	5.0	9.91	0.009	9.17	0.13	0.86	0.11	1.08	0.18
TOP	0.024	6.56	0.011	7.71	0.18	0.68	0.12	0.85	0.18
	0.144	5.40	0.012	6.47	0.10	0.67	0.06	0.83	0.12
	0.250	6.01	0.011	-	-	-	-	-	-
	0.565	5.37	0.012	6.17	0.12	0.70	0.08	0.87	0.14
	1.2	4.70	0.012	4.99	0.26	0.75	0.20	0.94	0.27
	5.0	2.92	0.016	2.86	0.26	0.82	0.21	1.02	0.29
BOTTOM	0.024	4.39	0.013	4.78	0.34	0.74	0.25	0.92	0.33
	0.144	3.89	0.014	5.37	0.11	0.58	0.06	0.72	0.11
	0.250	4.18	0.013	-	-	-	-	-	-
	0.565	3.95	0.014	5.38	0.13	0.59	0.08	0.73	0.13
	1.2	3.77	0.014	-	-	-	-	-	-
	5.0	2.52	0.017	2.43	0.18	0.83	0.15	1.03	0.22

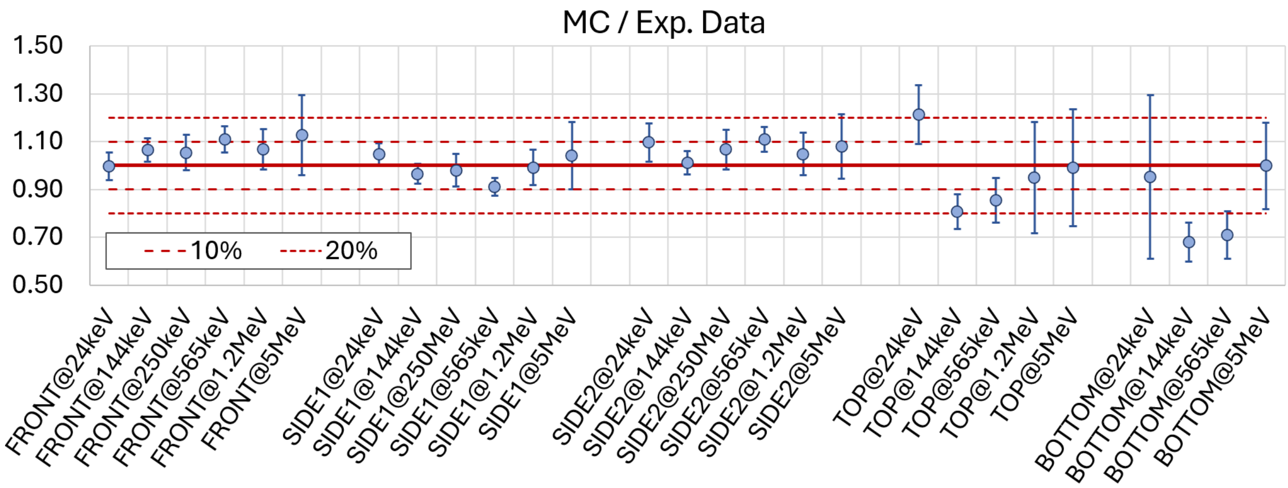

Figure 44. MC to measurement ratio for all irradiation configurations (see Table 10). The error bars correspond to the k = 1, i.e. ~68 % coverage for normal distribution.

3.2.3 Validation of MC model in broad range neutron fields (PTB)

To validate the MC model and extend the characterization of the device to a broader energy range, including the low-energy spectrum, the detector was exposed to three reference neutron sources based on radionuclides. These irradiations were performed in five different geometrical configurations (Front, Side 1, Side 2, Top, and Bottom, see Figure 41). All measurements were conducted at a reference distance of 170 cm, measured from the centre of the neutron source to the centre of the detector box. This time, the signal-to-noise ratio enabled useful measurements also for the bare detector.

The sources characteristics are the following:

^{241}Am-Be source:

- Emission rate: 2.92×10^6 s^{-1} ± 2.3 % (k = 1) to 1.3.2024
- Fluence rate @ 170 cm:
    - Direct neutrons: 8.055 ± 0.187 cm^{-2} s^{-1} (k = 2)
    - Direct + scattered neutrons: 14.147 ± 0.316 cm^{-2} s^{-1} (k = 2)

^{252}Cf source (Bare)

- Emission rate: 8.49×10^4 s^{-1} ± 0.7 % (k = 1) to 27.02.2024
- Fluence rate @ 170 cm:
    - Direct neutrons: 0.233 ± 0.002 cm^{-2} s^{-1} (k = 2)
    - Direct + scattered neutrons: 0.455 ± 0.008 cm^{-2} s^{-1} (k = 2)

^{252}Cf source (D_2O Moderated + 1 mm Cd)

- Emission rate: 8.49×10^4 s^{-1} ± 0.7 % (k = 1) to 27.02.2024
- Fluence rate @ 170 cm:
    - Direct neutrons: 0.194 ± 0.004 cm^{-2} s^{-1} (k = 2)
    - Direct + scattered neutrons: 0.405 ± 0.011 cm^{-2} s^{-1} (k = 2)

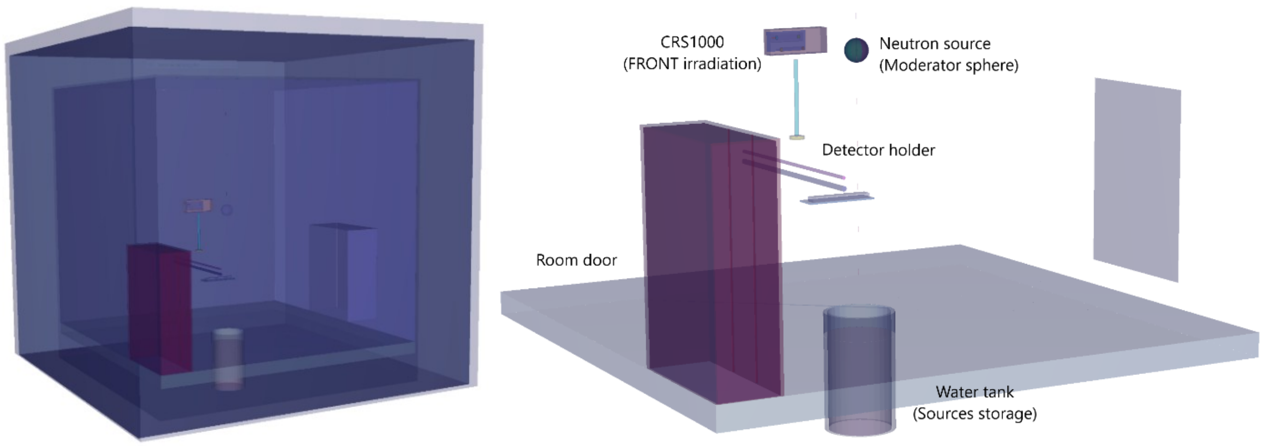

Figure 45. PTB MCNP model for the irradiation room showing the main elements.

Since no suitable shadowing object was available to block the entire detector, both direct and scattered neutron components were considered in the measurements. To account for background effects, a detailed MCNP simulation was performed. The MCNP geometry of the detector is included in a detailed simulation of the full experimental room. This MCNP room model, previously validated at PTB using the NEMUS Bonner sphere spectrometer, includes layers of various materials in the walls, floor, and ceiling, as well as key elements like the water tank beneath the floor (used for source storage), the room door, and detector support structures (Figure 45).

The data processing followed the methodology previously used for the measurements in monoenergetic neutron fields. However, due to significant fluence variations along the detector tubes (caused by the device's large size relative to the bunker), the dimensionless ratio (S_0) was defined from the counting rate in counts per second (*cps*):

$$S_o = \frac{cps_{\mathrm{MC}}}{cps_{exp}}$$

Where cps_{MC} is the simulated counting rate and cps_{exp}, the experimental counting rate.

The mean $\bar{S}$ was determined from 15 reference irradiation values, with standard deviation used to estimate uncertainty, yielding:

$$\bar{S}_{\mathrm{mod}} = 0.80 \pm 9\ \%$$

$$\bar{S}_{\mathrm{bare}} = 1.53 \pm 6\ \%$$

While the results for the moderated tube were consistent with measurements in monoenergetic neutron fields, a significant discrepancy was observed for the bare tube. This discrepancy arose due to a missing scaling factor in the MCNP room model, particularly affecting the thermal neutron spectrum.

Figure 46 compares the neutron fluence at the reference position (170 cm) obtained from the MCNP model versus BSS measurements. The discrepancy is attributed to the unknown water content in the concrete existing in the experimental room.

From the ratio between the integrated fluence in the thermal part (shaded area) between the MCNP model and the BBS measurements, a correction factor *C* was derived for the thermal component of each source:

$$C_{\mathrm{AmBe}} = 2.08,\ C_{\mathrm{Cf-252}} = 1.97,\ C_{\mathrm{Cf-252(mod)}} = 1.84$$

Applying these correction factors, the adjusted mean $\bar{S}$ values are:

$$\bar{S}_{\mathrm{mod}} = 0.80 \pm 10\ \%$$

$$\bar{S}_{\mathrm{bare}} = 0.79 \pm 9\ \%$$

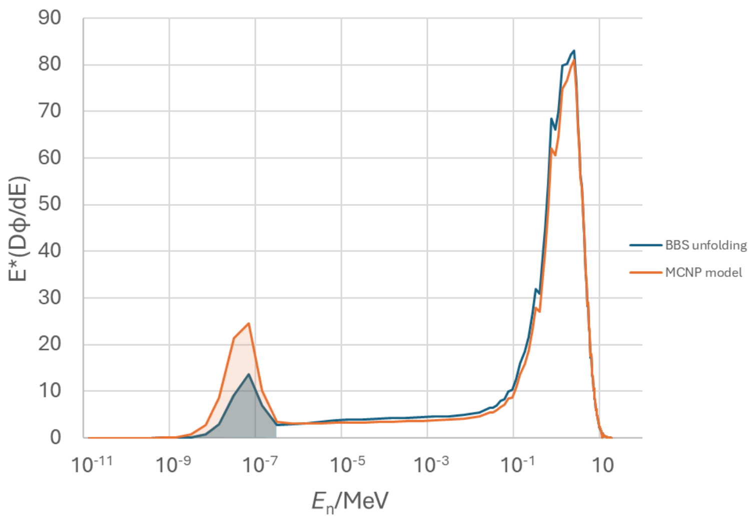

Figure 46. Comparison between the spectrum calculated with the MCNP (orange) model and the BBS measurements (blue) for the bare Cf-252 source at the reference position.

Using the corrected values, the MC to measurement ratio for different irradiation setups was recalculated as:

$$S = \frac{cps_{\mathrm{MC}}/\bar{S}}{cps_{exp}}$$

Tables 11 and 12 (moderated and bare detector respectively) summarize the experimental (cps_{exp}) and simulated (cps_{MC}) counting rates for each configuration, along with the corresponding S_o and corrected S values, including relative uncertainties.

Table 11. For the moderated counter: Summary of the experimental counts-per-second (cps_{exp}), the simulated counts-per-second (cps_{MC}) and the MC to measurement ratio before (S_o) and after (S) the adjustment by the scaling factor $\bar{S}$, for each irradiation configuration. All the quantities are written with the corresponding uncertainties.

Source	Irradiation	cps_{MC}	$u_{cps_{\mathrm{MC}}}$	cps_{exp}	$u_{cps_{\mathrm{exp}}}$	S_o	u_{S_o}	S	u_S
Am-Be	SIDE1	193.62	0.02	283.94	0.01	0.68	0.02	**0.85**	**0.09**
	SIDE2	190.91	0.02	269.56	0.02	0.71	0.02	**0.88**	**0.09**
	FRONT	190.96	0.02	271.11	0.01	0.70	0.02	**0.88**	**0.09**
	TOP	144.83	0.02	202.29	0.01	0.72	0.02	**0.89**	**0.09**
	BOTTOM	142.67	0.02	192.97	0.01	0.74	0.03	**0.92**	**0.09**
Cf-252 (Bare)	SIDE1	9.76	0.01	11.39	0.01	0.86	0.02	**1.07**	**0.09**
	SIDE2	9.17	0.01	10.58	0.01	0.87	0.02	**1.08**	**0.09**
	FRONT	9.31	0.01	10.81	0.01	0.86	0.02	**1.07**	**0.09**
	TOP	6.01	0.02	7.74	0.01	0.78	0.02	**0.97**	**0.09**
	BOTTOM	6.09	0.02	7.16	0.01	0.85	0.02	**1.06**	**0.09**
Cf-252 (Mod)	SIDE1	12.36	0.01	14.48	0.01	0.85	0.02	**1.07**	**0.09**
	SIDE2	11.11	0.01	12.56	0.01	0.88	0.02	**1.10**	**0.09**
	FRONT	11.79	0.02	13.77	0.01	0.86	0.03	**1.07**	**0.09**
	TOP	6.34	0.02	7.87	0.01	0.81	0.02	**1.01**	**0.09**
	BOTTOM	6.18	0.02	7.21	0.01	0.86	0.02	**1.07**	**0.09**

Table 12. For the bare counter: Summary of the experimental counts-per-second (cps_{exp}), the simulated counts-per-second (cps_{MC}) and the MC to measurement ratio before (S_o) and after (S) the adjustment by the scaling factor $\bar{S}$, for each irradiation configuration. All the quantities are written with the corresponding uncertainties.

Source	Irradiation	cps_{MC}	$u_{cps_{MC}}$	$^{Corr}cps_{MC}$	$u_{cps_{MC}}$	cps_{exp}	$u_{cps_{exp}}$	S_o	u_{S_o}	S	u_S
Am-Be	SIDE1	123.65	0.02	59.45	0.07	84.15	0.02	0.71	0.07	**0.90**	**0.09**
	SIDE2	120.89	0.02	58.12	0.07	84.67	0.02	0.69	0.07	**0.87**	**0.09**
	FRONT	121.10	0.02	58.22	0.07	85.20	0.02	0.68	0.07	**0.87**	**0.09**
	TOP	115.70	0.03	55.63	0.07	78.76	0.02	0.71	0.07	**0.90**	**0.09**
	BOTTOM	120.02	0.03	57.70	0.07	80.95	0.02	0.71	0.07	**0.91**	**0.09**
Cf-252 (Bare)	SIDE1	4.97	0.02	2.52	0.07	3.09	0.02	0.82	0.07	**1.04**	**0.09**
	SIDE2	5.03	0.02	2.56	0.07	3.12	0.01	0.82	0.07	**1.04**	**0.09**
	FRONT	4.91	0.02	2.49	0.07	3.10	0.02	0.80	0.07	**1.02**	**0.09**
	TOP	4.71	0.02	2.39	0.07	2.85	0.02	0.84	0.07	**1.07**	**0.09**
	BOTTOM	4.85	0.02	2.46	0.07	2.89	0.02	0.85	0.07	**1.09**	**0.09**
Cf-252 (Mod)	SIDE1	6.92	0.02	3.77	0.07	4.41	0.02	0.86	0.07	**1.09**	**0.09**
	SIDE2	8.02	0.02	4.37	0.06	5.53	0.02	0.79	0.07	**1.01**	**0.09**
	FRONT	7.32	0.03	3.99	0.07	5.05	0.02	0.79	0.07	**1.00**	**0.09**
	TOP	7.00	0.02	3.81	0.07	4.49	0.01	0.85	0.07	**1.08**	**0.09**
	BOTTOM	7.15	0.02	3.89	0.07	4.51	0.01	0.86	0.07	**1.10**	**0.09**

The corrected *S* values for both detector tubes are presented in Fig. 47, with error bars indicating k = 1 (~68 % confidence level for a normal distribution).

Considering all irradiation scenarios (monoenergetic neutron fields and radionuclide sources, see Tables 10 - 12), the global scaling factor for the MC model obtained is:

$$\bar{S}_{tot} = 0.80 \pm 10\ \%$$

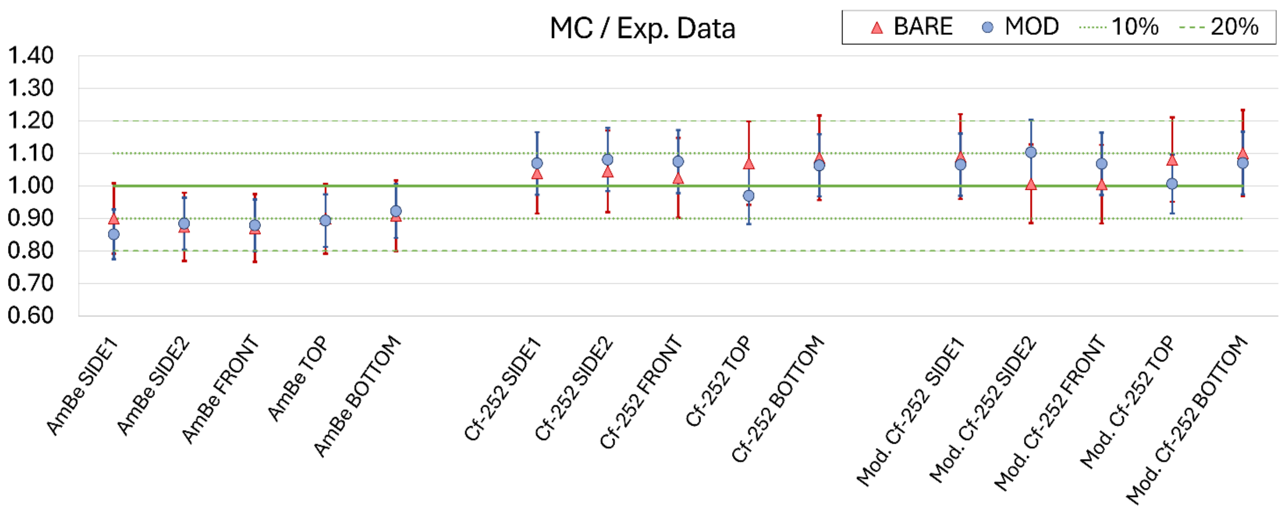

Figure 47. MC to measurement ratio for all irradiation configurations (see Tables 11 and 12). The error bars correspond to the *k* = 1.

3.3 Hydroinnova – BF_3-based CRS-2000/B

The CRS-2000/B system consists of bare and moderated neutron detectors, similar in concept to the Hydroinnova CRS-1000, but based on BF_3 proportional counters rather than ^3He.

Neutron detection is based on the $^{10}B(n,\alpha)^7Li$ reaction:

$$^{10}B + {}^1n \rightarrow {}^7Li + {}^4He + 2.31\ MeV$$

This reaction has a thermal neutron (0.025 eV) cross-section of σ = 3837 barn, with secondary particle energies of E_{Li} = 0.84 MeV and E_α = 1.47 MeV.

This detection mechanism is less efficient than the $^3He(n,p)^3H$ reaction, which has a cross section of σ = 5327 barn. Consequently, BF_3 detectors typically require a larger physical size than ^3He detectors to achieve comparable count rates.

The CRS-2000/B system comprises two cylindrical tubes (Figure 48), one moderated with high-density polyethylene (HDPE) and one bare. The assembly consists of an outer tube housing an internal BF_3 detector. The moderated detector is surrounded by HDPE, while the bare detector is surrounded by air. The BF_3 gas pressure cannot be disclosed. The detector tubes are integrated with a data acquisition system based on a data logger for measurement recording.

The CRS-2000/B was tested at PTB using several of the ISO 8529-1 recommended monoenergetic neutron fields to determine its response as a function of neutron energy.

The device was also tested at CIEMAT-LPN using reference radiation fields from radionuclide sources. In the initial campaign, only a weak ^{241}Am-Be neutron source (11.1 GBq) was used. Other available neutron sources were utilized in a subsequent campaign. However, these calibration sources were generally too intense for the CRS-2000/B detectors, leading to saturation and linearity loss. Consequently, many measurements had to be repeated.

3.3.1 MC model description (CIEMAT)

The MCNP 6.2 code was used to simulate the CRS-2000/B system, employing the ENDF/B-VIII.0 cross-section library. Two types of simulations were performed to obtain and validate the detector response against measurements.

In the first type, the model of each detector tube was simulated in a vacuum and irradiated by a monoenergetic point source at 222 energies from the thermal range up to 100 MeV. This provided a high-resolution intrinsic response of the tubes (Figure 49). These simulations were complemented with others using the specific monoenergetic neutron energies corresponding to the PTB measurement campaign, which served for validation.

In the second type of simulation, the complete CRS-2000/B system was modelled within the CIEMAT-LPN irradiation room to replicate the experimental conditions. The results from these simulations were compared directly with the measurement data.

The MCNP model was developed based on information provided by the manufacturer. The composition of main materials (dry air, HDPE, 304 stainless steel) was sourced from the PNNL-15870 Rev. 1 Compendium. The simulated model is shown in Figure 48. Due to the proprietary nature of the device, the BF_3 gas pressure and ^{10}B enrichment are not disclosed.

3.3.1.1 Determination of the response function with MC

The response function, *R*, was calculated using Monte Carlo and is defined as the number of alpha-producing reactions in the gas volume, *M*, divided by the neutron fluence over the detector's face of interest:

$$R[\mathrm{cm}^2] = \frac{M}{\Phi_{\mathrm{MC}}}$$

Concerning the source term and the tallies (or MCNP estimators) employed in the simulations, two different models have been used. In the first one a point monoenergetic source has been considered, and in the second one the traditional plane-parallel monoenergetic source was employed. Both models produce similar results.

a) Point source model

The F4 tally with the FM4 multiplier was used. The FM4 card included the gas volume and a negative sign to multiply the fluence by the (n,α) reaction cross-section (MT=107) and the atom density simultaneously. A complementary simulation of the fluence in an equivalent air volume was necessary to normalize the result and obtain the response function.

b) Plane-parallel source model

This standard method uses a homogenous plane-parallel neutron field irradiating the detector surface for each energy. The source area is included in the FM factor.

The differences between the models are only significant for the aligned orientation. The responses shown in Figure 49 correspond to the plane-parallel simulation. The number of simulated particles was 10^7 – 10^8, yielding a statistical uncertainty below 2 % for most energies, increasing to 5 % for energies above 4 MeV.

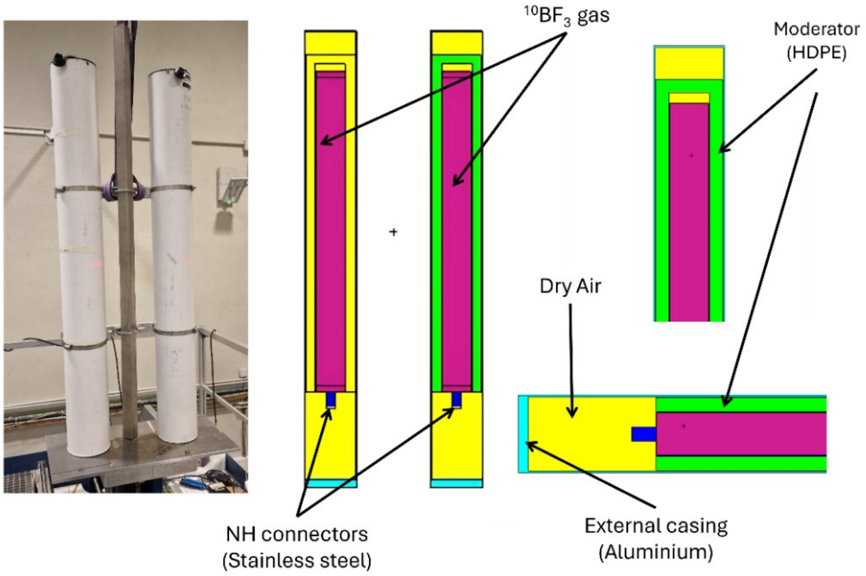

Figure 48. CRS-2000/B device (left) and the MCNP model (right) showing the relevant components.

The response functions for both tubes and different orientations are shown in Figure 49. Due to symmetry, an identical response is obtained for horizontal irradiation that is not aligned with the tube's axis. When the moderated tube is aligned with the irradiation axis, the response has a similar shape but lower magnitude. For the bare tube the response function essentially reflects the ^{10}B neutron absorption cross-section. The vertical orientation shows the characteristic 1/v dependence, while the aligned orientation shows a slightly shifted peak due to increased moderation along the detector's length.

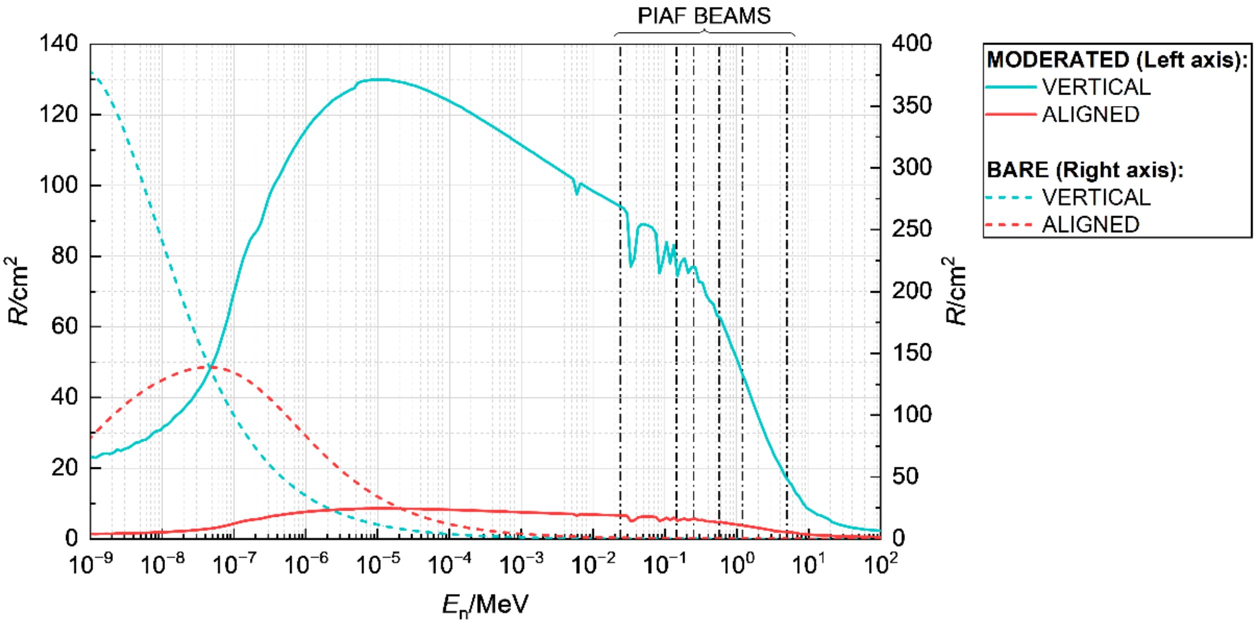

Figure 49. Response functions for the moderated and bare tubes of CRS-2000/B device, irradiated in vertical and aligned orientation.

3.3.1.2 Estimation of the response to CIEMAT-LPN neutron sources with MC

To complete the model validation, a series of simulations were performed to determine the CRS-2000/B response to the isotopic neutron sources at CIEMAT-LPN.

Two approaches were used:

1. **Intrinsic Response:** The same methodology for monoenergetic neutron fields was applied, convoluting the response function with the ISO spectrum of the neutron source. This provides results comparable to the direct contribution measured with the shadow cone technique.

2. **Full Facility Simulation:** A detailed model of the irradiation room, including the CRS-2000/B at the measurement position, was used. This simulation accounts for walls, floor, ceiling, air, and the irradiation bench, corresponding to the "direct + scatter" measurement condition without a shadow cone. Figure 50 show the detailed MCNP model of the CIEMAT-LPN facility

The results from these simulations were used to validate the CRS-2000/B model by comparison with experimental data from CIEMAT-LPN.

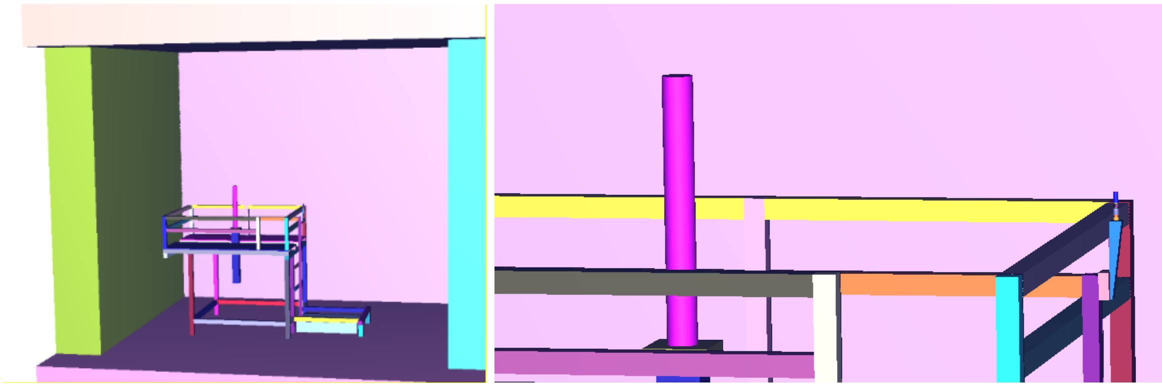

Figure 50. Left: Simulation of the CIEMAT-LPN facility showing the bench, storage pool, the ^{241}Am-Be neutron source, and the CRS-2000/B on the calibration bench. Right: Detailed view of the simulation, showing the CRS-2000/B detector on the calibration bench and the Am-Be source in its capsule holder.

3.3.2 Validation of MC model (CIEMAT) with measurements in neutron reference fields

3.3.2.1 Validation of CRS-2000/B response with monoenergetic neutrons at PIAF

A measurement campaign was conducted in March 2024 at PTB using the available ISO monoenergetic neutron fields (24 keV, 144 keV, 150 keV, 1.2 MeV, 5 MeV, see Table 9). The CRS-2000/B was tested in both vertical (Figure 51) and aligned orientations (Figure 52) with and without a shadow cone.

For each configuration, three measurements were derived: primary + scatter, scatter, and primary. The neutron monitor (NM) served as the reference for neutron fluence rate stability. The CRS-2000/B data logger recorded integrated counts NnCts (an extract is shown in Table 13) in a defined acquisition time NnET_sec, where *n* is the corresponding tube. Columns 1 and 2 correspond to the record number and date time (UTC).

Figure 51. Irradiation of the CRS-2000/B system with both tubes in vertical orientation and the corresponding shadow cone.

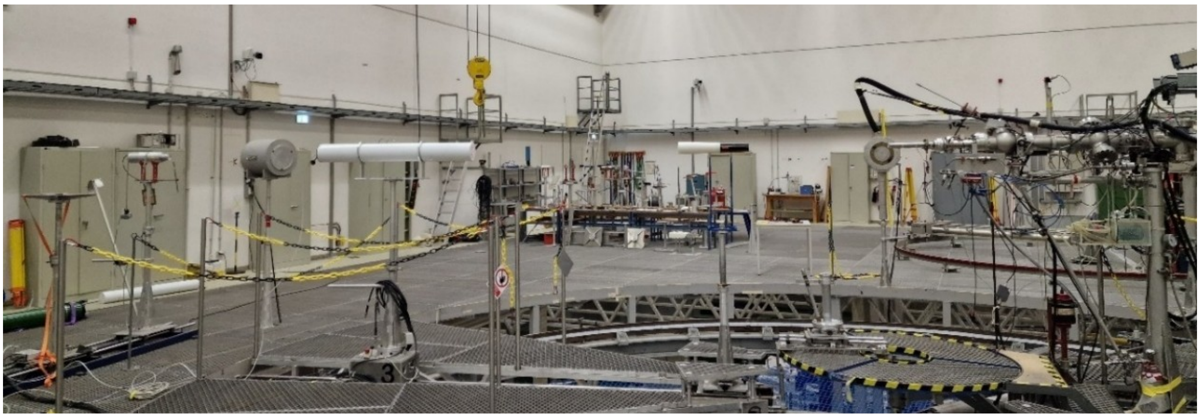

Figure 52. Irradiation of one detector of the CRS-2000/B system aligned with the ion beamline, neutron production target, and the shadow cone.

Table 13. Measurement data obtained from the data logger.

RecordNum	Date-Time (UTC)	Vbat	P1_mb	T1_C	N1Cts	N1ET_sec	P2_mb	T2_C	N2Cts	N2ET_sec
1	2024/02/13 20:43:24	15.305	1009	22.5	5	21	1009	-46.8	2	22
2	2024/02/13 20:44:00	15.306	1009	22.5	15	35	1009	-46.8	2	35
3	2024/02/13 20:46:00	15.306	1009	22.6	32	120	1009	-46.8	13	120
4	2024/02/13 20:48:00	15.306	1009.1	22.5	28	120	1009.1	-46.8	20	120
5	2024/02/13 20:50:00	15.306	1009	22.6	36	120	1009	-46.8	13	120
6	2024/02/13 20:52:00	15.306	1008.9	22.6	32	120	1008.9	-46.8	17	120
7	2024/02/13 20:54:00	15.306	1009	22.6	29	120	1009	-46.8	13	120
8	2024/02/13 20:56:00	15.306	1008.9	22.5	1763	120	1008.9	-46.8	448	120
9	2024/02/13 20:58:00	15.306	1008.9	22.6	4265	119	1008.9	-46.8	1135	120
10	2024/02/13 21:00:00	15.306	1008.9	22.6	4290	119	1008.9	-46.8	1208	120

The data provided by PTB includes the source, distance, irradiation time (expressed in 10 ms), readout of the NM with its uncertainty, NM rate, fluence with its uncertainty, and fluence rate, as can be seen in Table 14.

Table 14. Irradiation data provided by PTB during the measurements at PIAF facility.

Source	Contribution	Geometry	Distance [cm]	Irradiation time [10 ms]	NM	u(NM) [%]	NM rate	Phi [cm^{-2}]	u(Phi) [%]	Phi rate
250keV	primary+scatter	aligned-mod-nsc	589	84234	6141	0.0135	7.2906			
250keV	scatter	aligned-mod-sc	589	102381	7806	0.0122	7.6246			
250keV	primary	aligned-mod-nsc	589	84234	6141	0.0135	7.2906	243.30	2.70	0.289
250keV	primary+scatter	aligned-bare-nsc	589	152788	11194	0.0105	7.3266			
250keV	scatter	aligned-bare-sc	589	310058	22591	0.0080	7.2862			
250keV	primary	aligned-bare-nsc	589	152788	11194	0.0105	7.3266	443.49	2.63	0.290
250keV	primary+scatter	vertical-mod-nsc	646	240008	17978	0.0087	7.4907			
250keV	scatter	vertical-mod-sc	646	515855	39049	0.0068	7.5697			
250keV	primary	vertical-mod-nsc	646	240008	17978	0.0087	7.4907	587.21	2.69	0.245
250keV	primary+scatter	vertical-bare-nsc	646	240008	17978	0.0087	7.4907			
250keV	scatter	vertical-bare-sc	646	515855	39049	0.0068	7.5697			
250keV	primary	vertical-bare-nsc	646	240008	17978	0.0087	7.4907	587.21	2.69	0.245

The experimental response, R_{exp}, was calculated as:

$$R_{exp} = \left({}^{M_T}/_{NM_T} - {}^{M_{SC}}/_{NM_{SC}} \right) * {}^{NM_T}/_{\dot{\Phi}}$$

Where M_T and M_{SC} are the counts per second for the total contribution (primary + scatter) and for the scatter contribution (measurements with shadow cone) respectively. The same definition is applied to NM_T and NM_{SC} for the Neutron Monitor rates. Finally, $\dot{\Phi}$ corresponds to the fluence rate.

Table 15. CRS-2000/B response to monoenergetic neutron fields measured at PTB and simulated with MCNP.

	moderated vertical				bare vertical			
Energy [keV]	**R_{exp}**	**$u(R_{exp})$ [%]**	**R_{MC}**	**$u(R_{MC})$ [%]**	**R_{exp}**	**$u(R_{exp})$ [%]**	**R_{MC}**	**$u(R_{MC})$ [%]**
144	76.37	3.33	74.23	3.00	1.72	4.86	0.10	3.00
250	75.45	3.42	76.86	3.00	1.20	5.17	0.09	3.00
1200	32.32	2.95	46.68	3.00	0.69	3.69	0.01	3.00
5000	20.76	6.86	17.05	3.00	3.66	7.15	0.03	3.00
	moderated aligned				**bare aligned**			
Energy [keV]	**R_{exp}**	**$u(R_{exp})$ [%]**	**R_{MC}**	**$u(R_{MC})$ [%]**	**R_{exp}**	**$u(R_{exp})$ [%]**	**R_{MC}**	**$u(R_{MC})$ [%]**
150	6.87	3.72	5.05	3.00	-0.33	4.77	0.10	3.00
250	6.57	3.60	5.54	3.00	-0.22	5.31	0.07	3.00
1200	2.74	3.00	3.73	3.00	-1.14	2.93	0.02	3.00

The measured responses were compared with MCNP simulations (R_{MC}) in

Table **15**. Following the definitions employed in previous sections, the ratio S_0 was used for validation (see

Table **16**):

$$S_0 = \frac{R_{MC}}{R_{exp}}$$

where:

- R_{MC} corresponds to the MC calculation for the response of the detector to the specified energy.
- R_{exp} is the experimental detector response to such energy.

Good agreement was found for the moderated tube in the vertical orientation across energies (Figure 53). As in Section 3.2.2 for the CRS-1000 device, the response of the bare tube is limited to thermal neutrons, and the readouts obtained with and without shadow cone are essentially the same. This explains the S_0 values close to zero observed in

Table **16**. Figure 54 highlights that the available monoenergetic energies were insufficient to fully characterize the detector's epithermal response.

Table 16. Ratios between the simulated response to monoenergetic neutrons and the readouts for each orientation (vertical and aligned) and each tube (moderated and bare).

	moderated vertical		**bare vertical**	
Energy [keV]	**S_0**	**$u(S_0)$ [%]**	**S_0**	**$u(S_0)$ [%]**
144	0.97	4.48	0.02	5.71
250	1.02	4.55	0.02	5.98
1200	1.44	4.21	0.01	4.76
5000	0.82	7.49	0.21	7.76
	moderated aligned		**bare aligned**	
Energy [keV]	**S_0**	**$u(S_0)$ [%]**	**S_0**	**$u(S_0)$ [%]**
150	0.74	4.78	-0.30	5.63
250	0.84	4.68	-0.04	6.10
1200	1.36	4.24	-0.30	4.19

The uncertainties considered in the results shown in

Table **16** have the following components:

- Combined uncertainty of the neutron fluence provided by PTB: ~3 % (except for 5 MeV: 6.75 %)
- Statistical uncertainty of MC calculation: < 0.5 %
- Estimated systematic uncertainty of the MC model: 3 %
- Statistical uncertainty of measurements with CRS-2000/B: < 2 %

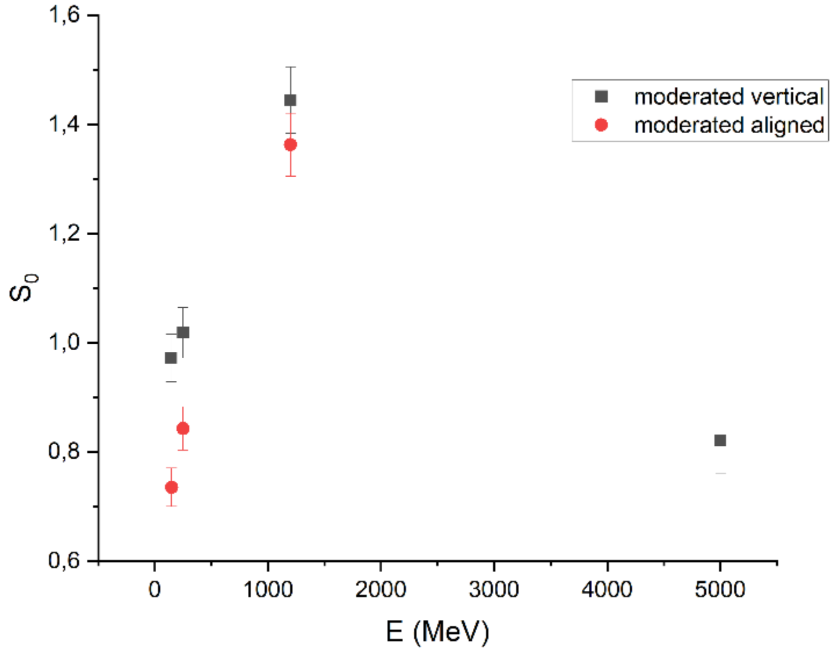

Figure 53. Ratios comparing measurements and simulations for moderated tube in different orientations, and irradiated with 144 keV, 250 keV, 1.2 MeV and 5 MeV.

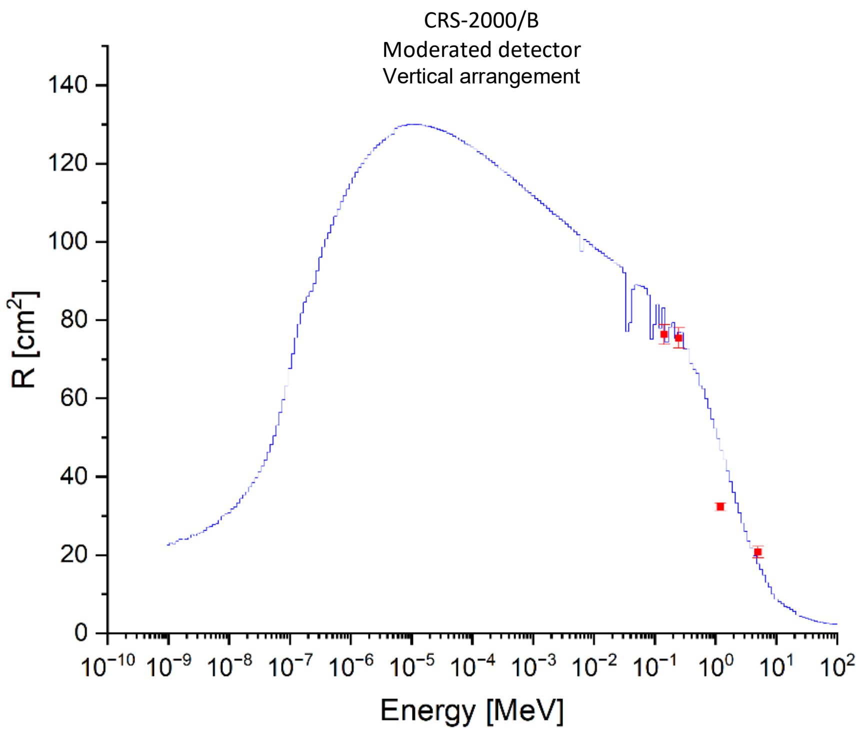

Figure 54. Response simulated for the CRS-2000/B with the experimental results obtained from the irradiations with monoenergetic neutrons superimposed covering only the high energy part of the response function.

3.3.2.2 Validation of CRS-2000/B response with isotopic neutron sources at CIEMAT

Two measurement campaigns were conducted at CIEMAT-LPN using different neutron sources. The measurements followed a similar methodology to the PTB campaign, irradiating both the moderated and bare tubes in various orientations (horizontal/perpendicular and aligned).

^{241}Am-Be source (AmBe-3):

- Type: Eckert & Ziegler AM1.N09
- Capsule: N09, Ø17.4 mm × 19.2 mm (H)
- Activity: 11.1 GBq (0.3 Ci)
- Emission Rate: 6.343 × 10^5 s^{-1} ± 1.4 % (k = 2) on 8 Aug 2024
- Emission Anisotropy @ 90°: 1.068 ± 0.45 % (k = 1)
- Fluence Rate @ 200 cm: 1.35 cm^{-2} s^{-1} ± 0.8 % (k = 1)

^{241}Am-Be source (AmBe-1):

- Type: AM1.N20
- Capsule: N09, Ø19.1 mm × 48.6 mm (H)
- Activity: 185 GBq (5 Ci)
- Emission Rate: 1.09 × 10^7 s^{-1} ± 1.4 % (k = 2) on 8 Aug 2024
- Fluence Rate @ 200 cm: 23.12 cm^{-2} s^{-1} ± 0.8 % (k = 1)

^{252}Cf source (Cf1):

- Type: QSA X1
- Capsule: X1, Ø7.9 mm × 10.15 mm (H)
- Activity: 5 GBq (136 µg)
- Emission Rate: 2.26 × 10^7 s^{-1} ± 1.30 % (k = 1) on 8 Aug 2024
- Emission Anisotropy @ 90°: 1.0502 ± 1.7 % (k = 1)
- Fluence Rate @ 200 cm: 47.22 cm^{-2} s^{-1} ± 2.2 % (k = 1)

3.3.2.2.1 Initial validation and challenges

The first campaign used the weak AmBe-3 source at 200 cm with a shadow object (see Figure 55). The experimental response was calculated as:

$$R_{exp} = \frac{M_T - M_{SC}}{\dot{\Phi}}$$

where *M* is the count rate with (SC) and without (T) the shadow cone, and $\dot{\Phi}$ is the fluence rate.

Table 17. Results for AmBe-3 source at 200 cm.

Am-Be	R_{exp} [cm²]	u(R_{exp}) [%]	R_{MC} [cm²]	u(R_{MC}) [%]	S_0
moderated aligned	5.17	1.61	8.65	0.98	1.67
bare aligned	25.33	1.16	0.07	1.10	0.00
moderated vertical	26.71	2.13	86.04	0.35	3.22
bare vertical	-0.32	1.80	0.07	0.45	-0.21

As in previous devices, the comparison with MC simulations showed poor agreement (Table 17), likely due to shadow object performance, as the signal is dominated for the low energy neutron scattering background.

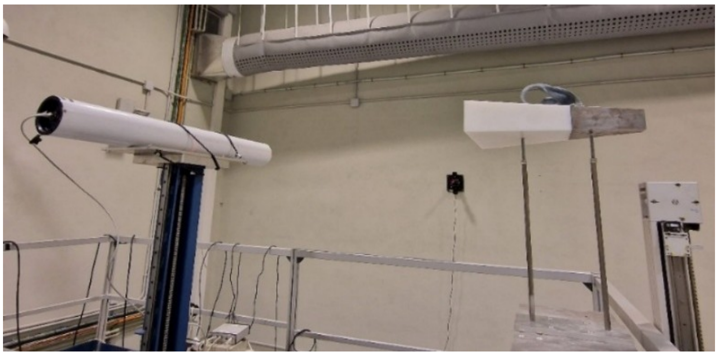

Figure 55. Pyramid cone used during measurements in horizontal orientation.

3.3.2.2.2 Improved agreement with full-simulation approach

Agreement improved significantly when total measurements (without shadow cone) were compared against full-facility MC simulations (which model walls, air, bench, etc.). Data from the first campaign and a more extensive second campaign with the AmBe-3 source at multiple distances (Table 18 and Figure 57 top) yielded consistent scaling factors:

$$\bar{S}_0\,(\text{mod}) = 1.35 \pm 4.8\ \%$$

$$\bar{S}_0\,(\text{bare}) = 1.61 \pm 2.1\ \%$$

The difference between these two values is consequence of the simulation of the laboratory. A discrepancy in the simulated thermal neutron spectrum was identified via Bonner Sphere Spectrometer (BSS) comparisons at 115 cm (

Figure **56**). The simulation overestimates the thermal contribution in a factor of S_{MC} = 0.83 ± 6.25 %.

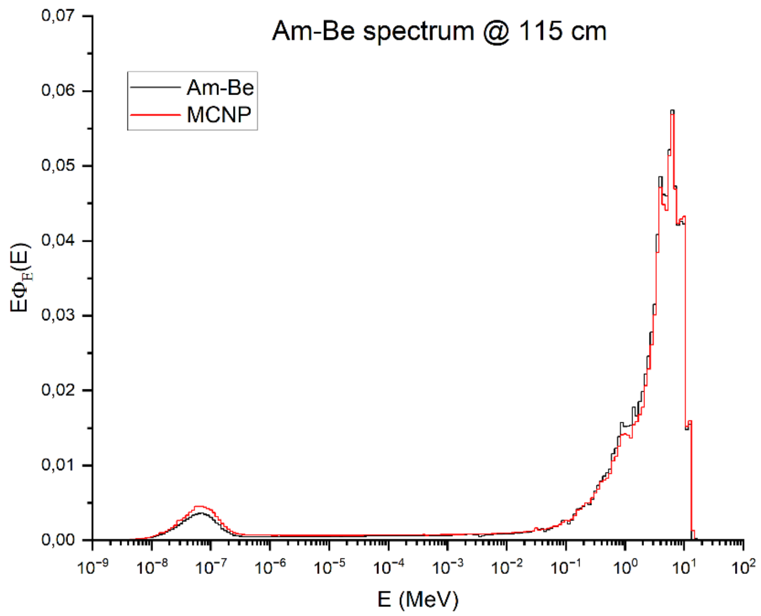

Figure 56. Am-Be spectrum measured with BSS and simulated with MCNP.

Applying a thermal correction factor (S_{MC} = 0.83 ± 6.25 %) to the bare detector simulation is obtained:

$$\bar{S}_0^* \text{ (bare)} = 1.34 \pm 6.6\ \%$$

And the mean value for both moderated and bare detectors is then:

$$\bar{S}_0^* = 1.34 \pm 3.6\ \%$$

The final results obtained for the AmBe-3 source, for the moderated and the bare tube, after applying the thermal correction, are shown in Figure 57 bottom.

Table 18. Results for AmBe-3 with irradiations at different distances.

Tube	Geometry	Distance [cm]	M_{exp} [CPS]	u(M_{exp}) [%]	M_{MC} [CPS]	u(M_{MC})	S_0	u(S_0) [%]
moderated	vertical	300	71.98	0.88	97.02	5.05	1.35	5.56
bare	vertical	300	34.47	1.55	56.08	5.03	1.63	5.69
moderated	aligned	250	59.51	0.89	83.72	5.05	1.41	5.57
bare	aligned	250	34.32	1.83	54.86	5.03	1.60	5.77
moderated	vertical	250	80.13	1.58	105.31	5.04	1.31	5.71
bare	vertical	250	34.64	2.00	56.26	5.03	1.62	5.83
moderated	aligned	200	64.21	1.16	88.72	5.05	1.38	5.61
bare	aligned	200	35.01	1.78	54.95	5.03	1.57	5.76
moderated	vertical	200	93.05	0.95	121.65	5.00	1.31	5.53
bare	vertical	200	34.53	1.94	56.16	5.03	1.63	5.81
moderated	aligned	150	73.44	1.26	102.64	5.04	1.40	5.63
bare	aligned	150	35.14	2.00	55.36	5.03	1.58	5.47
moderated	vertical	150	120.85	1.05	155.27	5.03	1.28	5.58
bare	vertical	150	34.83	1.97	56.59	5.03	1.62	5.82

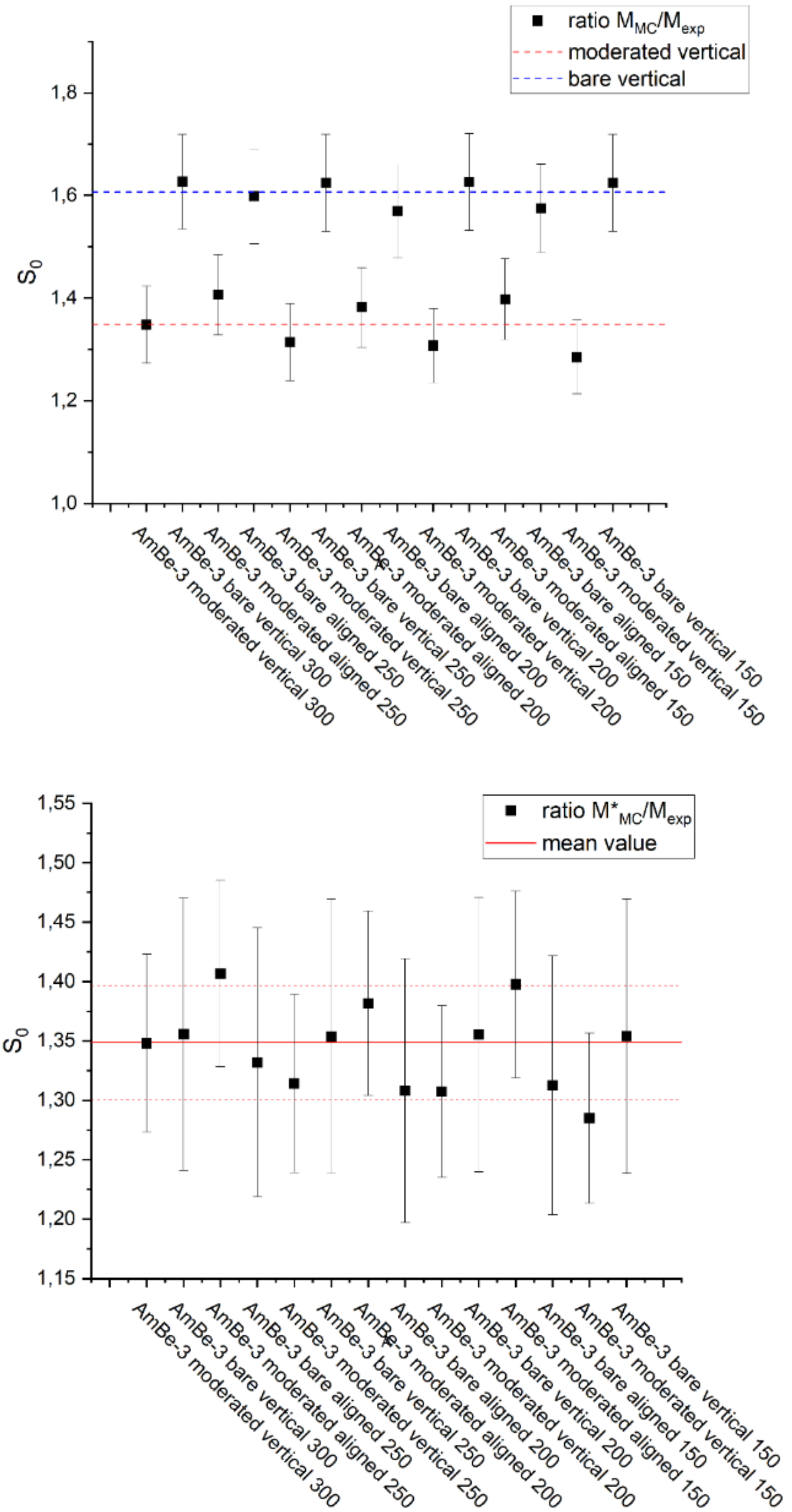

Figure 57. Top: Results for AmBe-3 before thermal correction. Bottom: Final results for AmBe-3 after applying the thermal correction.

3.3.2.2.3 Non-Linearity and final model validation

Measurements with more intense calibration sources (AmBe-1, Cf, D_2O-Cf, H_2O-Cf) revealed count rate saturation and non-linearity issues (Table 19). As can be seen, the count rate for AmBe-1 is nine times higher than for AmBe-3 but the relation between emission rates is 17.15. To solve this issue.

In Figure 58 is presented the ratio S_0 versus the experimental count rate, showing an exponential behaviour. An empirical linearity correction factor S_L, dependent on count rate, was derived from the data.

Table 19. Results for all the calibration sources at 200 cm.

Source	Geometry	M_{exp} [CPS]	$u(M_{exp})$ [%]	M_{MC} [CPS]	$u(M_{MC})$	S_0^*	S_L	$S_0^* \cdot S_L \cdot M_{exp}/M_{MC}$
AmBe-3	aligned-mod	64.21	1.16 %	88.72	5.05 %	1.38		1.03
AmBe-3	aligned-bare	35.01	1.78 %	45.79	5.03 %	1.31		0.98
AmBe-3	vertical-mod	93.05	0.95 %	121.65	5.00 %	1.31		0.98
AmBe-3	vertical-bare	34.53	1.94 %	46.80	5.03 %	1.36		1.01
AmBe-1	aligned-mod	532.94	0.35 %	1521.75	5.05 %	2.86	2.67	1.07
AmBe-1	aligned-bare	381.98	0.97 %	785.36	5.03 %	2.06	1.93	1.06
AmBe-1	vertical-mod	627.65	1.29 %	2086.51	5.00 %	3.32	3.56	0.93
AmBe-1	vertical-bare	379.01	0.47 %	802.67	5.03 %	2.12	1.92	1.10
Cf	aligned-mod	713.09	0.15 %	3521.52	5.04 %	4.94	4.89	1.01
Cf	aligned-bare	562.89	0.95 %	1788.49	5.02 %	3.18	2.90	1.10
Cf	vertical-mod	784.10	0.11 %	4997.80	5.03 %	6.37	6.59	0.97
Cf	vertical-bare	573.29	0.21 %	1807.67	5.02 %	3.15	2.99	1.05
D2O-Cf	aligned-mod	740.34	0.14 %	4154.14	5.14 %	5.61	5.47	1.03
D2O-Cf	aligned-bare	692.69	0.14 %	3221.79	5.11 %	4.65	4.52	1.03
D2O-Cf	vertical-mod	838.18	0.10 %	7263.23	5.12 %	8.67	8.42	1.03
D2O-Cf	vertical-bare	725.50	0.12 %	3565.52	5.10 %	4.91	5.14	0.96
H2O-Cf	aligned-mod	499.60	1.15 %	1050.38	5.41 %	2.10	2.45	0.86
H2O-Cf	aligned-bare	539.83	0.27 %	1945.84	5.26 %	3.60	2.72	1.33
H2O-Cf	vertical-mod	656.24	0.13 %	1835.04	5.33 %	2.80	3.94	0.71
H2O-Cf	vertical-bare	648.26	0.81 %	2658.67	5.17 %	4.10	3.83	1.07

The final validation involved correcting the MC-to-measurement ratio using both the unified scaling factor ($\bar{S}_0^*$) and the linearity factor (S_L). The resulting values for all sources at 200 cm are shown in the last column of Table 19 and Figure 59. After these corrections, the agreement between simulation and experiment is statistically acceptable for most sources, validating the CRS-2000/B model. The H_2O-Cf source showed the poorest fit, indicating a need for further refinement in simulating its significant thermal neutron component.

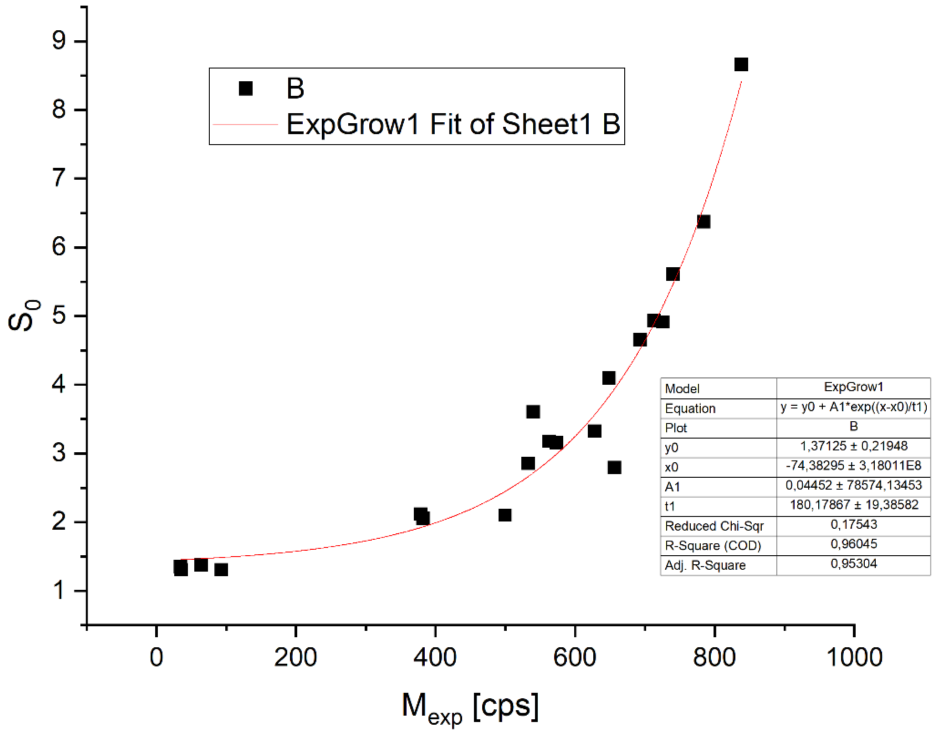

Figure 58. Loss of linearity for calibration sources: Am-Be, Cf, D_2O-Cf, and H_2O-Cf.

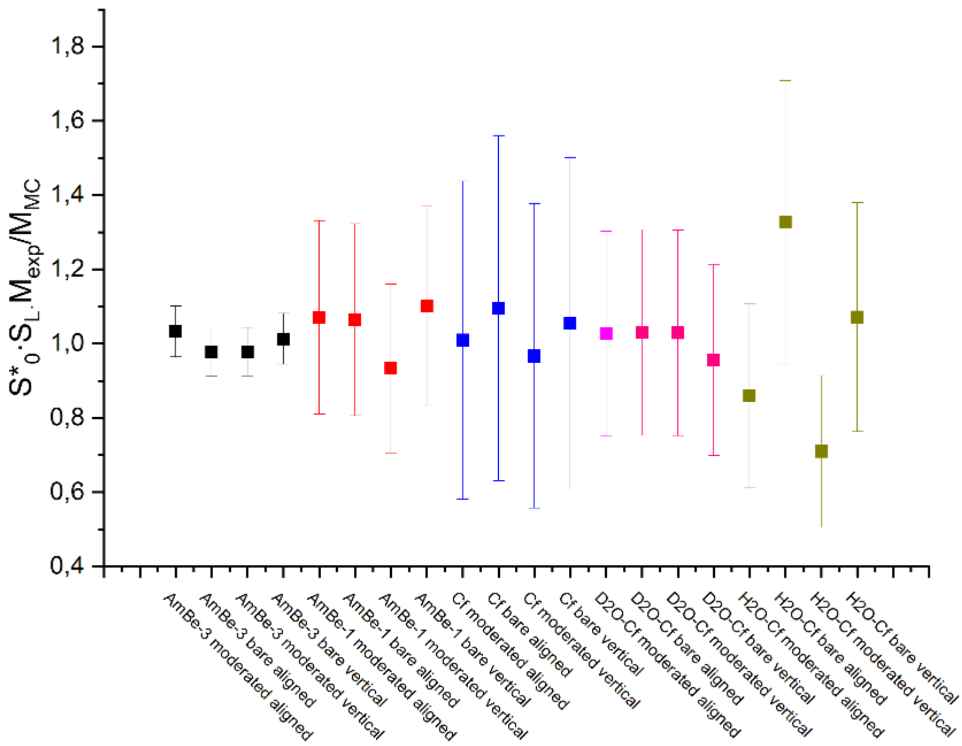

Figure 59. Final corrected ratios comparing measurements and MCNP simulations for all sources at 200 cm.

3.4 StyX Neutronica – System S1

As previous devices, System S1 detector, developed by StyX Neutronica GmbH (Germany), is a boron-lined proportional counter optimized for thermal neutron detection while maintaining low sensitivity to gamma radiation. Neutron capture occurs via the nuclear reaction:

$$^{10}B + {}^{1}n \rightarrow {}^{7}Li + \alpha + 2.79\ MeV$$

The resulting charged particles (alpha and lithium ions) ionize the detector gas upon escaping the converter layer, generating electrical pulses.

The detector consists of an aluminium tube 1250 mm in length, with an outer diameter of 56 mm and an inner diameter of 50 mm. The inner surface of the tube is coated with a 50 µm layer of high-purity copper onto which a 1.5 µm film of boron carbide (B_4C) enriched to 96 % in ^{10}B is sputtered. The gas filling is an argon–carbon dioxide mixture in a 90:10 ratio, optimized for proportional amplification and charge collection. The system is surrounded with a high-density polyethylene (HDPE) moderator to thermalize incoming neutrons.

The detector is protected by a 1 mm thick AlMg3 aluminium alloy sheet, which is internally coated with a Gd_2O_3-based paint. This gadolinium oxide layer, with an effective thickness of 200–250 µm, provides additional shielding by capturing thermal neutrons and thereby reducing background from scattered low-energy neutrons.

The detector outputs raw interaction pulses via a standard BNC connector, allowing connection to external acquisition systems. In this setup, the signals were recorded using a multichannel analyzer (MCA), enabling the acquisition of pulse-height spectra. The spectrum shows a broad energy distribution due to the varying escape depths of the reaction products within the gas volume. Discrimination from gamma-ray background is achieved by applying appropriate threshold settings.

3.4.1 MC model (PTB)

The S1 detector, developed by StyX Neutronica (Figure 60), is a boron-lined proportional counter optimized for thermal neutron detection. Its response function was calculated using the MCNP neutron transport code (v6.1.0), with the ENDF/B-VIII.0 cross-section library at 293.6 K and S(α,β) thermal scattering treatment. The modelling approach follows the methodology applied for the CRS-1000 system (see Section 3.2) but adapted to the specific geometry and materials of the S1. Unlike previous systems, all technical details of the detector geometry, materials, and construction were directly provided by the manufacturer, eliminating uncertainties associated with estimations. The key materials used in the MCNP model are the following:

- **Active medium:** Ar/CO_2 gas mixture (90:10), density 4.46×10^{-4} g/cm³.
- **Converter layer:** Boron carbide (B_4C), 96 % ^{10}B enriched, density 2.45 g/cm³.
- **Inner coating:** High-purity copper, density 8.96 g/cm³.
- **Detector housing:** Aluminium (pure), density 2.7 g/cm³.
- **External shield:** $AlMg_3$ alloy, density 2.66 g/cm³.
- **Moderator:** High-density polyethylene (CH_2), density 0.961 g/cm³.

- **Neutron absorber layer:** Gadolinium oxide (Gd_2O_3), density 7.41 g/cm³.
- **Internal air gap** / Gd_2O_3
- **World:** Dry air, density 1.29 × 10^{-3} g/cm³. Composed of 0.0124 % C, 75.527 % N, 23.18 % O, 1.28 % Ar.

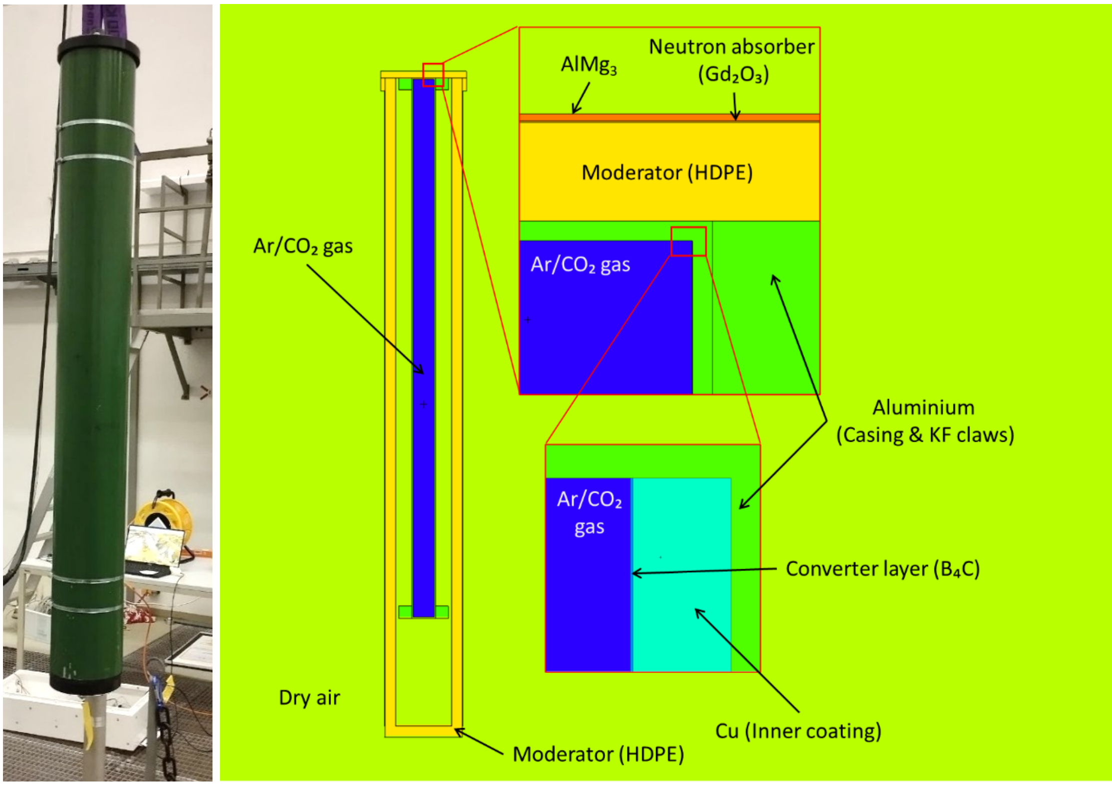

Figure 60. S1 system (left picture) and MCNP model (right picture).

A total of 163 monoenergetic neutron energies, ranging from thermal up to 100 MeV, were simulated using a plane-parallel source. This finer energy resolution allows a more detailed characterization of the detector response, particularly in the resonance region. The response function was calculated for two irradiation geometries: with the neutron field perpendicular to the detector's axis (SIDE configuration) and parallel to it (TOP configuration), and the results are shown in Figure 61.

Instead of tallying neutron capture reactions directly in the B_4C layer, the number of alpha particles reaching the gas volume was recorded using F4 tallies. This approach assumes that all detectable signals originate from alpha particles produced in the $^{10}B(n,\alpha)^7Li$ reaction, and that these alphas are fully stopped within the counting gas, contributing to the signal.

The neutron fluence was scored on the surface of the HDPE moderator block corresponding to each irradiation orientation. The response function R was defined as in previous cases:

$$R[\mathrm{cm}^2] = \frac{M}{\Phi_{\mathrm{MC}}}$$

where M is the number of alpha particles reaching the gas volume, and Φ_{MC} is the incident neutron fluence on the corresponding surface.

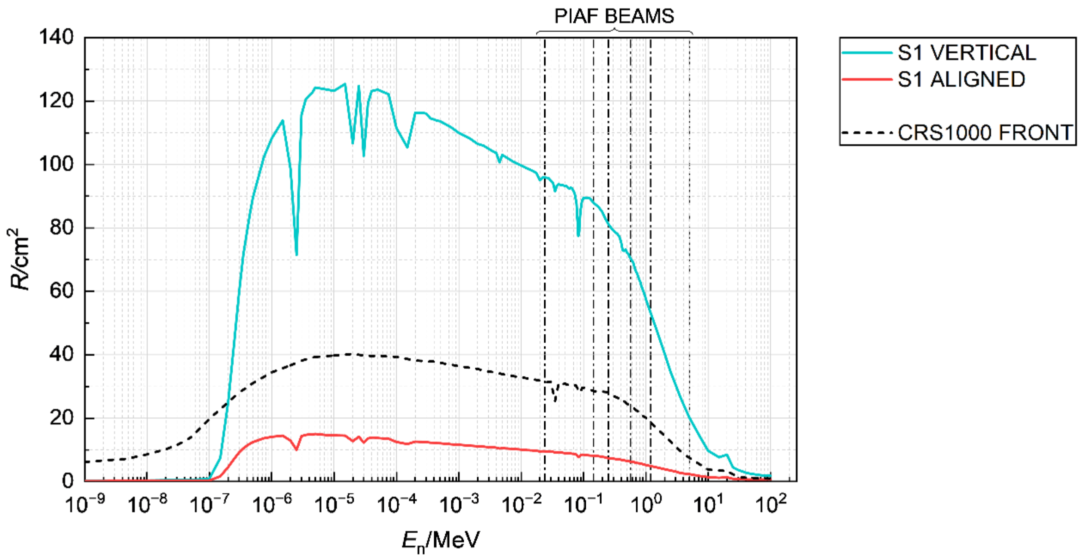

Figure 61. Response functions calculated with MCNP for the S1 system irradiated from the side (blue) and from the top (red). The CRS-1000 response (front orientation) is included for comparison (dashed lines).

3.4.2 Validation of MC model in the monoenergetic neutron fields (PTB)

As in previous sections, the MCNP model was validated by comparing simulation results with measurements performed in monoenergetic neutron reference fields at PTB (PIAF facility). In this case, the detector was irradiated with five neutron energies ranging from 144 keV to 5 MeV (the 24 keV field was not included; see Table 9).

During the measurements, the detector was placed 6 m from the neutron production target at a neutron emission angle of 0° (see Figure 62). Due to the inherently low detection efficiency observed in the TOP configuration (detector placed parallel to the ion beamline axis), only the SIDE configuration (detector placed perpendicular to the ion beamline axis, i.e. the detector was "standing" in its working position) was used for experimental characterisation.

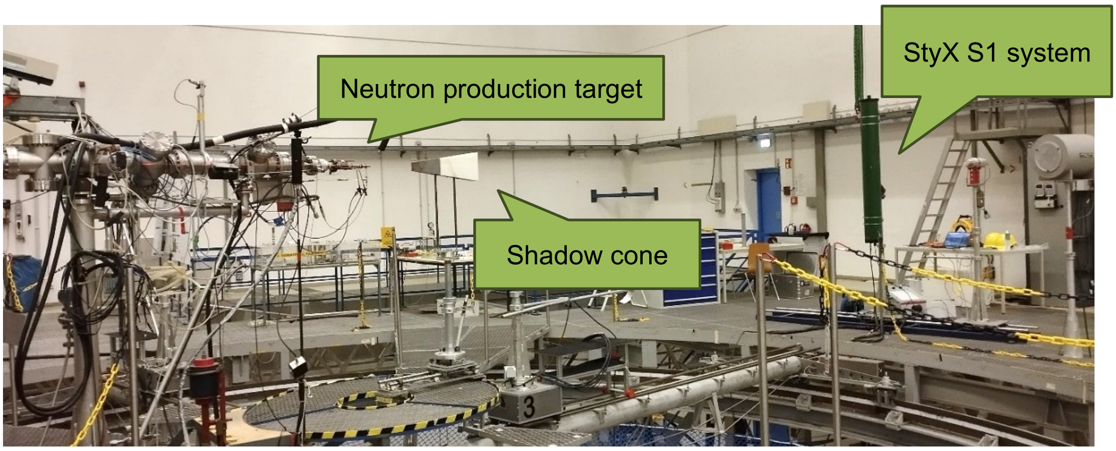

Figure 62. StyX Neutronica S1 and shadow cone in a typical experimental configuration at PIAF. The S1 device is placed 6 meters from the neutron production target.

The high sensitivity of the device, which was originally designed for low-fluence rate outdoor neutron environments, led to saturation of the internal data logger at counting rates above 20 counts per second. This limitation made it unfeasible to operate the system directly under the higher neutron fluence rate conditions present at the accelerator facility. To overcome this constraint and enable measurements at higher neutron fluences, an external multichannel analyser (FAST ComTec MCA4) was used to acquire detector signals, allowing the system to operate well beyond the saturation threshold of the original electronics.

As in previous cases, the shadow cone method (see Figure 62) was used to determine the neutron scattering background. The results indicated that, with the inclusion of the Gd neutron absorber layer in this system, the background contribution was reduced to approximately 20 %.

In addition to the experimental response, the device response to the monoenergetic neutron fields at PIAF was simulated for all irradiation configurations. To simulate the experimental conditions accurately, the neutron source was modelled with a Gaussian energy distribution with a variable full width at half maximum (FWHM) as follows:

- 1.2MeV → 100 keV FWHM
- 5 MeV → 200 keV FWHM
- Other energies → 15 keV FWHM

As in previous sections, to assess the agreement between experiment and simulation, a dimensionless ratio (S_0) was defined:

$$S_o = \frac{R_{\mathrm{MC}}}{R_{exp}}$$

Where R_{MC} is the simulated response and R_{exp} is the experimental response.

Following the same procedure that has been indicated with the previous probes, the mean $\bar{S}$ of 4 S_o values was calculated (the outlier for 1.2 MeV was excluded), and the standard deviation was used as estimation of $\bar{S}$ uncertainty:

$$\bar{S} = 1.28 \pm 6\ \%$$

To correct for this, $\bar{S}$ is introduced as a scaling factor, modifying the Monte Carlo to experimental measurement ratio:

$$S = \frac{R_{\mathrm{MC}}/\bar{S}}{R_{exp}}$$

The MC to measurement ratio is plotted in Figure 63, following the same protocol as in Section 3.2.2). Table 20 summarize the experimental (R_{exp}) and simulated (R_{MC}) responses for each configuration, along with the corresponding S_0 and corrected S values, including relative uncertainties.

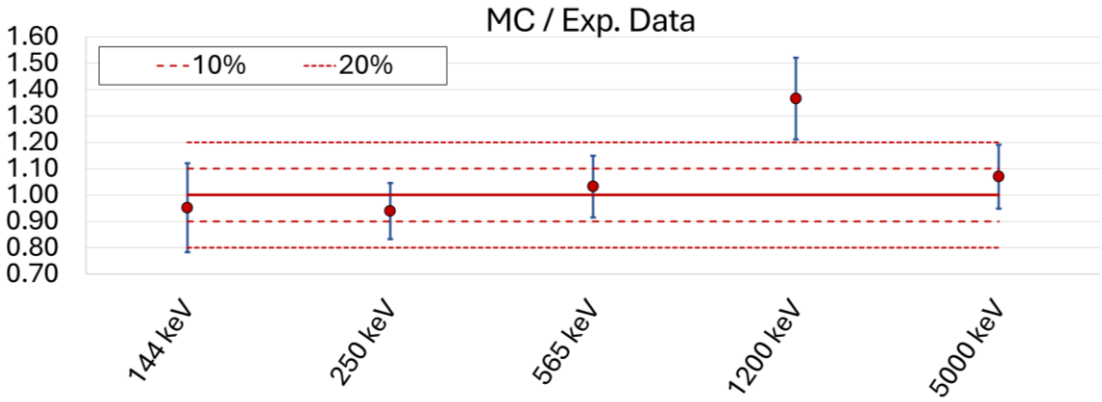

Figure 63. MC to measurement ratio for all energies (see Table 20). The error bars correspond to the *k* = 1, i.e. ~68 % coverage for normal distribution.

Table 20. Summary of the experimental response (R_{exp}), the simulated response (R_{MC}) and the MC to measurement ratio before (S_o) and after (S) the adjustment by the scaling factor $\bar{S}$. All the quantities are written with the corresponding uncertainties.

	E_n / MeV	R_{MC} / cm^2	$u_{R_{MC}}$	R_{exp} / cm^2	$u_{R_{exp}}$	S_o	u_{S_o}	S	u_S
	0.144	87.97	0.002	72.09	0.03	1.22	0.04	0.95	0.08
	0.250	82.04	0.002	68.15	0.06	1.20	0.07	0.94	0.10
FRONT	0.565	70.68	0.002	53.41	0.03	1.32	0.04	1.03	0.09
	1.2	53.82	0.002	30.74	0.08	1.75*	0.14	1.37*	0.17
	5.0	20.42	0.004	14.89	0.22	1.37	0.31	1.07	0.32

3.4.3 Validation of MC model in broad range neutron fields (PTB)

To validate the MC model and extend the characterization of the device to a broader energy range, including the low-energy region, the detector was irradiated with three reference neutron sources based on radionuclides. These measurements were conducted at three source-to-detector distances: 120 cm, 170 cm, and 220 cm, measured from the centre of the neutron source to the centre of the detector. The characteristics of the sources are the same as those described in Section 3.2.3.

As in the case of the CRS-1000 system, the MCNP geometry of the StyX S1 detector was included in the validated simulation of the entire experimental room (Figure 64). Additionally, a correction factor accounting for the thermal neutron component was applied, as shown in Figure 46.

The data processing followed the methodology previously described in Section 3.2.3. A dimensionless ratio S_o was defined from the counting rate in counts per second (cps) as:

$$S_o = \frac{cps_{\mathrm{MC}}}{cps_{exp}}$$

where:

- cps_{MC} = Simulated counting rate,
- c_{exp} = Experimental counting rate.

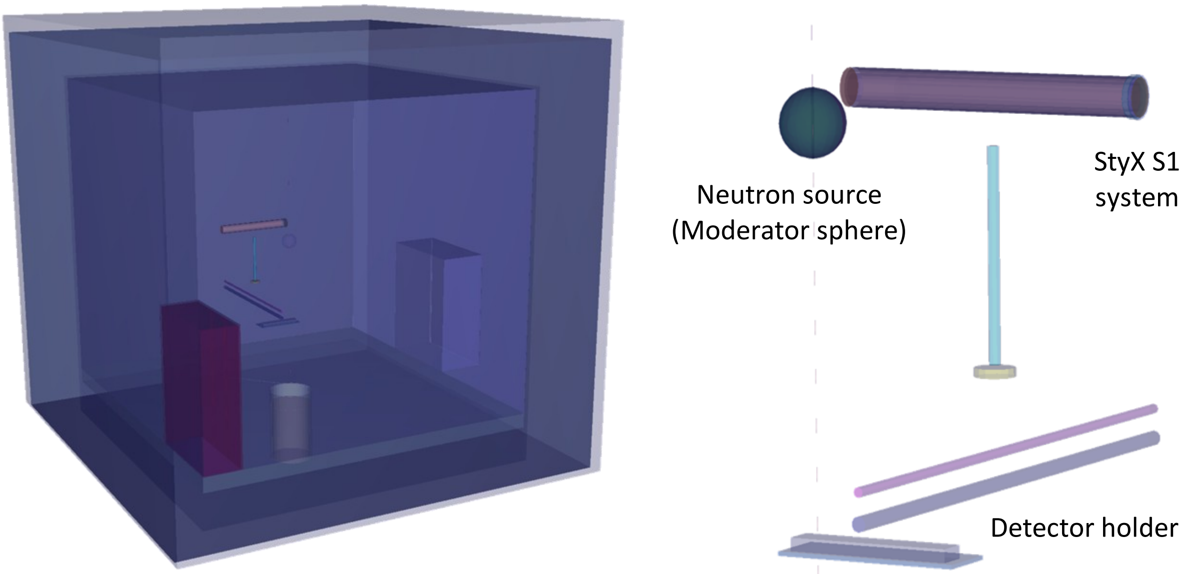

Figure 64. PTB MCNP model for the irradiation room showing the main elements.

The average value $\bar{S}$ was determined from 16 reference irradiations, with the standard deviation used to estimate the uncertainty, yielding:

$$\bar{S} = 1.26 \pm 12\ \%$$

The simulation-to-measurement ratio for different irradiation setups was then recalculated using the corrected expression:

$$S = \frac{cps_{\mathrm{MC}}/\bar{S}}{cps_{exp}}$$

Table **21** summarizes the experimental (cps_{exp}) and simulated (cps_{MC}) counting rates for each configuration, along with the corresponding S_o and corrected S values, including relative uncertainties.

The corrected *S* values are presented in Figure 65, with error bars indicating k = 1 (~68 % confidence level for a normal distribution).

Considering all irradiation scenarios (monoenergetic neutron fields and radionuclide sources, see Tables 20 - 21), the global scaling factor for the MC model obtained is:

$$\bar{S}_{tot} = 1.27 \pm 11\ \%$$

Table 21. Summary of the experimental counts-per-second (cps_{exp}), the simulated counts-per-second (cps_{MC}) and the MC to measurement ratio before (S_o) and after (S) the adjustment by the scaling factor $\bar{S}$, for each irradiation configuration. All the quantities are written with the corresponding uncertainties.

	Source	Distance	cps_{MC}	$u_{cps_{MC}}$	cps_{exp}	$u_{cps_{exp}}$	S_o	u_{S_o}	S	u_S
SIDE	Am-Be	120 cm	799.18	0.01	386.34	0.01	1.43	0.02	1.13	0.12
		170 cm	548.17	0.01	557.87	0.02	1.42	0.01	1.12	0.12
		220 cm	440.90	0.01	312.49	0.01	1.41	0.01	1.12	0.12
	Cf-252 (Bare)	120 cm	23.49	0.01	14.32	0.01	1.15	0.01	0.91	0.12
		170 cm	15.45	0.01	20.37	0.01	1.08	0.01	0.85	0.12
		220 cm	12.40	0.01	11.28	0.01	1.10	0.01	0.87	0.12
	Cf-252 (Mod)	120 cm	37.25	0.01	16.69	0.01	1.44	0.01	1.14	0.12
		170 cm	23.25	0.01	25.80	0.01	1.39	0.01	1.10	0.12
		220 cm	16.10	0.01	12.65	0.01	1.27	0.01	1.01	0.12
TOP	Am-Be	170 cm	340.71	0.01	243.86	0.01	1.40	0.01	1.10	0.12
	Cf-252 (Bare)	120 cm	19.80	0.01	9.74	0.01	1.25	0.01	0.99	0.12
		170 cm	9.93	0.01	15.89	0.01	1.02	0.01	0.81	0.12
		220 cm	8.23	0.02	7.91	0.01	1.04	0.01	0.82	0.12
	Cf-252 (Mod)	120 cm	31.35	0.01	9.49	0.01	1.70	0.01	1.34	0.12
		170 cm	12.91	0.01	18.50	0.01	1.36	0.02	1.07	0.12
		220 cm	9.22	0.02	7.63	0.01	1.21	0.01	0.96	0.12

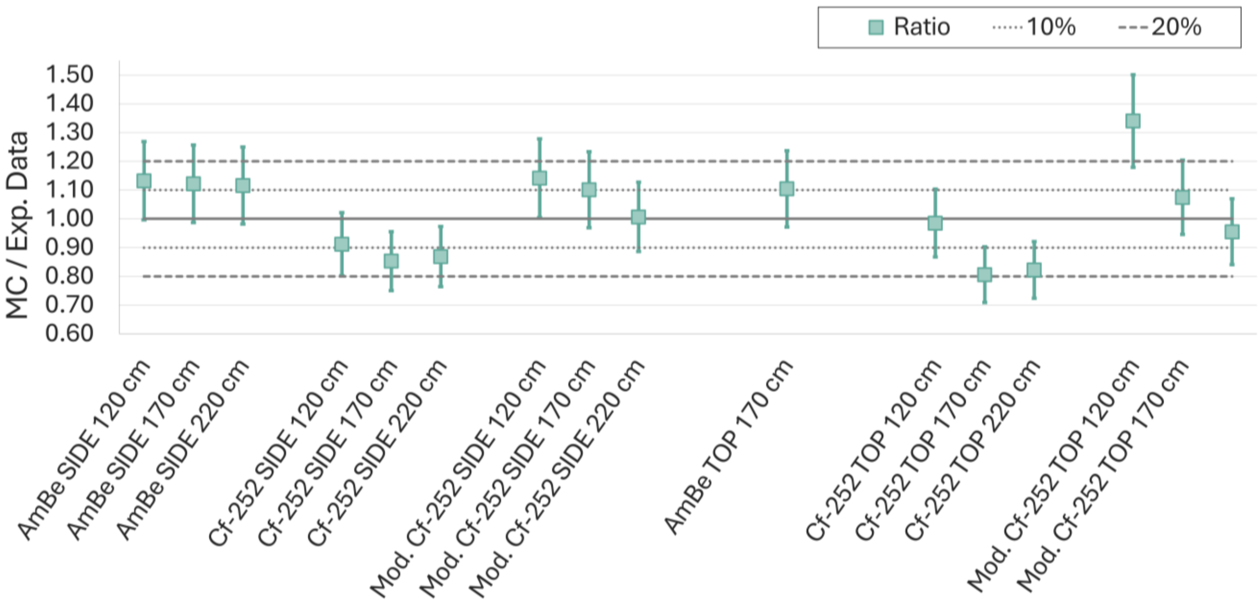

Figure 65. MC to measurement ratio for all irradiation configurations (see

Table **21** and 12). The error bars correspond to the $k = 1$, i.e. ~68 % coverage for normal distribution.

3.5 Summary of results

The following Table 22 summarizes the results of the Monte Carlo (MC) model validation procedure and the corresponding MC multiplication factors for all CRNS commercial systems characterised in this deliverable.

The MC multiplication factor *F* is a dimensionless quantity by which the results of the corresponding MC calculations must be multiplied to obtain the absolute CRNS probe response under simulated conditions. It is calculated as the reciprocal of the MC model scaling factor ($\bar{S}$) described in the previous Sections 3.1 to 3.4.

Table 22. Summary of the MC model scaling factors and the corresponding MC multiplication factors (F). The noted uncertainties correspond to k = 1 (~68 % coverage for a normal distribution).

Manufacturer	Detector model	MC model author	Particle transport code	Nuclear data	MC model scaling factor $\bar{S}$	$F = 1 / \bar{S}$
Finapp	Finapp Model 3	CMI	MCNP6.3	ENDF/B-VIII.0	1.47 ± 10 %	0.68 ± 10 %
Finapp	Finapp Model 3	SMU	MCNP6.2	ENDF/B-VII.0	1.29 ± 13 %	0.78 ± 13 %
Hydroinnova	CRS-1000 (^3He)	PTB	MCNP6.1	ENDF/B-VIII.0	0.80 ± 10 %	1.26 ± 10 %
Hydroinnova	CRS-2000/B (BF_3)	CIEMAT	MCNP6.2	ENDF/B-VIII.0	1.34 ± 4 %	0.75 ± 4 %
StyX Neutronica	System S1	PTB	MCNP6.1	ENDF/B-VIII.0	1.27 ± 11 %	0.79 ± 11 %

The selected CRNS probes were successfully modelled using the MCNP transport code, and these models were validated under laboratory conditions using well-characterized neutron reference fields. However, actual field operation conditions differ significantly in both neutron energy and angular distribution.

To enable a relevant intercomparison of different CRNS probe responses, it must be conducted under well-defined and harmonized conditions that accurately represent real operating environments. This activity is addressed under Task 2.2 within the project and is presented in the corresponding deliverable D3: *"Report on the comparison and validation of existing neutron transport models used to interpret CRNS signals measured under outdoor conditions".*

4 Outlook: Concept for a novel neutron reference field for the characterisation of CRNS devices

The laboratory characterisation of Cosmic-Ray Neutron Sensing (CRNS) probes, as detailed in this document, has highlighted a significant challenge: the mismatch between the probes' operational environment and the reference fields available at neutron metrology laboratories. CRNS devices are designed to measure low-intensity, broad-energy neutron fields, predominantly in the epithermal range, which are modulated by environmental factors like soil moisture. In contrast, standard laboratory calibrations utilise relatively intense, well-defined neutron spectra (from radionuclide sources or monoenergetic fields) that do not fully replicate the complex energy and angular distribution of the natural cosmic-ray neutron field.

CRNS probes are designed for environmental fluxes on the order of 10^{-2} cm^{-2} s^{-1}, while standard laboratory neutron fields typically operate between 10^{2} cm^{-2} s^{-1} and 10^{4} cm^{-2} s^{-1}. During the development of activity A1.3.4, this forced the use of only the weakest available sources (in the case of irradiations with radionuclide fields) and a reduction of the accelerator current in the case of irradiations with monoenergetic fields. Both measures reduced the statistics that could be collected during the allocated beam time and increased the statistical uncertainties. In cases where such low rates were not achievable, it was necessary to deal with non-linearity and saturation effects in the readout electronics, as observed with the Hydroinnova CRS-2000/B and StyX System S1 devices. The correction factors required in these situations introduced an additional source of uncertainty.

Validation of the Monte Carlo (MC) models showed that the probes' response depends strongly on neutron energy and angle of incidence. However, available laboratory neutron fields do not fully replicate the real-world neutron energy spectrum found in the natural environment, particularly in the epithermal energy range that is most relevant to the CRNS methodology. As a result, laboratory measurements with CRNS probes can be dominated by low-energy, room-return (scattered and moderated) neutrons, causing the observed CRNS count rate to be disproportionately weighted toward this scattered component rather than toward the primary neutrons emitted by a radionuclide source or produced at a neutron target.

In addition, the large size and asymmetric construction of CRNS probes (e.g. long cylindrical tubes) complicate the application of standard calibration techniques. Existing ISO shadow cones, where available, are suboptimal for the cubic or elongated geometry of the CRNS probes, leading to over-shielding or insufficient shielding and increasing the uncertainty in correcting for the scattered neutron component. These factors—high sensitivity to scattered neutrons and the lack of an appropriate background-subtraction technique—together increase the uncertainty, especially in cases where the background component must be addressed using MC simulations.

While the project successfully adapted existing reference facilities to accommodate the large size and unique response of CRNS probes, these adaptations introduced relatively large uncertainties (often between 10 % and 13 %). A dedicated neutron reference field, specifically designed for CRNS devices, would minimise the need for extensive corrections (such as the empirical linearity factors applied to the CRS-2000/B system or the thermal neutron corrections needed at PTB and CIEMAT to properly account for room-return in their detailed room simulations), thereby reducing the overall measurement uncertainty.

To address this need, two exploratory approaches are proposed to develop a novel neutron reference field tailored to CRNS applications.

4.1 Outdoor cosmic-ray neutron field

This approach uses the natural secondary cosmic-ray neutron field at ground level as the calibration source. To establish a traceable reference, a transfer instrument—such as the absolutely calibrated and SI-traceable extended range Bonner sphere spectrometer (ERBSS) operated by PTB—would be deployed alongside the CRNS probe under test. PTB has an outdoor area adjacent to its laboratory where a Bonner sphere spectrometer designed for outdoor neutron measurements (system NEMUS-UMW, described in SoMMet deliverable D3) can be deployed to characterise the local neutron energy spectrum and fluence rate, thereby providing an environmentally representative calibration baseline.

An additional variant of this concept is to perform measurements over a large body of water (e.g., a lake). The water effectively suppresses the soil "albedo" (ground-return) component of the neutron field—i.e., the component most sensitive to soil moisture—by acting as a quasi-infinite hydrogen-rich neutron moderator/absorber. Consequently, the near-surface epithermal contribution is strongly reduced, yielding a more stable reference environment with more stable fast and thermal neutron components, and reducing uncertainty associated with variations in the epithermal neutron fluence rate during extended measurement periods. This idea was recently explored by Schrön et al. [1], who reported a reduction of the epithermal neutron count rate by more than 50 %. PTB already operates the reference site for COsmic RAdiation DOSimetry (CORADOS) [2], a lake-based platform for cosmic radiation dosimetry, which could be adapted for this purpose.

4.2 Tailored laboratory-based field

For controlled laboratory conditions, the development of a dedicated moderator assembly is proposed. This device, based on a radionuclide neutron source (e.g., ^{241}Am-Be) or an accelerator-based neutron source (e.g., based on the Li(p,n)Be nuclear reaction), would use layers of moderating (polyethylene, AlF_3), reflecting (graphite, lead), and absorbing (cadmium, boron, lithium, titanium) materials to "shape" the output neutron energy spectrum, replicating the energy response of CRNS probes. The design would be inspired by beam-shaping assemblies used in Boron Neutron Capture Therapy (BNCT), as the one proposed in Montagnini et al. [3], which successfully mimics the characteristic CRNS response (see Figure 66).

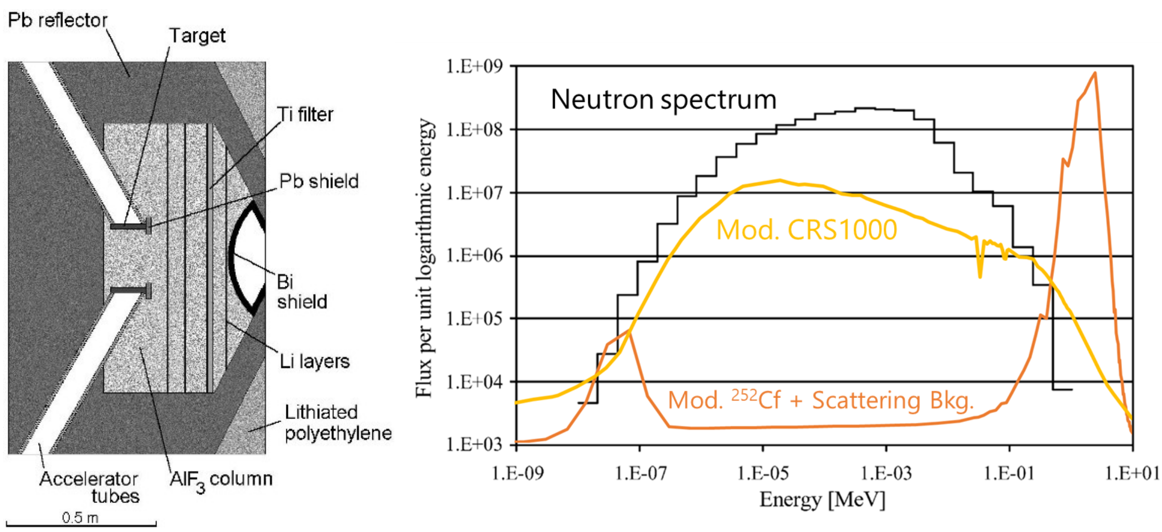

Figure 66. Moderator assembly from B. Montagnini et al. (left) and the achievable neutron energy spectrum (right). A typical CRNS response function is superimposed, together with the most suitable neutron field available at PTB (^{252}Cf neutron source including the scattering contribution). While the assembly reproduces the response function more closely, the ^{252}Cf field more closely matches a typical above-ground cosmic-ray neutron field.

Such a facility would require a very large, low-scattering experimental hall (already available at facilities such as PIAF@PTB or AMANDE@ASNR) to minimize room-return neutron contributions.

Furthermore, the design and characterization of customized shadow objects, tailored to the geometry of bulky CRNS probes, would be essential for accurately quantifying the scattering background.

Both exploratory concepts outlined above could, in principle, support community efforts to bridge the gap between laboratory calibrations and field operations, thereby contributing to more accurate, harmonised, and SI-traceable soil moisture data from global CRNS networks.

5 References

[1] M. Schrön, “Buoy-based detection of low-energy cosmic-ray neutrons to monitor the influence of atmospheric, geomagnetic, and heliospheric effects”, *Earth and Space Science,* vol. 11, p. e2023EA003483, 2024.

[2] S. Neumaier, “Improved assessment of $\dot{H}*(10)$ in the environment using two complementary active dosimetry systems”, *Radiation Measurements,* vol. 167, p. 106980., 2023.

[3] B. Montagnini, “Spectrum shaping of accelerator-based neutron beams for BNCT”, *Nuclear Instruments and Methods in Physics Research A,* vol. 476, p. 90–98, 2002.